DYNAMIC FILTRATION RESISTANCE OF FIBROUS FILTER MEDIA USED FOR GENERAL VENTILATION AND CLEAN AIR-CONDITIONING

ZHANG WANYI

PhD

The Hong Kong Polytechnic University

This programme is jointly offered by The Hong Kong Polytechnic University and Tongji University

2021

The Hong Kong Polytechnic University
Department of Building Services Engineering

Tongji University
School of Mechanical Engineering

Dynamic Filtration Resistance of Fibrous Filter Media Used for General Ventilation and Clean Air-Conditioning

Zhang Wanyi

A thesis submitted in partial fulfillment of the requirements

for the Degree of Doctor of Philosophy

April 2021

Certificate of Originality

I hereby declare that this thesis is my own work and that, to the best of my knowledge and belief, it reproduces no material previously published or written, nor material that has been accepted for the award of any other degree or diploma, except where due acknowledgement has been made in the text.

ZHANG Wanyi

Department of Building Services Engineering

The Hong Kong Polytechnic University

Hong Kong SAR, China

July 2021

Abstract

In recent years, the pursuit of people for better indoor air quality and the cleanliness requirement for the operating environments in factories have brought explosive growth to the market of air purifiers and clean air-conditioning systems. At present, the most effective method commonly used to separate particulate matters from air is to filter air with fibrous filter media. The performance parameters of a fibrous filter medium include filtration efficiency, resistance and dust loading capacity. These parameters would change gradually with the deposition of particles into the fibrous filter medium. The growth of filters' resistance can directly lead to an increase in energy consumption and a decrease in supply air volume for a ventilation system. Consequently, the dynamic filtration resistance of fibrous filter media directly determines the dust loading capacity, energy consumption and service life of air filters. However, there has been a lack of widely accepted theoretical models for the dynamic filtration resistance of fibrous media in the open literature.

It has been widely accepted that a dust loading procedure may be divided into three stages: the depth filtration, transition stage and surface filtration. However, for fibrous media used for general ventilation and cleaning air-conditioning, only the depth filtration and/or the surface filtration are usually experienced. Therefore, the research work reported in this Thesis focuses mainly on the dynamic filtration resistance models for fibrous media during depth filtration and surface filtration using both

theoretical modeling and experimental approaches, so as to improve dust loading capacity for Polytetrafluoroethylene (PTFE) high efficiency particulate air (HEPA) media.

In the research work reported in this Thesis, firstly, the influences of filtration velocity, air flow humidity and aerosol concentration on the dynamic resistance of fibrous filter media was studied experimentally. The experimental results showed that, in the filtration velocity range of 2~10 cm/s which was commonly used for general ventilation, the influence of an increase in filtration velocity on the dynamic resistance of fibrous filter media was not significant. However, an increase over 5% in relative humidity (RH) of passing air flow would lead to a significant decrease in resistance in a short time period when the media was loaded with polydisperse KCl aerosols. The resistance growth trend for a medium loaded with KCl aerosols at an air RH close to the deliquescence point of the KCl aerosol was similar to that loaded with a liquid aerosol. But polydisperse SiO_2 aerosols loaded into the media were not sensitive to the changes in air flow RH. In addition, the aerosol concentration had no significant influence on the dynamic resistance of a filter medium at the same filtration velocity.

Secondly, a layered resistance model by incorporating the mass concentration distribution of deposited particles into Bergman model was proposed to predict the depth filtration resistance for fibrous media. Experiments for five-stacked glass fiber

media loaded with four monodisperse SiO_2 aerosols and polydisperse SiO_2 aerosols were conducted to investigate the distribution of deposited particles. The resistance growths obtained respectively from experiments and model prediction showed good agreement when the modification of critical loaded dust mass was applied. To theoretically evaluate the distribution of deposited particles inside a loaded medium, the D-model was established by dividing a filter medium into unit layers and applying the definition of single fiber efficiency to calculating the mass of particles captured by each layer. The variation trends in loaded dust mass predicted using the numerical solutions for the D-model agreed well with those obtained from the dust loading experiments.

Thirdly, dust cake resistance models for both monodisperse aerosols and polydisperse aerosols were respectively developed by calculating the shielding effect of particles based on the kinetic theory. To monitor the changes in thickness and porosity for dust cakes during their formation, a laser scanning porosity measuring system was established and its accuracy and reproducibility demonstrated. When using this system to monitor the formation process of a dust cake, it was found that the thickness growth rate for a dust cake was gradually slowed down with an increase in loaded dust mass and finally leveled so that the dust cake porosity was decreased linearly. The results of dust loading experiments for PTFE membranes using monodisperse SiO_2 with different geometric mean diameters and polydisperse SiO_2 with different particle size

distributions suggested that, for monodisperse aerosols, the smaller the average diameter was, the faster the filtration resistance on the surface of PTFE films grew, and the dust layer porosity was higher under the same resistance growth. For polydisperse aerosols, the rate of increase in filtration resistance of the PTFE membrane and the porosities of dust cakes were decreased significantly with an increase in geometric standard deviation.

Finally, based on the above three parts of completed work, an experimental evaluation method for dust loading performances for HEPA filter media was developed from three aspects: the applicability of experimental aerosol in terms of particle size and humidity sensitivity, experimental setups and procedures, and the evaluation method of energy consumption. This method was used to compare the dust loading performances when using an H14 PTFE medium with those when using an H14 glass fiber medium. Scanning electronic microscope (SEM) photos were taken after the two media were loaded to having a resistance of 900 Pa at 5.3 cm/s. The comparison results showed that although the PTFE medium had a 50% lower initial resistance, its resistance growth rate was far greater than that for the glass fiber medium. To remove the application limit of PTFE media due to their poorer dust loading performances, composite PTFE media were developed by replacing the windward base materials of PTFE media. Three electret filter media of three different filtration efficiencies were used as the windward materials to make composite PTFE media. The average

resistances during dust loading for these composite PTFE media were experimentally obtained and compared. Results show that the dust loading performances of the above three PTFE media were significantly improved after compositing, all being better than that of a glass fiber HEPA medium. Among them, "PTFE + medium efficiency electret" had the best energy consumption performance when using an eligible experimental aerosol.

Keywords: dynamic resistance, monodisperse SiO_2 aerosol, single fiber efficiency, porosity, composite PTFE media

Publications Arising from the Thesis

Journal papers

- **Zhang Wanyi**, Deng Shiming, Wang Yongxiang, Lin Zhongping. Modeling the surface filtration pressure drop of PTFE HEPA filter media for low load applications[J]. Building and Environment, 2020, 177(7) (Based on Chapter 7)

- **Zhang Wanyi**, Deng Shiming, Wang Yongxiang, Lin Zhongping. Dust Loading Performance of the PTFE HEPA Media and its Comparison with the Glass Fiber HEPA Media[J]. Aerosol and Air Quality Research, 2018, 18(7): 1921-1931. (Based on Chapter 8)

Conference papers

- **Zhang Wanyi**, Deng Shiming, Wang Yongxiang, Lin Zhongping. Theoretical model for surface filtration pressure drop and accurate measurement method of dust cake porosity[C]//The International Symposium on Heating, Ventilation and Air Conditioning. Springer, Singapore, 2019: 173-180 (Based on Chapter 7)

- **Zhang Wanyi**, Deng Shiming, Lin Zhongping. Experimental Study on The Applicability of Solid Particles Used in Dust Loading Performance Evaluation

Experiments for HEPA Filter Media// the 8th International Conference on Energy and Environment of Residential Buildings, Wellington, New Zealand, November 19-21, 2018. (Poster) (Based on Chapter 5)

Acknowledgements

I must first express my sincere grateful thanks to my Chief Supervisor, Prof. Deng Shiming, from the Department of Building Services Engineering (BSE), The Hong Kong Polytechnic University, and my Co-Supervisor, Prof. Lin Zhongping, from the School of Mechanical Engineering, Tongji University for their readily available supervision, patient guidance and continuous helps throughout the course of my study.

Second, my special thanks go to The Hong Kong Polytechnic University and Tongji University for financially supporting my study. I would like to thank Prof. Fan Cunyang, Mr. Chu Jiaming, Mr. Wang Yongxiang, Mr. Zhao Chenyu, Mr. Fang Guanyu, Mr. Chen Wenjing and Ms. Yan Huaxia for their help during my study. I would like also to thank the manufactures of filter media and instruments for their assistance in the experimental work.

Finally, I would like to express my deepest gratitude to my parents, my elder sister and elder brother and my girlfriend. I could not have completed my work without their love, continuous supports and understandings.

Table of Contents

Page

List of figures

Chapter 5

Chapter 7

Chapter 8

List of tables

Chapter 7

Nomenclature

Variable	Description	Unit
A	Windward area of a porous medium	m^2
A_m	Filtration area of a fibrous medium	m^2
$\bar{c}$	Average velocity of air molecules	m/s
C_0	Upstream aerosol concentration	mg/m^3
C_o	Overlap coefficient	-
C_c	Cunningham slip correction factor	-
C_p	Free particle concentration in a fibrous medium	mg/m^3
d_f	Fiber diameter	µm
d_p	Particle diameter	µm
d_{pf}	"Particle fiber" diameter	µm
d_{pg}	Geometric mean diameter of particles	µm
d_{pm}	Mass mean diameter of particles	µm
d_{vg}	Geometric mean size of volume equivalent diameter	µm
$\mathrm{d}z$	Thickness of a medium unit	µm
D_{50}^{V}	Aerosol mass median diameter	µm
F_p	Drag force of a particle	N
F_c	Drag force of all particles in a dust cake	N
k	Permeability of a porous medium	-

k_2	Instantaneous growth rate of dynamic resistance	Pa·m^2/g
K_1	Resistance coefficient of a clean medium	Pa·s/m
K_2	Resistance coefficient of a dust cake	Pa·s·m/g
l	Total equivalent length of clean fibers in a unit medium	m
L_f	Total equivalent length of clean fibers	m
L_{pf}	Total equivalent length of "particle fibers"	m
N_p	Number of particles in the dust cake	-
m	Mass of a porous medium	g
$\bar{m}_a$	Average mass of air molecules	g
m_c	Dust mass per unit area	g/m^2
M_p	Deposited particle concentration in a fibrous medium	mg/m^3
M_c	Dust cake mass	g
r_p	Particle radius	μm
S	Area of a fibrous medium	m^2
t	Dust loading time	s
T_a	Thermodynamic temperature of air	K
V	Filtration velocity	cm/s
V'	Velocity around medium fibers	cm/s
Z	Thickness of a porous medium	m
Z_m	Thickness of a filter medium	m
Z_c	Thickness of a dust cake	m

ΔP	Resistance of a porous medium	Pa
ΔP_0	Resistance of a clean fibrous medium	Pa
ΔP_{pf}	Resistance of "particle fibers"	Pa
ΔP_c	Resistance of a dust cake	Pa
α	Packing density of a porous medium	-
α_c	Packing density of a dust cake	-
α_f	Packing density of a clean fibrous medium	-
α_m	Packing density of a fibrous medium	-
α_{pf}	Packing density of "particle fibers"	-
ε	Porosity of a porous medium	-
ε_c	Porosity of a dust cake	-
κ	Dynamic shape factor of particles	-
k_B	Boltzmann constant	J/K
η_f	Single fiber efficiency	-
η_{fp}	Loaded single fiber efficiency	-
λ	Single fiber efficiency growth coefficient	m^3/mg
λ_a	Mean free path of air molecules	m
ρ	True density of a porous medium	g/cm^3
ρ_a	Air density	kg/m^3
ρ_f	Fiber density	g/cm^3
ρ_p	Particle density	g/cm^3

σ_g	Geometric standard deviation of particle size distribution	μm
μ	Dynamic viscosity coefficient of a fluid	Pa·s
μ_a	Air viscosity	Pa·s

List of abbreviations

CFD	Computational fluid dynamics
CPC	Condensation particle counter
DEHS	DiEthylHexylSebacate
EPA	Efficient particulate air
FFU	Fan filter unit
HEPA	High efficiency particulate air
MMD	Mass mean diameter
MPPS	Most penetrating particle size
OPC	Optical particle counter
PSL	Polystyrene latex
PTFE	Polytetrafluoroethylene
RH	relative humidity
SEM	Scanning electronic microscope

Chapter 1

Introduction

Nowadays, people spend an average around 80% of their time indoors, which suggests that indoor air quality would have direct and significant impacts on occupants' health. However, the monitored atmospheric PM2.5 values due to air pollution and haze weather often exceeded the limits specified in related codes and regulations. On the other hand, indoor activities such as smoking and printing generate a large number of particles. Both outdoor and indoor sources of particulate matter would jointly lead to an increase in indoor particulate matter concentration. Therefore, in recent years, the pursuit of people for better indoor air quality and the cleanliness requirements for the improved operating environments in relevant factories have led to explosive growth of the market of air purifiers and clean air-conditioning systems.

At present, the most effective method commonly used to separate particulate matters from air is to filter the air with fibrous filter media. Various kinds of air filters made of fibrous media are being widely used for indoor air purification, environmental cleanness control and exhaust air treatment.

The performance parameters of a fibrous filter medium include filtration efficiency, resistance and dust loading capacity. These parameters would change gradually with the deposition of particles into the fibrous filter medium. For a fibrous medium made of fibers with no static electricity, its filtration efficiency is gradually increased with time unless it is damaged, implying that its filtration performance can be guaranteed within its life span. However, the growth of medium's flow resistance can directly lead to an increase in energy consumption and a decrease in supply air volume for a ventilation system.

The resistance of a fibrous filter is made of structure resistance and filter medium resistance, and the former can be considered to remain unchanged at a constant face velocity. Therefore, an increase in filter resistance is mainly caused by an increase in fibrous medium resistance. Consequently, the dynamic filtration resistance of fibrous filter media directly determines dust loading capacity, energy consumption and service life of air filters. Therefore, studying the dynamic resistance for fibrous filter media helps to evaluate their life cycle energy consumption and to optimize their structures so as to reduce the energy consumption of ventilation systems. However, there has been a lack of widely accepted theoretical models for the dynamic filtration resistance of fibrous media in the open literature.

It has been widely accepted that a dust loading procedure may be divided into three stages: depth filtration, transition stage and surface filtration. However, for fibrous media used for general ventilation and cleaning air-conditioning, only the depth filtration and/or the surface filtration are usually experienced.

In China, the PTFE HEPA filter medium has taken an increasingly large share of the HEPA media recently because of its lower initial resistance as compared to other traditional glass fiber HEPA media at the same efficiency level. Millions of PTFE HEPA filters have been used in low load applications such as the factories that produce liquid crystal displays and organic light-emitting diode panels to maintain a super clean production environment. However, the applicability of PTFE HEPA filters to general ventilation is still limited by their lower dust loading capacities.

Therefore, the research work reported in this Thesis focuses mainly on developing dynamic filtration resistance models for fibrous media during depth filtration and surface filtration using both theoretical modeling and experimental approaches, so as to improve the dust loading capacity for PTFE HEPA media.

To begin with, the previously reported studies related to the dynamic resistance of fibrous filter media in open literature are reviewed in Chapter 2. The current status of existing research and research gaps were identified by reviewing the relevant research

work on established models for initial resistance and dynamic resistance of fibrous media, influencing factors and simulation studies on the media dynamic resistance.

According to the research gaps identified in the literature review, Chapter 3 presents the proposal for the research work reported in this Thesis, including background, objectives and the methodologies to be adopted.

In Chapter 4, an experimental setup that was specifically established for dust loading experiments of fibrous media in the current research work is detailed, covering experimental air flow, experimental aerosol and experimental fibrous media. The operating performances of the experimental setup were validated through resistance test, Zero% efficiency test, 100% efficiency test and aerosol concentration test.

Chapter 5 reports on an experimental study on the influences of filtration velocity, air flow humidity and aerosol concentration on the dynamic resistance of fibrous filter media. The study results can be used as a useful reference for the parameter selection for the media dust loading experiments.

Chapter 6 presents a study on the depth filtration resistance of fibrous filter media by combining the classical depth filtration resistance calculation formula and the mass concentration distribution of deposited particles. Experiments for five-stacked glass

fiber media loaded with monodisperse SiO_2 aerosols and polydisperse SiO_2 aerosols were conducted to investigate the mass concentration distribution of deposited particles and validate the established depth filtration resistance model. Moreover, a D-model was built to theoretically evaluate the mass concentration distribution of deposited particles in a loaded medium.

A study on the surface filtration resistance of fibrous media is reported in Chapter 7. Dust cake resistance models for both monodisperse aerosols and polydisperse aerosols were respectively developed by calculating the shielding effect of particles based on the kinetic theory. To monitor the changes in the thickness and porosity of dust cakes during their formation, a laser scanning porosity measuring system was established and its accuracy and reproducibility demonstrated. Dust loading experiments for PTFE membranes were carried out using both monodisperse aerosols and polydisperse aerosols to verify established resistance models.

In Chapter 8, an experimental evaluation method for dust loading performances for HEPA filter media is presented. The method was developed based on the considerations of the applicability of experimental aerosol in terms of particle size and humidity sensitivity, experimental setups and procedures, and the evaluation of energy consumption for loaded media. This evaluation method was used to compare the dust loading performances when using an H14 PTFE medium with those when using an

H14 glass fiber medium. Composite PTFE media were developed by replacing the windward base materials of PTFE media with electret media to improve the dust loading performance of PTFE media. The average resistances during dust loading for these composite PTFE media were also experimentally obtained and compared.

Finally, the Conclusions of this Thesis and the future work are given in Chapter 9.

Chapter 2

Literature review

2.1 Introduction

At present, air filters have become indispensable in the ventilation systems in residential buildings and industrial plants [Chen et al. 2019, Bian et al. 2020]. The resistance increases of filters and filter media caused by captured particles have attracted extensive attention because of their significant impact on the service life of filters and the energy consumption of ventilation systems [Zaatari et al. 2016, Zuraimi et al. 2017, Ji et al. 2019].

The structure types and filter media used in air filters have been changed significantly over the past many years. Recently, the optimization of filter media becomes the key to improving the performances of air filters since the structure types of air filters have been virtually finalized. Research work on the dynamic resistance performance for various fibrous filter media has been carried out recently [Ji et al. 2003, Tian et al. 2018, Tian et al. 2019, Xia and Chen 2020] thus their basic understandings obtained.

As shown in Fig 2.1, with the continuous deposition of captured particles inside and on the surface of a fibrous filter medium, the filtration process may be roughly divided into three stages. The first one refers to a depth filtration stage, when captured particles deposit inside the medium and build “dendritic dust fiber”, resulting in a relatively low growth rate of resistance. For the second stage or the transition stage, with the clogging of the medium, particles are gradually unable to deposit into the medium, but only on its surface. At the third stage of filtration or surface filtration stage, “dust cake” is formed by the captured particles on the medium surface. During surface filtration stage, the resistance of loaded medium increases approximately linearly with an increase in loaded dust mass.

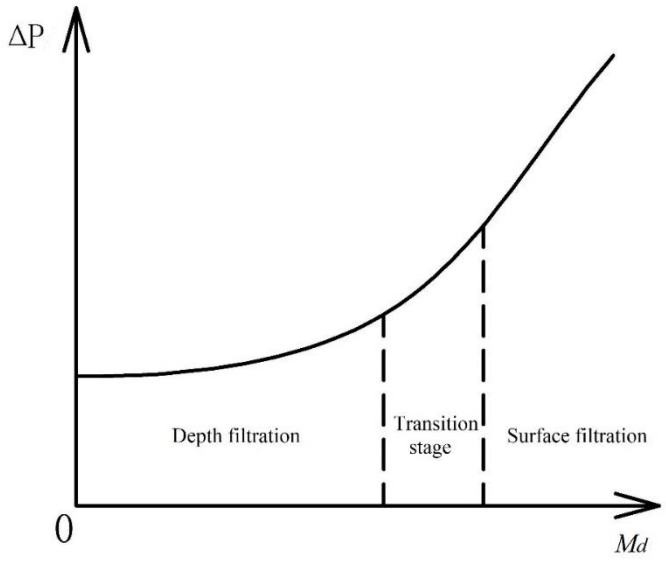

Fig 2.1 Resistance curve for a fibrous medium during dust loading

The widely used general ventilation and clean air-conditioning systems are sensitive to the increases in air flow resistance and thus energy consumption. Hence, in practice, in these systems, almost no fibrous media would be used to completely go through the three filtration stages and to reach very high final resistance. For example, the glass fiber HEPA filters used in clean air-conditioning systems are well protected by upstream filters and loaded with a limited amount of dust during their service life, such that only depth filtration is experienced. For a PTFE HEPA medium, most of the captured particles will directly deposit on the surface of the PTFE membrane, because the base material on the windward side has a very low filtration efficiency. Hence, it could be considered that only the surface filtration takes place for PTFE media.

The research work reported in this Thesis focused on studying the dynamic resistance of fibrous media used in general ventilation and clean air-conditioning systems. The types of fibrous media included medium and high efficiency glass fiber media and high efficiency PTFE media. Generally, only depth filtration and surface filtration were involved for these media. Therefore, in this research work, dynamic resistance performances of fibrous filter media during both depth filtration and surface filtration should be separately studied.

In order to understand the current situation of filtration theory and to identify the research gaps, an extensive literature review on the previous studies related to the

dynamic resistance of fibrous filter media has been carried out. The review covered four aspects: initial resistance models for clean fibrous media, the dynamic resistance models for fibrous media during dust loading, the influencing factors and the simulation studies for the dynamic resistance of fibrous media. These will be presented in Sections 2.2 to 2.5, respectively.

2.2 Initial resistance models for clean fibrous media

Studies on the initial resistance of clean fibrous media lay a foundation to understand their dynamic resistance. Fibrous filter medium is a kind of porous material. When air passes through a fibrous medium, the total air pressure is reduced. However, the changes in kinetic energy and potential energy of air are usually ignored. Therefore, the pressure drop, i.e., the resistance of a fibrous medium, mainly refers to the difference in air static pressure between upstream and downstream of the medium. One the other hand, the resistance of clean fibrous media is affected by their internal structure, such as thickness, fiber diameter distribution, packing density, etc., and external environmental parameters, such as filtration velocity, air flow temperature, relative humidity, etc.

The Darcy law which was derived from Darcy's experiments on water flowing over sand granular beds, has been adopted to describe the resistance characteristics of clean

fibrous media. The law specified a linear relationship between the pressure gradient and the velocity of fluid through a homogeneous isotropic porous medium at a steady flow rate, expressed as

$$\frac{\Delta P}{Z} = \frac{1}{k}\mu V \tag{2-1}$$

where ΔP is the resistance, Z the thickness and k the permeability of the porous medium, μ the dynamic viscosity coefficient of the fluid and V the flow velocity.

Fiber diameter and porosity of a fibrous medium were introduced to represent the parameter k, for quantitatively calculating the medium resistance, as shown in Equation (2-2),

$$\frac{\Delta P_0}{Z_m} = \frac{4f(\alpha_m)}{{d_f}^2}\mu_a V \tag{2-2}$$

where ΔP_0 is the resistance, Z_m the thickness, α_m the packing density of the clean fibrous medium, which is the ratio of the non-porous packed volume of a medium to the actual volume, $f(\alpha_m)$ a parameter related to the packing density, representing the force per unit area of the fiber surface exerted on air flow, which can be calculated according to the arrangement of fibers relative to air flow, d_f the fiber diameter and μ_a the air viscosity.

Jackson and James [1986] conducted a more comprehensive review of modeling studies on $f(\alpha_m)$ based on air flow direction relative to fibers, and divided available models into the following three categories: theoretical models based on air flow direction parallel to that of fibers, theoretical models based on air flow perpendicular to that of fibers, and empirical and theoretical models based on air flow through a random arrangement of fibers. Among them, the models in the first category mainly included the single fiber models by Langmuir et al. [1942] and Happel [1959], and the models for fibers with the arrangements of square, regular triangle, regular hexagon and rectangular by Drummond and Tahir [1984]. The theoretical models in the second category mainly included the Kuwabara [1959] model, the approximation of the Kuwabara model by Fuchs and Stechkina [1963], the Hasimoto [1959] model, the resistance model of square and regular hexagonal fiber arrangement [Sangani and Acrivos 1982], etc. The models in the last category mainly included the empirical model by Chen [1955], Spielman and Goren [1968] theoretical model, Davies [1973] empirical model, Jackson and James [1986] theoretical model, and Henry and Ariman [1983] theoretical model.

By comparing the predictions for the resistance of clean fibrous media from a number of existing model with experimental results as shown in Fig 2.2, Thomas et al. [2016] showed that the use of these models would lead to significant errors at the packing

density of less than 0.01 and greater than 0.4. Among these models, the Davies model would have the best prediction and has been thus widely used.

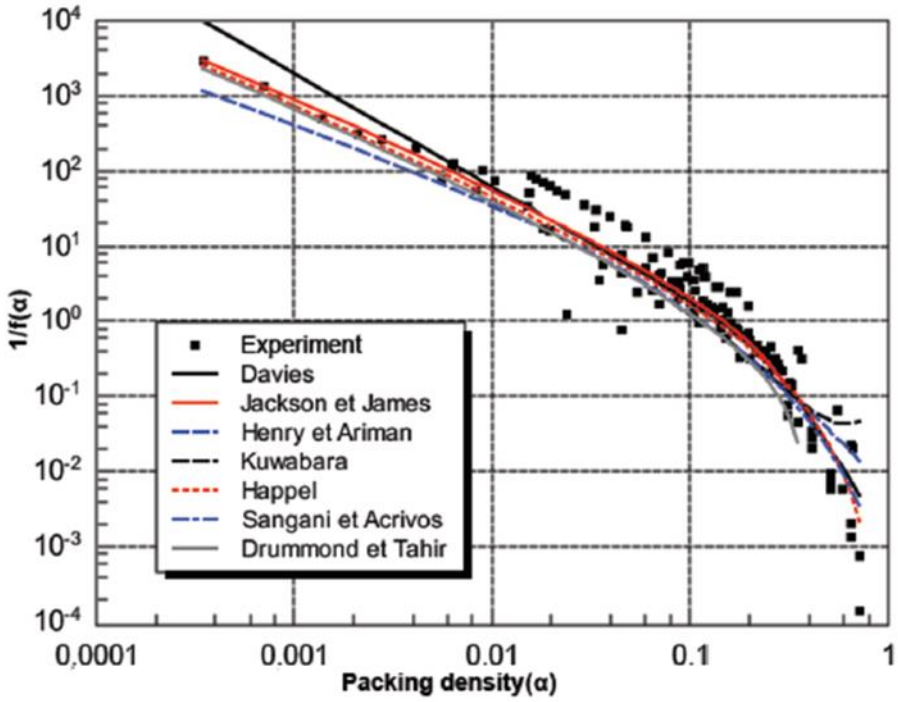

Fig 2.2 Comparison between the predictions by a number of theoretical models for the resistance of clean fibrous media and experimental results [Thomas et al. 2016]

The Davies model for the resistance of clean fibrous media is expressed as

$$\frac{\Delta P_0}{Z_m} = \frac{64{\alpha_m}^{\frac{3}{2}}(1 + 56{\alpha_m}^3)}{{d_f}^2}\mu_a V \tag{2-3}$$

The model would predicate the best when the packing density was between 0.006 to 0.3.

2.3 Dynamic resistance models for fibrous media during dust loading

Existing studies on the dynamic resistance of fibrous filter media are very complicated, and only their representatives are reviewed in this Section. These included the "particle dendrite" hypothesis and Bergman model for depth filtration resistance, dust cake resistance models for surface filtration resistance and the related studies on loaded media porosity.

2.3.1 "Particle dendrite" hypothesis and Bergman model

Based on the previous observations on the particles' deposition inside fibrous media through electronic microscopes, the dendritic deposition structure of particles was discovered [Cai 1992]. A "particle dendrite" hypothesis was proposed [Payatakes 1976, Payatakes and Tien 1976, Payatakes 1977] to build the resistance models for loaded media. However, in these models, the captured particles were thought to be stacked along the direction of air flow. This would overestimate the filtration efficiency and the growth rate of resistance for fibrous media [Xu 2014]. To study the

shape and growth of particle dendrites, Kasper et al. [2010] used a confocal microscope to observe dendritic particles suspended on thin steel fibers in an aerosol stream.

A resistance model, Bergman model, for loaded fibrous media was proposed based on the Davies model [Bergman et al. 1978]. The Bergman model considered a loaded fibrous medium as a superposition of the original clean medium fibers and the new fibers formed by captured particles, and may be used to evaluate the loaded medium resistance as the total from clean medium and particle fiber, as Equation (2-4).

$$\Delta P = \Delta P_0 + \Delta P_{pf} \tag{2-4}$$

where ΔP is the total resistance, and ΔP_{pf} the resistance of particle fibers.

ΔP and ΔP_{pf} in Bergman model were supposed to be independent of each other, but in practice, the influence of particle fibers on the air flow inside the medium cannot be ignored. In order to quantify this influence, Bergman increased the packing density of clean fibers and particle fibers by $(L_f + L_{pf})/L_f$ and $(L_f + L_{pf})/L_{pf}$, respectively, as follows,

$$L_f = \frac{4\alpha_f Z_m}{\pi {d_f}^2} \tag{2-5}$$

$$L_{pf} = \frac{4\alpha_{pf} Z_m}{\pi {d_p}^2} \tag{2-6}$$

where L_f is the total equivalent length of clean fibers of the loaded fibrous medium, L_{pf} the total length of particle fibers, α_f the clean fiber packing density, d_f the diameter of clean fibers, α_{pf} the particle fiber packing density, and d_p the captured particle diameter.

Then the Davies empirical model on the resistance for clean media, i.e., Equation (2-3), was applied to calculating the resistance of clean fibers and particle fibers, by omitting the coefficient $(1 + 56\alpha^3)$. As a result, the resistance of a loaded fibrous medium may be evaluated by:

$$\Delta P = 16\pi\mu_a V \left[L_f (\alpha_f \frac{L_f + L_{pf}}{L_f})^{1/2} + L_{pf} (\alpha_{pf} \frac{L_f + L_{pf}}{L_{pf}})^{1/2} \right] \tag{2-7}$$

Replacing L_f and L_{pf} according to Equations (2-5) and (2-6), Equation (2-7) became:

$$\Delta P = 64\mu_a V Z_m (\frac{\alpha_f}{{d_f}^2} + \frac{\alpha_{pf}}{{d_{pf}}^2})^{1/2} (\frac{\alpha_f}{d_f} + \frac{\alpha_{pf}}{d_{pf}}) \tag{2-8}$$

It was assumed in Bergman model that the particles were deposited uniformly inside the fibrous medium. However, Letourneau et al. [1991] considered that this assumption was not consistent with the experimental observations, and thus proposed a modified model where a fibrous medium was separated into several uniformly thin layers along the thickness direction, assuming that captured particles were deposited uniformly in each thin layer, expressed by

$$\Delta P = 64\mu_a V \int_0^{Z_m} \left(\frac{\alpha_f}{{d_f}^2} + \frac{\alpha_{pf}(Z)}{{d_{pf}}^2}\right)^{1/2} \left(\frac{\alpha_f}{d_f} + \frac{\alpha_{pf}(Z)}{d_{pf}}\right) \mathrm{d}Z \qquad (2\text{-}9)$$

However, as seen, this modified model actually relied on the captured particle mass distribution which was determined experimentally in Letourneau's study. In addition, the change in the packing density of the loaded fibrous medium during dust loading was considered by the model.

Another model for filtration efficiency and resistance of fibrous HEPA filters during dust loading was proposed [Thomas et al. 1999, Thomas et al. 2001], based on the work of Letourneau et al. [1991], which was an important progress in the study of dynamic filtration. Based on the analysis of the experimental data and the observation of the loaded HEPA media using a SEM, Thomas believed that the accumulation of particles inside the HEPA media had an exponential distribution. Therefore, the proposed model took this inhomogeneity into consideration, and the resistance and

filtration efficiency for a loaded fibrous medium under unsteady conditions may be evaluated layer by layer on an on-going basis. Dust loading experiments were designed to verify this model, and fluorescein sodium aerosol was used to measure the penetration rate. Joubert et al. [2011] studied the dust loading resistance of HEPA filters under high humidity exposure using this model.

In recent years, a nonlinear differential equation for particle concentration distribution in a fibrous medium was derived by Lin et al. [2013] based on the Navier-Stokes equation for viscous fluids. An empirical formula for dynamic filtration efficiency was obtained by fitting experimental results using nonlinear regression.

2.3.2 Dust cake resistance models

The Bergman model aimed mainly at the resistance increase during depth filtration. For the surface filtration situation, particles would deposit on the surface of fibrous media to form dust cakes, and the resistance of a dust cake was increased linearly with collected dust mass.

The available resistance calculation methods for the dust cakes has been summarized by Rudnick and First [1978]. They compared the "free surface" resistance model proposed by Happel [1959, 1983, 1983] with Kozeny-Carman's empirical resistance

model for porous media [Carman 1956] and considered the latter less accurate. Cheng and Tsai [1998] conducted dust loading experiments at filtration velocities of 1~9 cm/s using three types of dust: fly ash having a mass mean diameter (MMD) of 6.28 μm, limestone dust of an MMD of 2.53 μm and fine powder of an MMD of 3.88 μm used for air cleaner test. The experimental results were used to obtain the resistance coefficients of the cakes of three types of dust, and they also believed that the Rudnick-Happel model agreed better with the experimental results.

In general, the total resistance of a fibrous medium covered with a dust cake during surface filtration was the sum of the clean medium resistance and the dust cake resistance, as follows,

$$\Delta P = \Delta P_0 + \Delta P_c \tag{2-10}$$

where ΔP_c is dust cake resistance.

For a clean medium with a high filtration efficiency, its initial resistance and the rate of resistance increase after being covered with a dust cake were linearly related to filtration velocity. Then, a coefficient of K_1, can be used as the resistance coefficient for a clean medium, and a coefficient of K_2, that for the dust cake, so that the resistance of a medium covered with a dust cake was

$$\Delta P = \Delta P_0 + \Delta P_c = K_1 V + K_2 \frac{V M_c}{A_m} \quad (2\text{-}11)$$

where M_c is the dust cake mass, A_m the filtration area.

K_2 was first proposed by Billings [1966]. Dennis and Dirgo [1981] conducted an experimental study to determine K_2, and Novick et al. [1992] recommended to use K_2 to integrate Bergman model, Rudnick-Happel model and Kozeny-Carman model. Song et al. [2006] used Equation (2-11) to evaluate the resistance of HEPA media loaded with monodisperse aerosols.

In the studies on dust cake resistance, a widely accepted hypothesis was that the resistance of a dust cake was the sum of the forces exerted by each particle that made up the dust cake in the flow field, divided by the effective filtration area, expressed as follows,

$$\Delta P_c A_m = \frac{\sum F_p}{\varepsilon_c} \quad (2\text{-}12)$$

where F_p is the drag force for a single particle in the dust cake, ε_c the dust cake porosity. The correction of $1/\varepsilon_c$ was made to reflect the influence of dust cake structure on inner air flow velocity.

The drag force for each particle obeyed Stokes law when the Reynolds number was less than 0.1 and can be expressed as follows,

$$F_p = 6\pi r_p \mu_a V = 3\pi d_p \mu_a V \tag{2-13}$$

where r_p is the radius and d_p the diameter of the particle.

The Stokes law was derived under the assumption that the air flow was continuous. However, when the particle size was very small at less than 15 μm, air flow may no longer be considered as continuous, so that the Cunningham slip coefficient correction [Cunningham 1910] was introduced to Equation (2-13) as

$$F_p = \frac{3\pi d_p \mu_a V}{C_c} \tag{2-14}$$

where C_c is the Cunningham slip correction factor, evaluated by

$$C_c = 1 + \frac{2\lambda_a}{d_p} \cdot (A_1 + A_2 \cdot e^{\frac{-A_3 \cdot d_p}{2\lambda_a}}) \tag{2-15}$$

where λ_a is the mean free path of air molecules, A_1, A_2, A_3 the empirical coefficients, assumed at 1.165, 0.483 and 0.997, respectively [Kim et al. 2005].

A representative theoretical model for calculating the dust cake resistance due to drag force of particles was developed by Endo et al. [1998, 2002], as follows,

$$\Delta P_c = 18\frac{\mu_a V}{C_c}\frac{\varphi(\varepsilon_c)}{{\varepsilon_c}^2}\frac{\kappa}{d_{vg}^2 \exp\left(4\ln^2\sigma_g\right)}\frac{m_c}{\rho_p} \tag{2-16}$$

where $\varphi(\varepsilon_c)$ is the structure correction factor, κ the dynamic shape factor of particles, d_{vg} the geometric mean size of volume equivalent diameter, σ_g the geometric standard deviation of particle size distribution, m_c the dust mass per unit area, ρ_p the density of the particles.

Although this model provided an effective method to link the resistance of a dust cake to the drag force of the particles inside the cake, the shielding effect of neighboring particles in direct contact with one another was not quantitatively expressed and hence an empirical correction was still required. Therefore, it became difficult to directly evaluate the surface filtration resistance using this model.

Kim et al. [2009] experimentally investigated the deposition of soot nanoparticles on glass fiber media at a filtration velocity of 10 cm/s. The Endo model was applied using the size of primary particles and it was found that the predicted results were consistent with the experimental resistance results. However, it should be pointed out that the

Endo model was established for dust cake resistance during surface filtration and may not be applicable to dynamic resistance of glass fiber media where depth filtration took place. Liu et al. [2013] attempted to evaluate the resistance of membrane filters loading with diesel particulate matters and the study results showed that the available resistance expressions differed greatly from one another.

Thomas et al. [2014] proposed a hypothesis that a dust cake consisted of “particle fibers”, so that Davies empirical resistance model for clean fibrous media may be used to obtain a resistance model for nanostructured dust cakes, as follows,

$$\Delta P_c = \frac{64{\alpha_c}^{0.5}(1+56{\alpha_c}^3)}{C_c{d_p}^2\rho_p}\frac{(1-C_o)}{\left[\frac{2}{3}-{C_o}^2(1-\frac{C_o}{3})\right]}\mu_a m_c V \qquad (2\text{-}17)$$

where α_c is the packing density of the dust cake and equal to $1-\varepsilon_c$, d_{pm} the mass mean diameter of particles in the dust cake and C_o the overlap coefficient.

It should be noted that Davies empirical resistance model was applied to clean filters, inside which fibers were perpendicular to air flow direction. Actually, the captured particles in a dust cake were more likely to form "dust fibers" that were nearly parallel, rather than perpendicular, to air flow direction due to the collecting mechanism of "dust filter". Thus, the resistance of the fibers parallel to air flow direction was

obviously different from that of the fibers perpendicular to air flow direction, leading to errors when using the model.

Bourrous et al. [2016] established a simplified model based on Thomas dust cake resistance model to predict the resistance increase of ultrafine particle filters. Ribeyre et al. [2017] studied the resistance of three dust cakes formed by different non-hygroscopic ultrafine aerosols and established a semi-empirical model to evaluate the duat cake resistance based on Thomas model. The established model took into account the changes in dust cake porosities and thicknesses and was found having a maximum deviation of 10% compared to the experimental results.

There have also been various studies on the dust cake resistance by the researchers from the Chinese Mainland. Tan et al. [1990] and Rong et al. [1992] assumed that the dust cake structure remained unchanged, and based on the Kozeny- Carman Equation, the filtration efficiency and resistance formulas for dust cakes were derived. Xiang et al. [2002a, 2002b] and Liu et al. [2002] proposed a simplified resistance formula for both fibrous media and dust cakes during dynamic filtration by combining both micro and macro analysis methods. Fu et al. [2003, 2004, 2006, 2008, 2009] carried out a number of investigations on the dynamic filtration of fibrous media in recent years. They studied the changes in resistance and filtration efficiency of fibrous media during dust loading by theoretical analysis, experiments and simulations. They also

introduced the concept of "fractal" to describe the structure of dust cakes by referring to Xu's study on dust cakes [Xu et al. 1993], which provided a new idea for the study of dynamic filtration performance of fibrous filter media.

2.3.3 Loaded media porosity

Among various parameters in resistance models, porosity was of particular concern because it reflected the structural characteristics of a loaded fibrous medium/dust cake and thus affected the resistance of a loaded fibrous medium/dust cake. A smaller porosity implied a greater air flow velocity inside the medium at the same inlet velocity and resulted in an intenser gas-solid two-phase flow friction and a higher air flow resistance. The porosity of a loaded medium/dust cake may be evaluated by:

$$\varepsilon = 1 - \alpha = 1 - \frac{m}{\rho A Z} \tag{2-18}$$

where m is the mass, A the windward area, Z the thickness of the loaded medium/dust cake and ρ the true density of medium fibers/particles.

It was easy to calculate the porosities for clean fibrous media and loaded media after their masses and thicknesses were measured. But for a dust cake, its porosity was relatively hard to obtain because the thickness of a dust cake made of

submicron/nanoparticles was less than 100 μm and the dust cake had a non-negligible surface roughness due to the rough surface of medium underneath.

Aguiar and Coury [1996] developed a calculation formula for dust cake resistance based on the Ergun resistance model [Ergun and Orning 1949, Ergun 1952] for a particle fluidized bed, and adopted the resin embedding method proposed by Schmidt and Löffler [1990, 1991] to solidify dust cakes, and evaluated the porosity through microscopic images of a solidified cake. Cheng and Tsai [1998] proposed a method of measuring the dust cake thickness with a laser distance sensor to enable the calculation of dust cake porosity. Ito and Aguiar [2009] studied the porosity of dust cakes formed by different dust sources through optical microscope imaging and found that with an increase in filtration velocity, the porosity of dust cakes was decreased. Although various methods have been applied to dust cake porosity measurements, the measuring accuracy was still limited by the number of measuring points.

2.4 The influencing factors for dynamic resistance of fibrous media

The dynamic resistance of a fibrous medium was affected by several factors during the process of filtering particles, including the characteristics of a filter medium (fiber diameters, medium structure, fiber static electricity, porosity, thickness and filtration efficiency), parameters of air flow (velocity, relative humidity, temperature),

characteristics of filtered aerosols (concentration, particle size distribution, particle shape, physical and chemical properties), etc. Some of these factors were already used in dynamic resistance models, such as porosity, thickness and filtration efficiency of a fibrous medium, particle size distribution of the aerosol. Some of these factors would also interact with one another. For example, the influence of air flow relative humidity on the dynamic resistance of a fibrous medium mainly depended on the hygroscopicity of experimental aerosols. There were also certain factors that may change the dynamic resistance of a fibrous medium by affecting its filtration efficiency, such as fiber diameters and medium structure. The studies on the factors influencing the dynamic resistance of fibrous media have been reviewed from the aspects of fiber diameter, medium structure, fiber static electricity, filtration velocity, air flow relative humidity, air flow temperature, aerosol concentration and aerosol type, as follows.

2.4.1 Fiber diameters

According to Davies model for the resistance of clean fibrous filter media, the fiber diameter directly affected the initial resistance of a clean medium. However, its influences on the medium dynamic resistance may be mainly achieved by affecting medium filtration efficiency.

The filtration efficiency of a fibrous medium was increased as fiber diameter was decreased according to the single fiber efficiency calculation formula, because a thinner fiber had a stronger interception and diffusion during filtration. Hinds [1999] measured the filtration efficiency of three media with the same resistance but of different fiber diameters under the same filtration velocity. The filter media packing density was 0.05, and the fiber diameters 0.5 μm, 2 μm, and 10 μm, respectively. The measured results showed that the medium with the thinnest fiber had the highest filtration efficiency.

Yun et al. [2007] measured the filtration efficiency of polyacrylonitrile nanofiber media prepared by the electrospinning method for monodisperse NaCl particles in the particle size range of 10~80 nm and at a filtration velocity of 0.053 m/s. The study results showed that for a given particle size, the filtration quality factor and single fiber efficiency of a nanofiber medium depended on the packing density and fiber diameter. More recently, Hung and Leung [2011] conducted a study on the filtration efficiency of nanofiber media with three fiber diameters of 94 nm, 185 nm and 220 nm, respectively. It was shown that due to the more significant diffusion and interception effects, finer fiber media had a higher filtration efficiency for particles with diameter between 50 and 200 nm, but their resistance was correspondingly higher.

2.4.2 Medium structure

The influences of medium structure on the dynamic filtration performances of fibrous media mainly focused on the filtration efficiency, and study results showed that the medium structure had a significant impact on the filtration efficiency of fibrous media [Kirsch and Stechkina 1973, Kirsch et al. 1974].

A fibrous medium had a complex structure and its three-dimensional model was therefore difficult to be built [Brown 1993]. Hence, most researchers tended to simplify a fibrous medium into a uniform fiber array. The studies on the inhomogeneity of medium structure can be divided into two categories: one for the uneven arrangement of fibers in a fibrous medium [Heidenreich et al. 1991, Adam et al. 1992, Molter and Fissan 1997, Dhaniyala and Liu 2001], and the other for where the diameter of fibers was widely distributed in a fibrous media [Bao et al. 1998, Sakano et al. 2000, Podgorski et al. 2006].

There were also studies where three-dimensional models for fibrous media were established to simulate the deposition of particles under different fiber arrangements and their influences on the dynamic resistance of the media. Wang et al. [2013] used a probabilistic model for the lattice Boltzmann-cellular automata of particle flow to simulate the filtration process of multi-layer fibers and to study the effects of different

fiber arrangements, such as parallel arrangement, staggered arrangement and separation ratio, on filtration efficiency and resistance. Qian et al. [2013] studied the influence of medium structure and particle characteristics on particle deposition and agglomeration characteristics in a filtration process, where 6 different fiber structures were used.

Steffens and Coury [2007] proposed an assumption where a fibrous medium was regarded as a superposition of layered media. Each layer was composed of fibers with a narrow diameter distribution and its parameters may be evaluated according to the thickness, fiber diameter and packing density of the layer medium. Then a theoretical model for the performances of a fibrous medium under different fiber diameter distributions can be obtained. However, this assumption cannot be used to study the effects of particles deposition on medium filtration efficiency and resistance. Therefore, it was only suitable for studying the performance of clean fibrous media, but not for studying the dynamic resistance.

2.4.3 Fiber static electricity

The static electricity carried by fibers can help greatly improve the filtration efficiency of a fibrous medium. The electrostatic effect was usually used to improve the filtration efficiency of particles having the size from 0.15 μm to 0.5 μm, which were difficult to

be captured using other effects. The filtration efficiency in the presence of static electricity was affected by the chemical composition of particles and fibers, the charge on the particles, the charge density on the surface of fibers, and the strength of the electric field around fibers [Mostofi et al. 2010].

However, the static electricity on the fibers would not remain unchanged during dust loading, and would gradually weaken or even disappear as the particles were deposited on the fibers. For the macroscopical performance of the electrostatic fibrous media, their overall filtration efficiency was firstly reduced due to the gradual weakening of static electricity, but then the overall filtration efficiency gradually became higher as the rate of increase in the mechanical filtration efficiency caused by particle deposition was greater than the rate of decrease in the electrostatic filtration efficiency [Walsh and Stenhouse 1997].

2.4.4 Filtration velocity

The effect of filtration velocity on dynamic resistance of fibrous media would include those on both the media filtration efficiency and the formation and structure of the trapped particles.

Filtration velocity significantly impacted on the overall filtration efficiency of fibrous media [Kousaka et al. 1990, Alonso et al. 1997, Mostofi et al. 2010]. At low filtration velocities, due to the relatively long residence time of particles in the filter media, fibers mainly relied on the diffusion and electrostatic effects to capture particles. As the filtration velocity was increased, the inertia of particles was also increased, making particles more difficult to be captured. Therefore, an increase in the filtration velocity would result in a significant drop in the filtration efficiency of the fibrous media. Boskovic et al. [2007, 2008] studied the filtration efficiency of a filter for particles of different shapes, in the size range of 50~300 nm and at the filtration velocities from 5 cm/s to 20 cm/s. The study results showed that at a lower filter velocity, the filtration efficiency for particles of all shapes was higher.

Silva et al. [1999] experimentally studied the influence of filtration velocity on the formation of dust cakes during dust loading. The experimental results showed that the porosity of a dust cake was decreased with an increase in filtration velocity, and the resistance of the dust cake was increased with an increase in the filtration velocity.

2.4.5 Air flow relative humidity

The air flow relative humidity was one of the main factors affecting the filtration efficiency and resistance of fibrous filter media [Mostofi et al. 2010, Mahdavi et al.

2015]. Chen et al. [2015] experimentally studied the influence of the air flow relative humidity on the resistance of the glass fiber HEPA media and PTFE HEPA media, and the study results demonstrated that the relative humidity had no effect on the initial resistance of the glass fiber and PTFE media. Dust loading experiments under different air flow relative humidity were conducted by Joubert et al. [2011], and the results suggested that an increase in air flow relative humidity in the range of 20 to 60% would cause a decrease in dust cake resistance. Generally, a high relative humidity would help reduce the resistance of the fibrous media loaded with hygroscopic particles, but had no effect on those loaded with non-hygroscopic particles [Gupta et al. 1993, Miguel 2003, Joubert et al. 2010].

The air flow relative humidity mainly affected the dynamic resistance through its interaction with hygroscopic particles. The hygroscopicity of nanoparticles was affected by their particle size, which occurred when air flow relative humidity was below the deliquescent point of nanoparticles [Biskos et al. 2006]. When the air flow relative humidity was increased but still below 70%, the size of nanoparticles was larger compared to that under drier conditions. The particle size ratio was defined as a growth factor. The study by Hu et al. [2010] showed that when air flow relative humidity was at 0 to 70%, the growth factor of particles in the size range of 20 to 200 nm was between 0 and 10%. NaCl particles were also experimentally proved to have reversible absorption of liquid water on their surface when air flow relative humidity

was below the deliquescent point, which might affect the shape and structure of the particles [Wise et al. 2008].

2.4.6 Air flow temperature

In aerosol filtration related studies, the influence of air flow temperature on the filtration performance of fibrous media has not been investigated in detail. When air flow temperature was lower than a specific value that can affect the fiber shape of a fibrous media, the influences of air flow temperature on the dynamic resistance was mainly the change in the Brownian motion of the particles and that in air density and viscosity. De Freitas et al. [2006] studied the filtration performance of a double-layer ceramic filter at high air flow temperatures. The study results demonstrated that a higher air temperature led to a lower filtration efficiency, due possibly to that an increase in air flow temperature may increase the number of particles rebounded from the filter.

2.4.7 Aerosol concentration

Wang et al. [2016] investigated the effect of aerosol concentration on the dynamic resistance of fibrous media using Arizona road dust. It was shown that aerosol

concentration had a significant influence on the resistance curve of tested fibrous media. However, the studies by Thomas et al. [2001] and Zhang et al. [2018] indicated that the change in aerosol concentration within a certain range had no effect on the dynamic resistance of fibrous media.

2.4.8 Type of aerosol

Generally, aerosols were different in the following three aspects: physical and chemical properties, size distribution and shape. The influences of physical and chemical properties on the dynamic resistance are discussed earlier in this Chapter in Sub-section 2.4.5. The size distribution of aerosols was an important parameter in resistance models, and is also covered earlier in Sub-sections 2.3.1 and 2.3.2. On the other hand, the effect of particle shape on the filtration efficiency of filter media was studied by Boskovic et al. [2005, 2007]. Spherical polystyrene latex (PSL) particles, spherical iron oxide particles and cubic magnesium oxide particles were used to test the filtration efficiency of polypropylene fibrous media. The results showed that in the particle size range of 50~300 nm, at the same size, the filtration efficiency for cubic particles was significantly lower than that for spherical particles, but the differences in filtration efficiency were gradually decreased as the particle size was increased.

The explanation given by Boscovic was that particles of different shapes move in different ways on the fiber surface. Spherical particles were sided or rolled before being stationary, while cubic particles were sided or turned over. Turning over can significantly change the contact area between the particle and the fiber surface, thereby increasing the separation possibility between particles and fiber. The influence of aerosol particle shape on the dynamic resistance may be generally taken into consideration by adding a shape factor in the models like Equation (2-16).

2.5 Simulation studies on the dynamic resistance of fibrous media

With the rapid development of computer technology, numerical methods have been widely applied to studying the filtration performance of fibrous media and filters. These numerical studies covered the collision between fibers and particles, the filtration efficiency and resistance of clean media and filters, and the dynamic filtration performance of loaded media and filters. However, in this Chapter, only the existing simulation studies on the dynamic resistance are reviewed from the following three aspects: particle depositing on fibers, particle deposition in filters and particle deposition on the fibrous medium surface and the formation of dust cakes.

2.5.1 Particle deposition on fibers

The simulation studies of particle deposition on fibers covered the deposition of particles on a single fiber and that on multiple fibers with different structures. Zhu et al. [2013] used the Monte Carlo stochastic method to simulate the growth process of "dust fiber" on a single fiber, and the collision/rebound model developed by Dahneke [1971, 1972, 1973] was used to analyze the collision, adhesion and rebound of particles on fibers and deposited particles.

Wang et al. [2013] applied the probabilistic model of the lattice Boltzmann-cellular automata of particle flow to simulating the filtration process of multi-layer fibers and the effects of different fiber arrangements, such as parallel arrangement, staggered arrangement, separation ratio, on filtration efficiency and resistance. Qian et al. [2010b] used a Computational Fluid Dynamics (CFD) software to numerically study the gas-solid two-phase flow inside a fibrous medium to investigate the influence of the fiber structure on its filtration performance. The numerical results showed that the horizontal distance, vertical distance and the filtration velocity had an important influence on the filtration efficiency and resistance of the fibrous medium. Qian et al. [2013] also numerically studied the influence of medium structure and particle characteristics on particle deposition and agglomeration characteristics in a filtration process.

Three-dimensional models for fibrous media were established to study the deposition of particles. For example, Maze et al. [2007] built up the three-dimensional structure of a nanofiber fibrous media with fiber diameters of less than 200 nm, and loaded with nanoparticles. The structures of nanoparticles deposition under high and low temperature conditions were simulated.

By developing custom C++ subroutines running in the Fluent environment, which incorporated both particle collection caused by interception and Brownian diffusion, and the slipping effects on the surface of nanofibers into CFD calculations, Hosseini and Tafreshi [2010] constructed the three-dimensional geometry of the internal microstructure of electrospun fiber media to simulate their resistance and filtration efficiency when capturing particles having diameters from 25 nm to 1000 nm. Saleh et al. [2013] also used this custom C++ subroutine to further simulate the instantaneous resistance of a fiber medium when particles were captured. With the rapid development of computer technology, three-dimensional micro-scale simulation has been expected to become the preferred method of filter design in the future.

In studies conducted by Zhu et al., [2013], Wang et al. [2013] and Qian et al. [2010a, 2010b, 2013], only the filtration interactions of inertia, interception and collision were considered, but that between the electrostatic force and the fiber structure on the

filtration performance of fibrous media was not covered. By modeling the three-dimensional structure and electrostatic charge of some fibrous media, their resistance, filtration efficiency and dust loading capacity were numerically studied by Rief et al. [2006]. The particle size, the microstructure of the media, the electrical field and the shape of the fiber were considered in the numerical study and the results indicated that the filtration performances of a fibrous medium, in particular the performances related to electrostatic force, were highly related to the medium structure.

Different from the above mentioned simulation methods, Zhong and Pan [2016] used statistical methods to incorporate the Monte Carlo simulation in the Ising model to study the particulate matter filtration process.

2.5.2 Particle deposition inside filters

Most of the existing studies on the simulation of the performances of filters focused on flat pleated filters, which had regular structures and were easy to be built into a three-dimensional model. Rebai et al. [2010a, 2010b] proposed a mathematical model for the dust loading of dense pleated filters used for gas filtration. Two main clogging scenarios were identified and analyzed based on numerical prediction, and the predicted changes in overall resistance caused by clogging compared with experimental data.

On the basis of the CFD simulation method incorporating the C++ subroutine, Fotovati et al. [2012] developed a macro model for a dense pleated filter to simulate its instantaneous filtration efficiency and resistance. The study results showed that increasing the number of pleats can reduce the resistance and enhance the filtration efficiency. Fotovati et al. [2011] also proposed a modeling method to study the influence of dust load on the resistance of a dense pleated filter. Feng et al. [2016] established two models based on the Lagrangian method and Euler method to simulate the unsteady filtration process in a dense pleated filter.

In order to investigate the filtration process consisting of both depth filtration and surface filtration, Llive et al. [2018] established a mixture model where one-dimensional depth filtration was modeled, and studied the filtration efficiency variation law of flat and densely pleat fibrous filters under constant air flow rate.

2.5.3 Particle deposition on the fibrous medium surface

In addition to the simulation studies on the interaction between particles and fibers or filters, there have been other studies on the simulation for the particle deposition on the fibrous medium surface and the formation of dust cakes during surface filtration. Zhu [2009] conducted an investigation on the deposition process of particles on the

surface of a single fiber, at three-dimensional conditions. The results showed when the diffusion of particles was stronger than the convection, the dust cakes formed by deposited particles would be looser. Lindquist et al. [2014] studied the formation of dust cakes based on the dynamic simulation method by Langevin [Ermak and Buckholz 1980] for monodisperse particles deposited on a flat substrate.

The above mentioned two studies on the formation of dust cakes were only for monodisperse particles. When simulating the formation of a dust cake composed of polydisperse particles, since the size of particles may distribute over a large range, the choice of numerical resolution was more difficult. Becker et al. [2016] developed a method that enabled the filtration simulation for the dust cake made of polydisperse particles at any grid resolution. They simulated the formation of dust cakes on the fibrous medium surface and established a percolation model using the Stokes-Brinkman Equation, and the local packing density and flow resistance of each porous grid unit were used as the input to the Equation.

2.6 Conclusions

The following conclusions are made based on the literature review of the dynamic resistance of fibrous filter media presented in this Chapter.

Firstly, although there existed extensive studies on various factors influencing the dynamic resistance of fibrous filter media, the influences of the working environment of filters on dust loading in certain applications, such as general ventilation and clean air-conditioning, were yet to be studied. In these applications, with regards to filtration velocity, although the air velocities upstream of a filter were relatively high at 0.5~2.5 m/s, a pleated folding design for the fibrous media in the filter would reduce the filtration velocity to only 2~10 cm /s. However, studies mainly looked into high filtration velocities. Besides, the influences of humidity change and aerosol concentration on the dynamic resistance have not been fully covered in the applications of general ventilation and clean air-conditioning.

Secondly, depth filtration and surface filtration have not been correctly distinguished and the related theoretical models often misused in many existing studies. For example, glass fiber or synthetic fiber HEPA media were widely used in studying surface filtration resistance, but in fact, captured particles would firstly penetrate the surface and enter the filter media, so that depth filtration rather than surface filtration in these media took place. Therefore, the existing surface filtration resistance models cannot be directly applied to these media.

Thirdly, the existing dynamic resistance models were established based on a number of assumptions and, therefore, prediction errors may occur when they were directly

applied to actual operating conditions. For example, the theoretical resistance models for depth filtration cannot reflect the changes in filtration efficiency and resistance at different thicknesses of a fibrous medium. In addition, for surface filtration, the Stokes law was used in Endo model to calculate the drag force of particles in a dust cake. However, the shielding effect among neighboring particles was neglected.

Lastly, although various numerical methods like Monte Carlo, lattice Boltzmann and CFD have been widely applied to studying particle deposition in fibrous filters and media, in these methods, ideal situations were assumed and specific applications defined. Besides, existing theoretical models for particle filtration were largely used in related numerical studies, and new filtration theories cannot therefore be developed.

The literature review on the dynamic resistance of fibrous media presented in this Chapter has identified a number of research gaps, as the four points summarized above. These gaps are therefore the targets of the research work reported in this Thesis.

Chapter 3

Proposition

3.1 Background

Clean air can be used to help protect people's health and maintain a suitable environment for industrial production. The most effective way to separate particles from air and generate clean air is to use fibrous filter media. However, during the service life of fibrous media, the deposition of particles would lead to an increase in the dynamic resistance of media and the energy consumption of a ventilation system. Therefore, carrying out a study on the dynamic resistance of filter media can help understand their dust loading process and optimize their structures to lower the energy consumption during their service life.

Although various studies have been conducted on the dynamic resistance of fibrous media, there still existed research gaps as identified in Chapter 2. In fact, existing studies in the open literature mostly focused on investigating dynamic resistance performances of fibrous media used for specific applications but not on optimizing structure and improving dust loading performance for fibrous media. Therefore,

research work on understanding dynamic filtration resistance and improving the dust loading performances for fibrous filter media applied to general ventilation and clean air-conditioning has been carried out and is presented in this Thesis.

3.2 Project title

The research work reported in this Thesis focused on studying the dynamic resistance of fibrous filter media during depth filtration and surface filtration for general ventilation and clean air-conditioning applications. The research work is therefore entitled “Dynamic filtration resistance of fibrous filter media used for general ventilation and clean air-conditioning”.

3.3 Aims and objectives

The aims and objectives of the research work are as follows:

- To establish an experimental setup suitable for testing the filtration efficiency and resistance of fibrous filter media and for conducting the dust loading experiments;
- To experimentally investigate the effects of filtration velocity, air flow humidity and aerosol concentration on the dynamic resistance of filter media during dust

loading, and to develop an experimental scheme for subsequent theoretical modeling studies;

- To theoretically model and experimentally study the mass concentration distribution of deposited particles and the dynamic resistance for filter media during depth filtration;
- To build the surface filtration resistance models based on the investigation into the shielding effect between neighboring particles in a dust cake, and validate and verify the models through dust loading experiments using monodisperse and polydisperse aerosols;
- To develop an experimental evaluation method for dust loading performances for HEPA filter media and invent composite PTFE media based on the modeling study on depth filtration and surface filtration.

3.4 Research methodologies

Both theoretical modeling and experimental study will be adopted in the research work reported in this Thesis. Numerical approaches will also be used when analytical results cannot be obtained from using the established theoretical models.

For the theoretical modeling of depth filtration resistance, a mass concentration distribution model for the deposited particles will be built by dividing a filter medium

into unit layers and applying the definition of single-fiber efficiency to calculate the mass of particles captured by each layer, where the classical depth filtration resistance calculation formula will be applied to evaluate the depth filtration resistance. Surface filtration resistance models for both monodisperse aerosols and polydisperse aerosols will be respectively developed by calculating the shielding effect of neighboring particles based on the kinetic theory.

Based on established theoretical models, numerical approaches will be introduced to simulate the mass concentration distribution for deposited particles during depth filtration and to evaluate the effect of particle size distributions on the surface filtration resistance.

For experimental study, a filter media performance experimental setup containing an aerosol generation section, a media test section and an air flow rate control section will be established. The effects of filtration velocity, air flow humidity and aerosol concentration on the dynamic resistance of filter media will be experimentally investigated.

Dust loading experiments for filter media with different filtration efficiency levels will be carried out using either monodisperse or polydisperse SiO_2 aerosols, when the filtration efficiency and resistance of filter media will be measured and recorded. The

experimental results will be used to validate and verify the theoretical models established in the research work reported in this Thesis.

Chapter 4

The experimental setup

4.1 Introduction

An experimental setup with reliable performance and stable operation for the carrying out performance tests for fibrous filter media is needed for the research work reported in this Thesis. This Chapter provides an overview on the construction and performance verification of the experimental setup, and the dedicated experimental devices and methods applicable to each part of the research work are detailed in relevant Chapters.

4.2 Descriptions to the experimental setup

The experimental setup built for the research work reported in this Thesis can be used to evaluate the filtration efficiency and resistance of a filter medium, and to carry out dust loading experiments. The setup was established based on the European Standard EN 1822-3: 2009 High efficiency air filters (EPA, HEPA and ULPA) - Part 3: Testing flat sheet filter media; the International Standard ISO 29463-3: 2011 High-efficiency

filters and filter media for removing particles in air — Part 1: Classification, performance testing and marking; and the Chinese Standard GB 2626: 2006 Respiratory protective equipment - non-powered air-purifying particle respirator.

Fig 4.1 shows the photo of the experimental setup for filter media performance test, and Fig 4.2 the schematic diagram of the setup. As seen in Fig 4.2, the setup was composed of three sections: an aerosol generation section, a filter media test section and an air flow rate control section.

Fig 4.1 Photo of the experimental setup

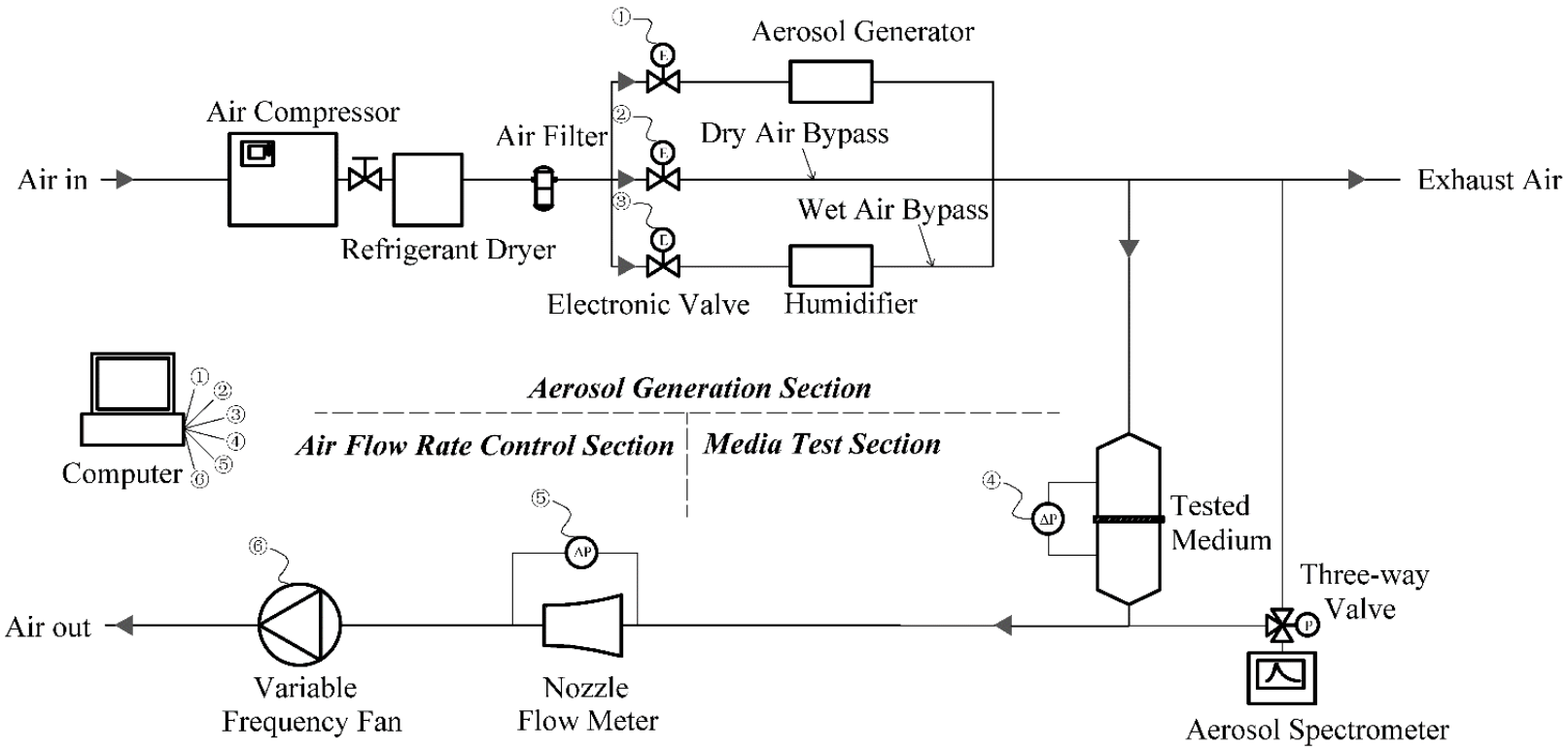

Fig 4.2 Schematic diagram of the experimental setup

Firstly, in the aerosol generation section, compressed dry air was supplied to an aerosol generator with a target aerosol solution, and then mixed with dry air and wet air to generate experimental aerosol at a controlled humidity. Secondly, in the filter media test section, a pressure difference meter was equipped to monitor the changes in air flow resistance for filter media, and an aerosol particle size spectrometer to measure aerosol concentration and particle size distribution both upstream and downstream of the filter media. Lastly, in the air flow rate control section, a nozzle air flow meter was used to monitor the changes in air flow rate real-time, and a computer to adjust the operating frequency of a variable speed fan to maintain the experimental air flow rate at its preset value. The specifications of this setup are given in Table 4.1.

Table 4.1 Specifications of the experimental setup

Items	Specifications
Standards	GB 2626: 2006，EN 1822-3: 2009，ISO 29463-3: 2011
Air flow rate	20~100 L/min
Efficiency range	10%~99.999%
Resistance range	0~2000 Pa
Aerosol type	NaCl/KCl，DiEthylHexylSebacate (DEHS)

Fig 4.3 shows a user interface of the computer used in the experimental setup. Through this interface, users were able to adjust the pressure of air supplied to aerosol generator,

the dry air pressure and experimental air flow rate, to control the opening and closing of media holders, and to monitor the air flow rate and the resistance of tested media.

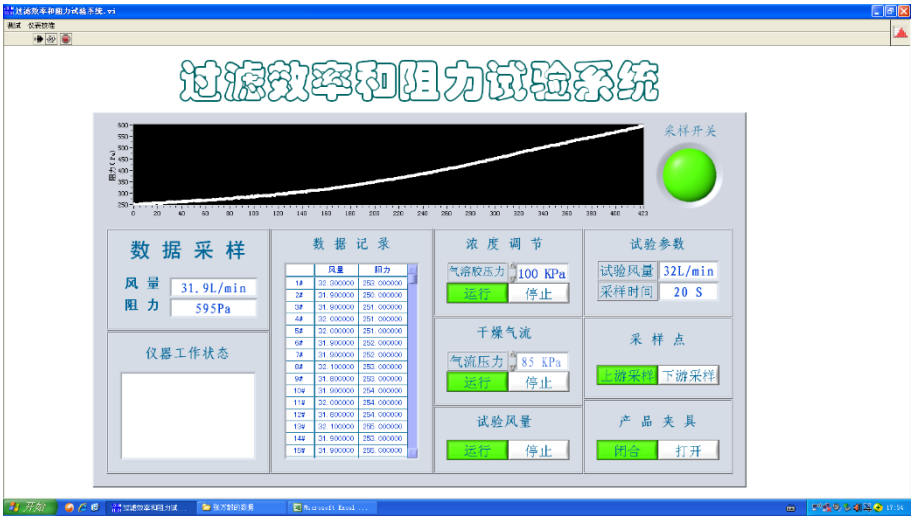

Fig 4.3 User interface of the experimental setup

The structure of medium holders used to hold the tested fibrous filter media is illustrated in Fig 4.4. The upper holder could be moved vertically while the lower holder was stationary. The opening and closing of the holders were controlled by a piston driven by compressed air. During experiments, a tested medium was clamped between the upper and lower holders. The effective filtration area of the filter medium in the holders was 100 cm^2, and two silicone gaskets were used to seal the holder.

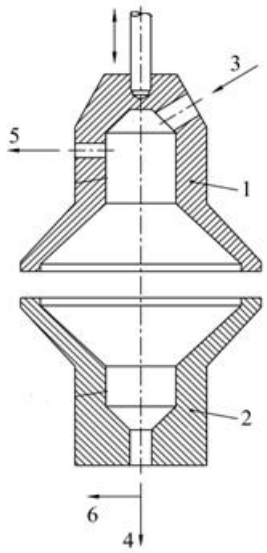

1. Upper holder
2. Lower holder (stationary)
3. Air flow inlet
4. Air flow outlet
5. Upstream static pressure sampling point
6. Downstream static pressure sampling point

Fig 4.4 Structure of the medium holders

The details of the experimental setup are introduced in Sections 4.3 - 4.6, from the following four aspects, respectively: experimental air flow, experimental aerosols, experimental filter media and the performance verification.

4.3 Experimental air flow

As mentioned in Section 4.2, compressed dry air was supplied to an aerosol generator bypass, a dry air bypass and a wet air bypass. To generate experimental air flow at a controlled humidity and temperature, the generation of compressed air and the control of its flow rate, air humidity and temperature were required.

Ambient air was compressed by an air compressor as shown in Fig 4.2, stored in a compressed air tank, and dried and filtered before being put into use. A screw air compressor, which was a positive displacement gas compression device, was used to generate compressed air. The compressed air tank with a pressure range of 0.50~0.75 MPa was used to store the generated compressed air.

The setup used a nozzle flowmeter, a vortex pump and a frequency converter to measure and negatively-feedback control the air flow rate passing through tested filter media. Based on the mechanism of air throttling, the nozzle flowmeter was able to measure the air flow rate quickly through the real-time static pressure difference obtained by pressure difference sensors upstream and downstream of the nozzle. The measurement range of the nozzle flowmeter was 20~100 L/min, and the measurement accuracy 0.1 L/min. A high-precision differential pressure sensor with a measuring range from -1000 Pa to 1000 Pa, and a measuring accuracy of ±1.5%, was selected to measure the nozzle static pressure difference.

When expanding into experimental air flow, compressed air would absorb heat, causing air flow temperature to decrease. The temperature of the experimental air flow can be adjusted by an air conditioner in the laboratory where the setup was located, because the air flow can fully exchange heat with the ambient when flowing through

air pipe before reaching the medium holders. On the other hand, the outlet air temperature of the air conditioner was set at 23 °C.

Since the relative humidity of dry compressed air was as low as 10%, but the required relative humidity of experimental air flow should be generally higher than 10%, the control of air flow humidity required to humidify the air to the target relative humidity. Considering that the experimental setup already had a compressed air source, it was more convenient to use the air-water mixing method for the required humidification. In a humidifier of the experimental setup shown in Fig 4.2, compressed air was sprayed into distilled water through a Laskin nozzle to produce fine water droplets of 5~8 μm diameter and compressed air was in full contact with water droplets to achieve the required humidification. A humidification efficiency of over 80% and the relative humidity control accuracy of 3% were achieved.

4.4 Experimental aerosols

4.4.1 Types of Aerosol

It can be seen from the literature review on the dynamic resistance of fibrous filter media in Chapter 2 that the types of aerosols used for dust loading in various studies

were different. Some of these studies determined the experimental aerosols based on the types of particles captured in the specific applications of the filter media, and other studies used common types of aerosols that may be easily generated.

According to the filter test standards and practice, common aerosol types included KCl solid aerosol, DEHS liquid aerosol, A1-A4 solid Arizona road dust, ASHRAE A1 dust, PSL monodisperse solid aerosol, etc. Among them, KCl solid aerosol and DEHS liquid aerosol were often used for filtration efficiency test of filters/filter media, A1-A4 road dust and ASHRAE A1 dust for dust loading experiments of general ventilation filters, and PSL monodisperse solid aerosol for the calibration of aerosol spectrometers.

The fibrous filter media studied in the research work were used in general ventilation and clean air-conditioning systems for capturing particles of small size and with complex solid components. Therefore, DEHS liquid aerosol and A1 -A4 road dust of large particle size and ASHRAE A1 artificial dust that contained cotton batting were excluded. Furthermore, the particle size distribution and concentration of solid polydisperse KCl aerosol can be adjusted through the generation situations, and monodisperse PSL aerosol can be conveniently used for validating and verifying the dynamic resistance models for fitter media. Therefore, these two aerosols were used in the research work.

The high price of monodisperse PSL aerosols would lead to higher dust-loading experiment costs, so monodisperse SiO_2 aerosols with lower cost but similar properties were used as experimental aerosols. Also, monodisperse SiO_2 aerosols with different average particle sizes can be combined to form polydisperse SiO_2 aerosols with a controllable particle size distribution, which was also helpful to study the influence of aerosol polydispersity on the growth of medium dynamic resistance.

4.4.2 Generation methods of aerosol

The polydisperse KCl aerosol generator used a gas-liquid two-phase flow nozzle, which was more stable than the Laskin nozzle commonly used for aerosol generation. The concentration and particle size distribution of the aerosol generated through the two-phase flow nozzle during long-term operation were stable. The siphon effect occurred when compressed air passed through the gas-liquid two-phase flow nozzle, then KCl solution was sucked into compressed air and decomposed into droplets. The KCl droplets that entered the pipeline were dried by the compressed air in the dry air bypass and dehydrated to form KCl solid particles. Changing the pressure of compressed air or the concentration of the KCl solution can adjust the concentration and particle size distribution of the KCl aerosol generated.

Different from the KCl being dissolved in a solution, SiO_2 existed as solid particles suspended in a suspension. Consequently, precipitating and blocking may be easily caused if the polydisperse KCl aerosol generator was used to generate SiO_2 aerosol through SiO_2 suspension. In addition, the cost was very high to produce the amount of SiO_2 suspension required when using KCl aerosol generator. Therefore, a SiO_2 aerosol generator, which had a small suspension capacity and was not easy to be blocked, was needed.

The SiO_2 aerosol generator used in the research work was a medical atomizer. The atomizer can be used to periodically input compressed air into the nozzle of a atomization cup at a certain frequency and to spray SiO_2 suspension in the atomization cup to become droplets. The atomizer can be directly applied to the aerosol generator bypass shown in Fig 4.2, and the droplets containing SiO_2 particles can be dried by the dry air bypass. The concentration and particle size distribution of SiO_2 aerosol were determined by the amount and size distribution of SiO_2 powder used in the suspension. The capacity of the atomizer cup of this atomizer was 8 mL, and SiO_2 suspension needed to be added periodically during dust loading.

4.4.3 Measurements of aerosol concentrations and size distributions

Aerosol particle counters mainly included condensation particle counters (CPC) and optical particle counters (OPC). Condensation particle counters can only be used to measure the total number of aerosol particles but not the particle size distribution. However, the optical particle counters can be used to not only detect the total number of aerosol particles but also obtain the particle size distribution by measuring the number of particles in each particle size range. Therefore, they were more suitable for both monodisperse and polydisperse aerosols. Optical particle counters also had the advantages of non-interference with particle size distribution, wider range, shorter photoelectric conversion response time, higher resolution, and easier maintenance. Therefore, an optical particle counter was selected as the measuring device for aerosol concentration and particle size distribution in the experimental setup. The optical particle counter used in the research work was Palas Promo 2000 aerosol particle size spectrometer and its technical specifications are shown in Table 4.2.

Table 4.2 Specifications of Palas Promo 2000 aerosol particle size spectrometer

Items	Specifications
Measuring principle	Optical light-scattering
Ranges of size	0.2~10 μm, 0.3~17 μm, 0.6~40 μm, 2~100 μm
Size channels	Up to 128
Limit of concentration	$< 1\times10^{6}$ P/cm^{3}
Sampling rate	5 L/min

4.4.4 Concentrations and size distributions of aerosols generated

In order to understand the generation characteristics of the polydisperse KCl aerosol generator, KCl aerosol concentration and MMD emitted by 2% mass concentration KCl solution under different pressures of the generation air and the dry air are shown in Fig 4.5 and Fig 4.6, respectively. From these two figures, it can be seen that an increase in the generation air pressure and/or a decrease in the dry air pressure can lead to an increase in the KCl aerosol concentration, while a decrease in the generation air pressure and/or dry air pressure would result in an increase in the MMD of the generated KCl aerosol. For SiO_2 aerosols, their particle size distributions were determined by the solid SiO_2 powder used for suspension preparation.

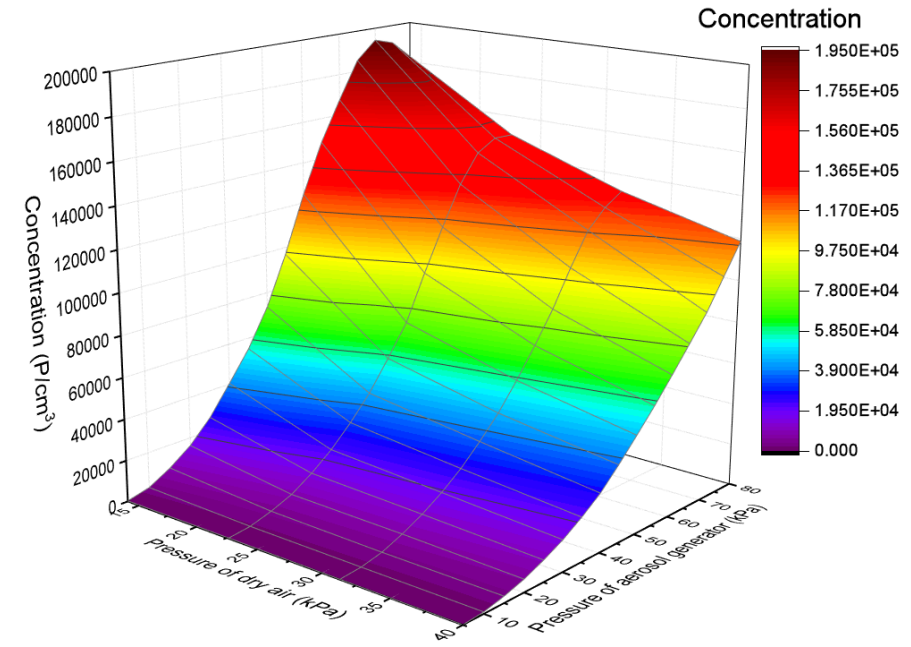

Fig 4.5 KCl aerosol concentrations under different generation pressures

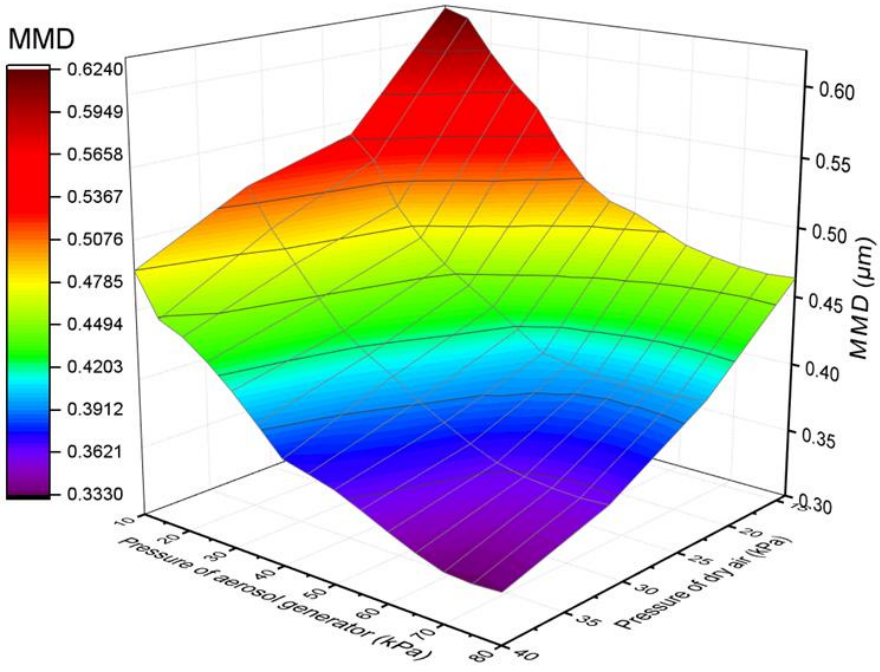

Fig 4.6 MMDs of KCl aerosols under different generation pressures

4.5 Experimental filter media

As mentioned in Chapter 3, the dynamic resistance of the fibrous filter media during dust loading would be targeted. According to the different pattern of particle deposition, depth filtration and surface filtration may be experienced for a filter medium. In order to study the dynamic resistance during the two filtration processes, medium-efficiency glass fiber filter media, glass fiber HEPA media and PTFE HEPA media were used. Here, the HEPA medium referred to a fibrous filter medium with a filtration efficiency of not less than 99.97% for the most penetrating particle size (MPPS) particles.

According to European Standards EN 779: 2012 Particulate air filters for general ventilation -Determination of the filtration performance and EN 1822-3: 2009, various levels of filters and their corresponding performance requirements are shown in Tables 4.3 - 4.4, respectively.

Table 4.3 Classification of air filters for general ventilation

Group	Class	Final pressure drop (Pa)	Average arrestance (A_m) of synthetic dust (%)	Average efficiency (E_m) to 0.4 μm particles (%)	Minimum efficiency* to 0.4 μm particles (%)
Coarse	G1	250	$50 \leq A_m \leq 65$	-	
	G2	250	$65 \leq A_m \leq 80$	-	
	G3	250	$80 \leq A_m \leq 90$	-	
	G4	250	$90 \leq A_m$	-	
Medium	M5	450	-	$40 \leq E_m \leq 60$	
	M6	450	-	$60 \leq E_m \leq 80$	
Fine	F7	450	-	$80 \leq E_m \leq 90$	35
	F8	450	-	$90 \leq E_m \leq 95$	55
	F9	450	-	$95 \leq E_m$	75

*. Minimum efficiency is the lowest one among the initial efficiency, discharged efficiency and the lowest efficiency throughout the loading procedure of a test.

Table 4.4 Classification of efficient particulate air (EPA) filters, HEPA filters and ultra low penetration air (ULPA) filters

Group	Class	Integral value		Local value	
		Efficiency* (%)	Penetration (%)	Efficiency (%)	Penetration (%)
EPA	E10	≥ 85	≤ 15	-	
	E11	≥ 95	≤ 5	-	
	E12	≥ 99.5	≤ 0.5	-	
HEPA	H13	≥ 99.95	≤ 0.05	≥ 99.75	≤ 0.25
	H14	≥ 99.995	≤ 0.005	≥ 99.975	≤ 0.025
ULPA	U15	≥ 99.9995	≤ 0.0005	≥ 99.9975	≤ 0.0025
	U16	≥ 99.99995	≤ 0.00005	≥ 99.99975	≤ 0.00025
	U17	≥ 99.999995	≤ 0.000005	≥ 99.9999	≤ 0.0001

*. The efficiency and penetration in this table refers to MPPS efficiency and penetration.

In the research work reported in the Thesis, G1~F9 and E10~U17 were used to naming the fibrous media that can be made into filters that have classes of G1~F9 and E10~U17, respectively.

A glass fiber filter medium was manufactured using molten glass, with fiber diameters ranging from several microns to tens of microns. It was generally white in color, and its windward side can be easily distinguished from its leeward side, as the former was generally of a plush texture, but the latter can be relatively smooth, as shown in Fig 4.7.

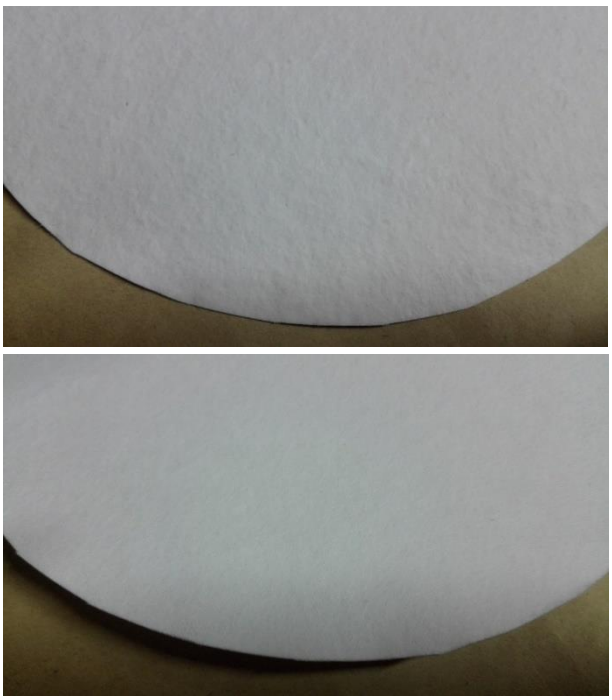

Fig 4.7 Photos of windward side (up) and leeward side (down) of a glass fiber filter medium

The PTFE medium was invented in the 1980s and had stable chemical properties and low resistance. At present, the PTFE filter medium can satisfy the filtration efficiency requirements for HEPA and ULPA media, and thus became a substitute to traditional glass fiber HEPA media. Unlike the glass fiber medium which was only made of glass

fiber, the PTFE medium generally had a three-layer structure, with a PTFE membrane in the middle, and a layer of non-woven fabric on both the windward and leeward sides. The sandwiched PTFE membrane had a three-dimensional network-like porous structure and thus a very high filtration efficiency, and the membrane fibers were very thin, with diameters between 10 nm to 100 nm. Due to the insufficient strength of the PTFE membrane, it cannot be used as a filter media alone. Hence, non-woven fabric substrates of a PTFE medium played a role in protecting and supporting the PTFE membrane. A photo of showing a PTFE HEPA medium is given in Fig 4.8.

Fig 4.8 Surface photo of a PTFE HEPA medium

4.6 Performance verification for the experimental setup

The purpose of carrying out performance verification for the experimental setup was to ensure the validity and accuracy of the setup through certain tests before it was put into actual use. To meet the needs of the research work for dynamic resistance and filtration efficiency monitoring during dust loading of the filter media reported in this Thesis, the performance verification of the experimental setup was carried out from three aspects: resistance measurement accuracy, Zero% efficiency test and 100% efficiency test, and experimental aerosol concentration stability.

4.6.1 Accuracy of resistance measurement

Given the objectives of the current research work on studying the dynamic filtration resistance of fibrous filter media, the accuracy of resistance measurement was of vital importance. Actually, the accuracy of resistance measurement was affected by the following three factors: air flow rate adjustment, resistance measurement method and the precision of the pressure difference meter. These three factors were fully examined during the construction of the experimental setup. Therefore, the resistance measurement accuracy of the experimental setup can be verified by comparing the

measured resistance results using the experimental setup with those from other two reference setups which were calibrated annually using the same testing filter medium.

The same testing filter medium was installed at the experimental setup and the other two reference setups, and the filter medium resistances at different filtration velocities when installed at the three setups were measured and compared. The measured resistance results are shown in Fig 4.9. As seen, the resistance curves obtained from the three setups were very close to one another. Therefore, the resistance measurement accuracy from the experimental setup was verified.

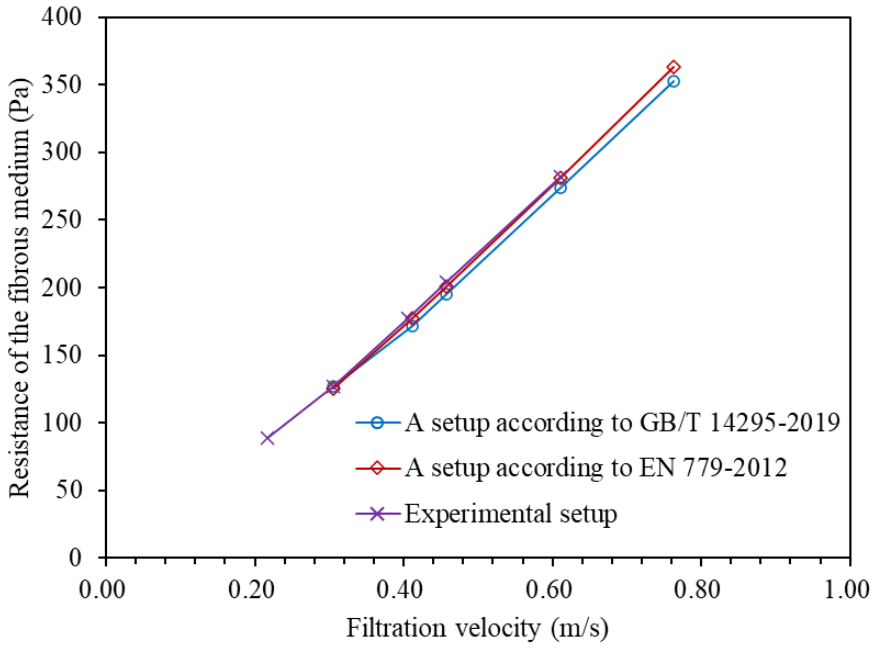

Fig 4.9 Comparison of resistance measurement results using three different setups

4.6.2 Zero% efficiency test and 100% efficiency test

A Zero% efficiency test referred to the generation of experimental aerosols and the filtration efficiency test for a setup without installing tested filters. This test can be used to check the appropriateness of the entire pipeline, the aerosol generation, sampling and measurement devices.

According to European Standard EN 779: 2012, a Zero% efficiency of a qualified setup should meet the following requirements: the filtration efficiency for particles not greater than 1.0 μm of 0±3%, and that for particles larger than 1.0 μm of 0±7%. In order to reduce statistical errors, the total number of each particle sample used for filtration efficiency calculation should be greater than 500. The Zero% efficiency test result for the experimental setup is shown in Fig 4.10, which satisfied the requirements in EN 779: 2012.

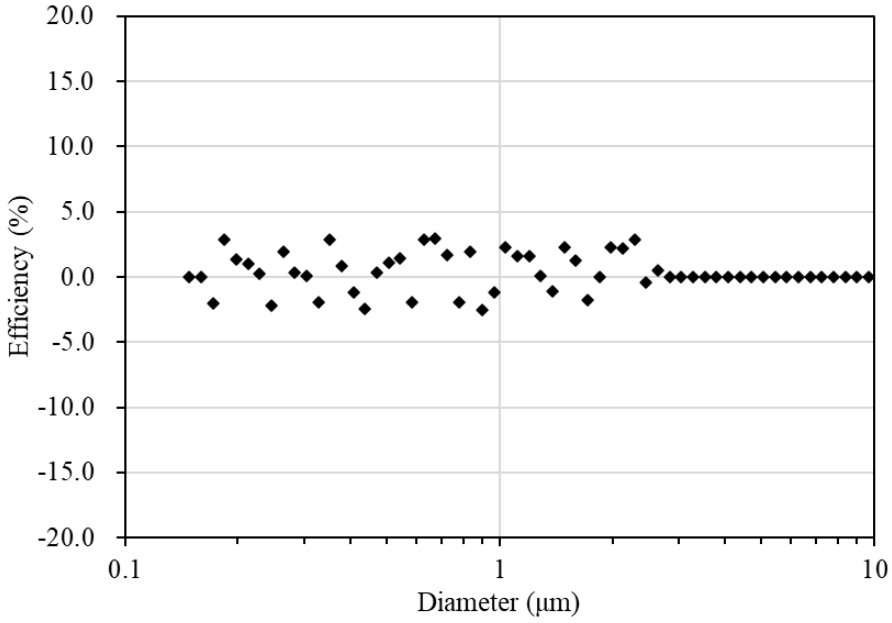

Fig 4.10 Zero% efficiency test results of the experimental setup

A 100% efficiency test referred to when using the experimental setup for HEPA or ULPA filters if was ensured that the pipeline and sampling devices of the setup could meet the requirements of 100% efficiency determination. The filtration efficiency of all particle diameter channels of a qualified setup should be greater than 99%.

The filtration efficiency of each particle size channel for an H14 glass fiber filter medium was measured using the polydisperse KCl aerosol at a filtration velocity of 5.33 cm/s and the measured results are shown in Fig 4.11. It can be seen that the efficiencies of all the particle size channels measured by this experimental setup were greater than 99.9%, which satisfied the requirements of 100% efficiency test.

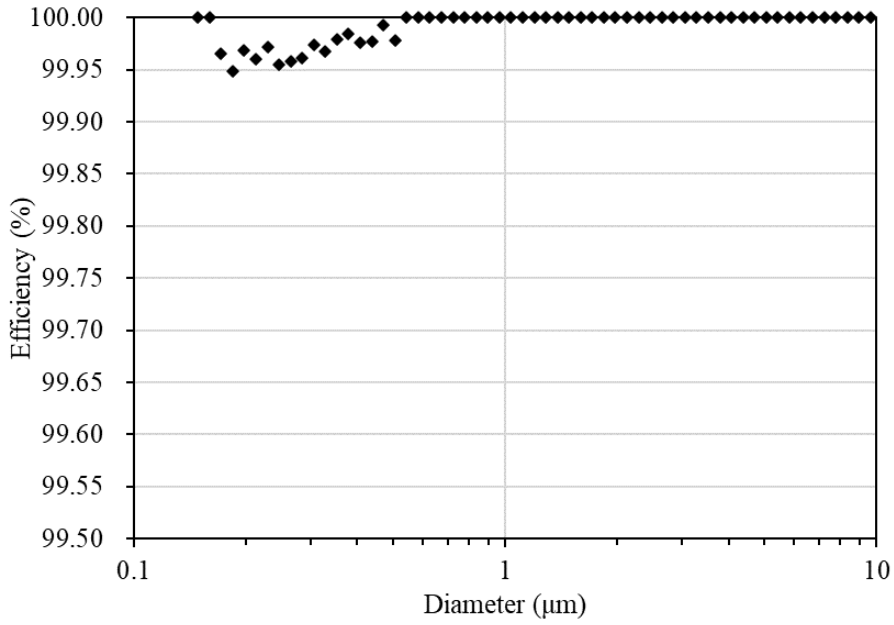

Fig 4.11 100% efficiency test results of the experimental setup

4.6.3 Concentration stability of generated aerosols

In order to avoid the influence of aerosol concentration fluctuations on the dynamic resistance of fibrous media during dust loading, and at the same time to make the loaded dust mass in proportion to dust loading time, aerosol concentration for the experimental setup should be kept stable. Fig 4.12 shows the number concentrations of KCl aerosols generated in the experimental setup at different loading time. It can be seen that the concentration of aerosols remained virtually stable during dust loading.

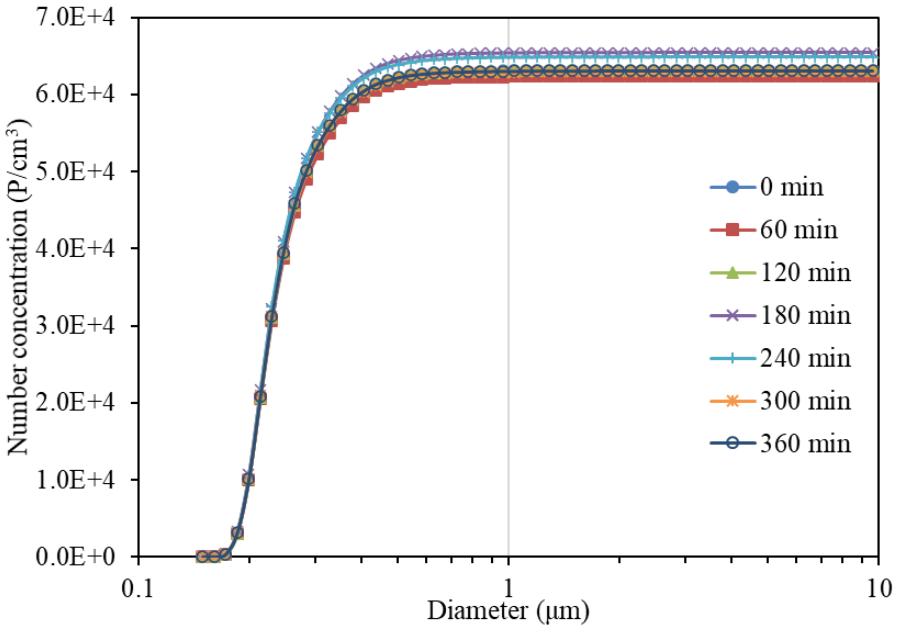

Fig 4.12 Stability test results of aerosol concentration for the experimental setup

4.7 Conclusions

An experimental setup has been established for carrying out the performance test and dust loading experiments of the fibrous filter media. In this Chapter, the construction of the setup, experimental air flow, experimental aerosols and the filter media are detailed. The performance verifications for the experimental setup are also reported, and the verification results demonstrated that the setup can meet the needs of the experimental part of the research work reported in this Thesis.

Chapter 5

Effects of operating factors on dynamic resistance of fibrous media

5.1 Introduction

Fibrous filter media have been widely used in different environments and their actual performances were closely related to the operating condition of different environments. Hence, the effects of certain operating factors such as filtration velocity, air flow humidity and temperature, and aerosol concentration on the dynamic resistance of fibrous media have attracted increased research attention. Therefore, the effects of these operating factors on the dynamic resistance of fibrous media have been experimentally studied and the study results are presented in this Chapter.

Generally, filtration velocity had a significant influence on the filtration efficiency of fibrous media. Different filtration efficiencies of fibrous media due to different filtration velocities would result in different number of particles captured by fibrous media, and thus directly affect the dynamic resistance of fibrous media. However, it should be noted that the filtration velocity was relatively high in previous studies on the influence of filtration velocity on the medium dynamic resistance. For example,

the filtration velocity adopted by Balazy [2005] in studying its influence on the filtration performance of fibrous media for 10~500 nm particles was set at 30 cm/s, which was much higher than that adopted for general ventilation and clean air-conditioning applications. On the other hand, the change in filtration velocity would also affect the deposition of particles on fibers and hence the dynamic resistance of fibrous media, which however received limited attention in existing studies. Therefore, it was necessary to study the effects of filtration velocity on the dynamic resistance of fibrous media in filtration velocity range appropriate to those used in general ventilation and clean air-conditioning systems.

In addition, air flow humidity was one of the key factors affecting the filtration efficiency and resistance of fibrous media. Related studies on the effects of air humidity on the dynamic resistance of fibrous media have been reviewed in Chapter 2. In general ventilation applications, an increase in air humidity was often caused by rainy weather, where air relative humidity can be increased from 50%~60% to 70%~100%. An increase in air flow relative humidity would affect the dynamic resistance of fibrous media in the following two manners: i) the loaded media were treated with air flow of high relative humidity and ii) the media were loaded with particles in a high air relative humidity environment. In the research work reported in this Thesis, both hygroscopic KCl aerosols and non-hygroscopic SiO_2 aerosols would

be used to study the influence of air flow humidity on the dynamic resistance of fibrous media in the two above mentioned manners.

Experimental aerosols were usually used to conduct dust loading experiments for fibrous media to examine their filtration performances and dust holding capacities in actual applications. Relatively high aerosol concentrations were always adopted to reduce the dust loading time duration in these experiments. However, there existed different opinions among the existing relevant studies on the effects of aerosol concentration on the dynamic resistance of fibrous media. For instance, Wang et al. [2016] considered that aerosol concentration had a noticeable influence on the resistance curve of the tested filter media, but Thomas et al. [2001] believed that the changes in aerosol concentration within a certain range had little influence on the growth of dynamic resistance of fibrous media. Therefore, it became necessary to examine the influence of aerosol concentration on the dynamic resistance of fibrous media.

The effects of air flow temperature on the dynamic resistance of fibrous media were both the change in Brownian motion state of particles caused by the intensification of air molecular, and the influences from air density and viscosity. In the applications of general ventilation and clean air-conditioning, the temperature of air flow passing through fibrous media was relatively low and its variation range was narrow. Thus, air

flow temperature had little influence on the dynamic resistance of fibrous media, so that this was not studied in this Chapter.

Therefore, the influences of the following operating factors including filtration velocity, air flow humidity and aerosol concentration on the dynamic resistance of fibrous media were experimentally investigated and the experimental results are reported in this Chapter. The experimental results can provide a guideline when selecting certain parameters for the experimental studies presented in Chapters 6 to 8.

5.2 Filtration velocity

The influence of filtration velocity on the dynamic resistance of fibrous media was reflected by filtration efficiency, because a higher filtration velocity could enhance the inertia of particles, and the deposition of particles on the fibers and media surface.

To examine the influence of filtration velocity on the dynamic resistance of fibrous media applied to general ventilation and clean air-conditioning, the actual filtration velocity of fibrous media in these applications should be firstly defined. Then the influence of filtration velocity on filtration efficiency and deposition of particles could be respectively studied, by theoretical analysis and experimental approaches.

Filtration efficiency and dust loading resistance for fibrous media under different filtration velocities were tested using polydisperse KCl aerosols.

There were three types of filters commonly used in general ventilation and clean air-conditioning, including medium efficiency bag filter, medium efficiency V-bank filter and high efficiency box filter. Their photos, structures and sizes and rated air flow rates are given in Table 5.1. According to the rated air flow rate and filter structure and size, the corresponding filtration velocity ranges for the fibrous media were evaluated and are also given in Table 5.1. As seen, the rated filtration velocity of fibrous media applied to general ventilation and clean air-conditioning ranged from 2 cm/s to 10 cm/s. This velocity range was adopted in the study presented in this Chapter.

Table 5.1 Filtration velocity ranges of fibrous medium used in three different types of filters

			
Type	Medium efficiency bag filter	Medium efficiency V-bank filter	High efficiency box filter
Structure and size	6 bags, 600*600*750 mm^3	600*600*300 mm^3	600*600*250 mm^3
Rated air flow rate	1000~2000 m^3/h	2000~3400 m^3/h	3400 m^3/h
Filtration velocity range	5~10 cm/s	5~8 cm/s	2~5 cm/s

5.2.1 Effects of filtration velocity on filtration efficiency

A fibrous filter medium was featured with not only the MPPS but also the most penetrating filtration velocity, below which its filtration efficiency would decrease with an increase in filtration velocity. A previous study on filtration efficiency for two kinds of fibrous media indicated that the most penetrating filtration velocity for synthetic fiber media and glass fiber media were at 0.7 m/s and 0.9 m/s, respectively [Xu 2014], which were far greater than the rated filtration velocity for fibrous media used for general ventilation and clean air-conditioning. Hence, an increase in the filtration velocity within the range of 2~10 cm/s would lead to a decrease in the filtration efficiency for the fibrous media targeted in the research work reported in this Thesis.

According to Table 4.3 and Table 4.4, a fibrous medium in “F”, “E” or “H” class had a relatively high filtration efficiency which may not easily be affected by the change in filtration velocity. Therefore, an M5 glass fiber medium was selected and its filtration efficiency curves at 3 cm/s, 5.33 cm/s and 10 cm/s tested using polydisperse KCl aerosols. Three obtained efficiency curves are plotted in Fig 5.1. As seen, as filtration velocity was increased from 3 cm/s to 5.33 cm/s and finally to 10 cm/s, the filtration efficiency of the M5 medium basically remained unchanged when particle diameters were less than 1.0 μm, but was decreased otherwise.

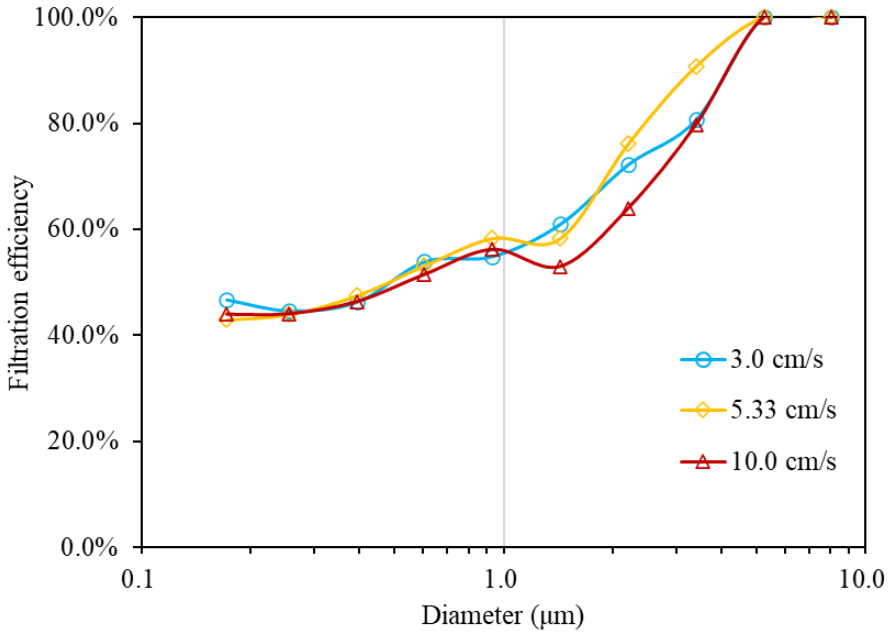

Fig 5.1 Filtration efficiency curves for an M5 medium at three filtration velocities

As the air flow resistance of a loaded fibrous medium came from the collision among air molecules, captured particles and medium fibers, a decrease in filtration efficiency may affect the medium dynamic resistance through changing the number and surface area of captured particles. Fig 5.2 shows both the number distribution and surface area distribution for the experimental aerosol. As seen, almost no particles and only limited particle surface area were distributed in the size range over 1.0 μm. Consequently, it can be concluded that even for an M5 medium, an increase in filtration velocity within 2~10 cm/s had no significant effect on filtration efficiency and thus its dynamic resistance.

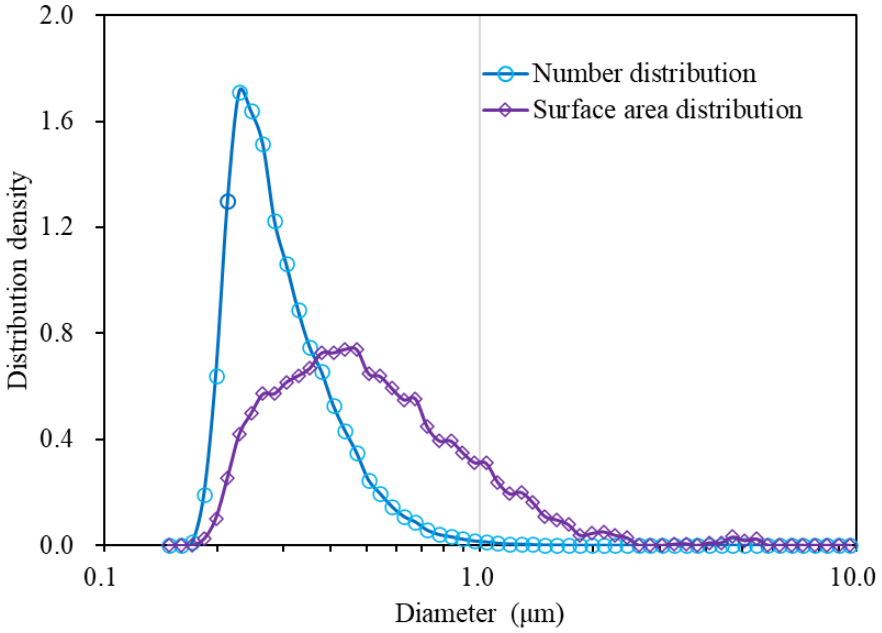

Fig 5.2 The distributions of number and surface area for the experimental aerosol

5.2.2 Effects of filtration velocity on particle deposition

It was a common practice to study the effects of filtration velocity on particle deposition through observing particle deposition structures using an optical microscope or a scanning electron microscope. However, an optical microscope or a scanning electron microscope may actually be inappropriate for the observation, because the two kinds of microscopes can only provide statistical information of particle deposition structure in two-dimension rather than three-dimension. Therefore, in the research work reported in this Thesis, the effects of filtration velocity on particle

deposition were examined through comparing dynamic resistance curves of fibrous media at different filtration velocities.

The effects of filtration velocity on particle deposition may occur during depth filtration, transition stage and surface filtration for a fibrous medium. However, for a fibrous medium with the filtration efficiency class of “G” or “M”, surface filtration was not easy to take place as its filtration efficiency was relatively low. Therefore, F7 and H14 glass fiber media were selected to study the effects of filtration velocity on particle deposition. Polydisperse KCl aerosols were used for dust loading experiments for F7 and H14 glass fiber media at filtration velocities of 3 cm/s, 5.33 cm/s and 10 cm/s, respectively.

Fig 5.3 shows the resistance curves for three F7 media at three filtration velocities during dust loading. For each curve, its y axis was normalized by corresponding filtration velocity, so that the clogging of the three F7 media could be easily compared with one another at three filtration velocities. It can be seen from Fig 5.3 that, three curves were close to one another during dust loading. Although an increase in filtration velocity brought a slight decrease in medium filtration efficiency, the resistance curve comparison shown in Fig 5.3 suggested that a change in filtration velocity had almost no effect on the resistance for F7 medium and consequently the particle deposition.

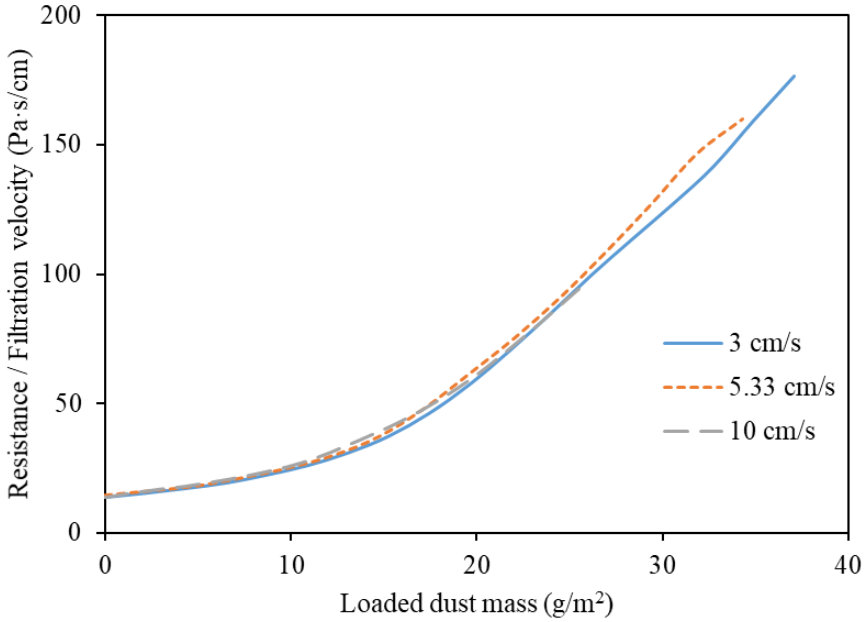

Fig 5.3 Resistances for three F7 media at three filtration velocities during dust loading

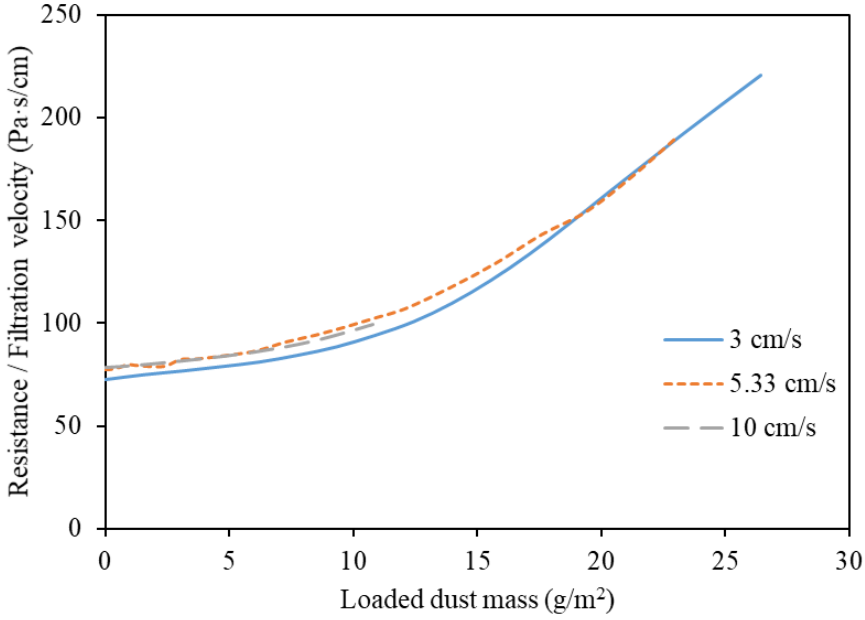

Fig 5.4 Resistances for three H14 media at three filtration velocities during dust loading

Fig 5.4 shows the resistance curves for three H14 media at three filtration velocities during dust loading. As seen, a change in filtration velocity had either no significant effect on the dynamic resistance of H14 media, during depth filtration, transition stage or surface filtration.

For a particle in microscopic movement, a larger movement velocity could enhance its inertia and weaken its diffusion. It was easier for a particle with a higher velocity to deposit at a deeper place, leading to a greater packing density of a dust cake or loaded fibrous medium. However, according to the simulation study by Zhu [2009] on dust cake formation, only when the Peclet numbers, i.e., the filtration velocity under the same characteristic scale of flow field and molecular diffusion coefficient, became over 10 times greater, the effects of particle/filtration velocity change on dust cake structure could be slightly significant. Therefore, in the filtration velocity range of 2~10 cm/s applied to general ventilation and clean air-conditioning, a change in filtration velocity had no considerable effect on particle deposition during dust loading of fibrous media.

In summary, in the filtration velocity range of 2~10 cm/s used in general ventilation and clean air-conditioning, an increase in filtration velocity for a fibrous medium would lead to a decrease in its filtration efficiency for larger particles and may bring a change in particle deposition. However, according to the experimental results and

theoretical analysis presented in this Section, the effects of filtration velocity on medium dynamic resistance were not significant. Then a filtration velocity of 5.33 cm/s can be adopted in the subsequent experiments conducted in the research work reported in this Thesis. This velocity is also commonly used in existing standards and literature.

5.3 The humidity of air flow

Since glass fiber media and PTFE media targeted by the research work reported in this Thesis did not have the ability for moisture absorption, their resistance would hence not change when passing through air flow of high relative humidity. Therefore, the effects of air flow humidity on the dynamic resistance of fibrous media would be mainly demonstrated through influencing aerosols used in dust loading experiments. In this Section, polydisperse KCl aerosol and polydisperse SiO_2 aerosol were selected as the representatives of hygroscopic aerosol and non-hygroscopic aerosol, respectively. They were used to examine the influences of both changes in air flow humidity on the resistances of loaded fibrous media and different air flow humidity on the dust loading performances of clean fibrous media.

5.3.1 Effects of the changes in air flow humidity on the resistance of loaded media

To investigate the effects of changes in air flow humidity on the resistance of loaded fibrous media, parts of the experimental setup as shown in Fig 4.2 including the aerosol generation bypass, dry air bypass and wet air bypass were used to generate the experimental aerosol/air flow at required RH.

Four dust loading experiments were carried out using H14 glass fiber media, among them three H14 media were loaded with polydisperse KCl aerosol and one polydisperse SiO_2 aerosol, respectively. During the four dust loading experiments, the RH of experimental aerosols was kept at about 40% and the filtration velocity at 5.33 cm/s. The final resistance for the three H14 media loaded with KCl aerosol was set at 900 Pa and the one loaded with SiO_2 at 950 Pa, so as to distinguish and compare resistance curves corresponding to different aerosols.

For each H14 medium, when the final resistance arrived, the aerosol generation bypass was shut down while the holders were kept closed. Then the pressures of dry air bypass and wet air bypass were immediately set at pre-designed values to generate experimental air flow with the required RH. Three H14 media loaded with KCl aerosol were treated with experimental air flow at different levels of RH at about 30%, 50% and 80%, respectively, and one loaded with SiO_2 aerosol with that of about 75% RH.

The resistances of H14 media and the RH values of the experimental air flow were recorded during the four experiments.

Fig 5.5 shows the changes in the resistance for four loaded H14 media when passing through air flow at different RH levels. As seen, the resistance of the H14 medium loaded with KCl aerosol remained unchanged when the RH of the passing air flow was at 30.5%, which was lower than that applied to dust loading experiments. However, the resistances of the H14 medium loaded with KCl aerosol were decreased significantly over a short time period when the RH of passing air flow was at a higher RH level between 47.8% and 77.8%. For H14 medium loaded with SiO_2 aerosol, no changes in its resistance may be observed at an air flow RH of 75.2%.

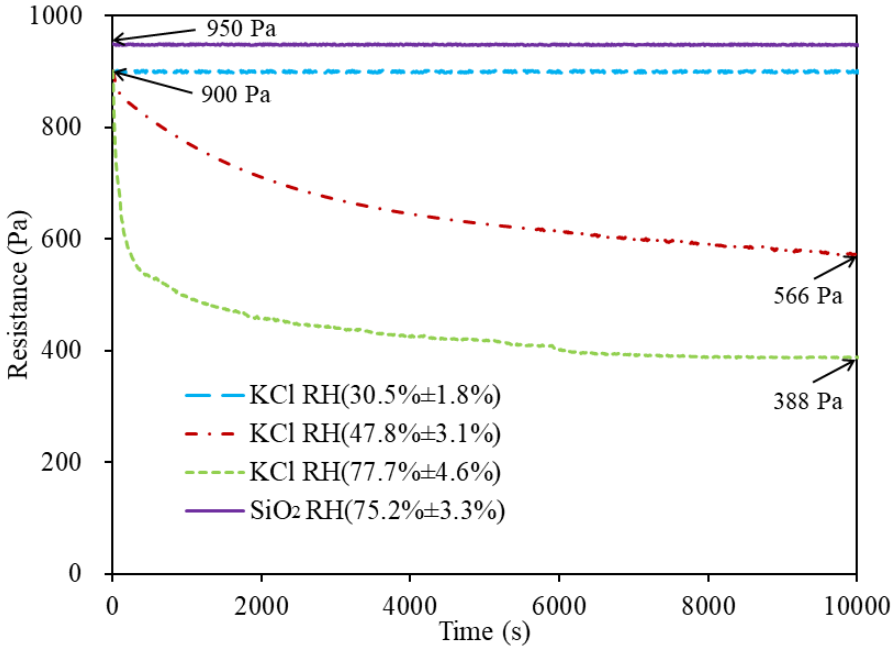

Fig 5.5 Resistances of H14 media loaded with KCl/SiO_2 aerosols at different RH levels of passing air flow

Generally, a constant resistance of loaded fibrous media would suggest a stable particle deposition structure, but a sudden drop in resistance would imply that a particle deposition structure was changed. In order to observe the differences in particle deposition structure before and after introducing the air flow of a higher RH level to the medium loaded with KCl aerosol, SEM photos were taken for both a loaded media treated with higher RH air and the other loaded media not treated with higher RH air, respectively, as shown in Fig 5.6.

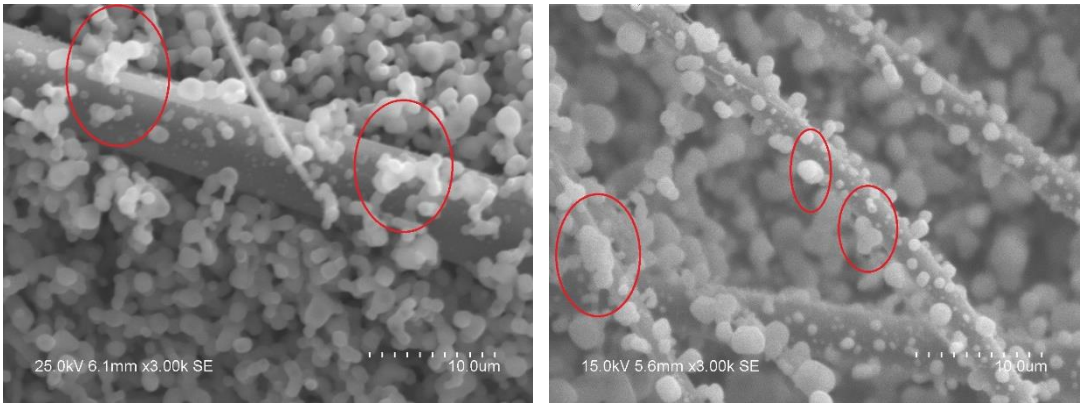

a) Untreated medium b) Treated medium

Fig 5.6 SEM photos for two H14 media loaded with KCl aerosol with one treated, and the other not treated, with high RH air flow

As seen in Fig 5.6, the depositions of KCl particles in the medium not treated with high RH air flow had dendritic structures and the particle size was relatively small. However, KCl particle depositions in the medium treated with high RH air flow had fusion structures rather than dendritic structures. Hence, it can be inferred that for KCl particles which were able to absorb moisture, a high RH air flow disintegrated the dendritic deposition structures and caused small particles to fuse into large particles. Both the collapse of dendritic structures and the formation of large particles led to a decrease in obstruction when air flow passed through at the micro level, which was reflected by a sudden drop in the resistance of the loaded medium at the macro level.

In certain cases, the holders in the experimental setup needed to be opened to finish certain operations for tested fibrous medium for the subsequent dust loading

experiments in Chapters 6 to 8. Due to the effects of changes in air flow RH on the resistance of loaded fibrous media, errors may be brought in to these dust loading experiments because there would be a difference in RH level between the experimental air flow and ambient air. To determine whether opening holders and exposing loaded media to ambient air would affect their resistance, two H14 media loaded with polydisperse KCl aerosol and one with SiO_2 aerosol under an RH level of about 40% were exposed to ambient air or placed in closed holders without air flow passing through. Their resistances and the RH level of ambient air were recorded and are illustrated in Fig 5.7.

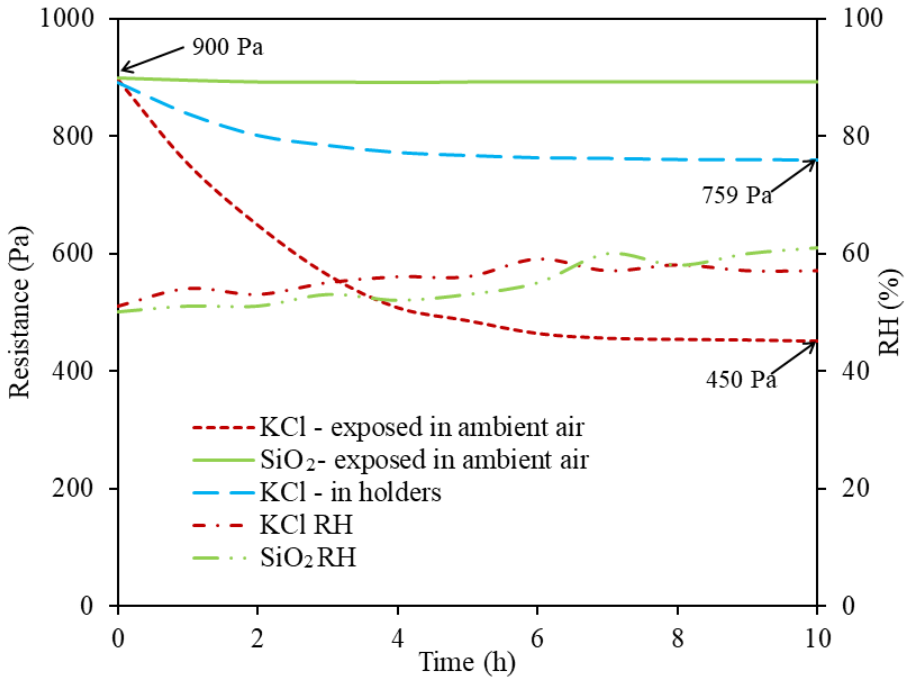

Fig 5.7 Resistances of three H14 media loaded with KCl/SiO_2 aerosols when exposed to ambient air or placed in closed holders

In Fig 5.7, although the RH of ambient air was all greater than 40%, the resistance of the medium loaded with SiO_2 and exposed to ambient air basically remained unchanged. This was similar to what happened when it was treated with high RH air flow.

However, the resistance of the two media loaded with KCl aerosol exposed to closed holders and ambient air would gradually be decreased from 900 Pa to 759 Pa and 450 Pa, respectively. This indicated that the resistance of fibrous media loaded with hygroscopic particles would be decreased even when being placed in a high RH environment. Therefore, SiO_2 aerosol should be used instead of KCl aerosol if it was necessary to open the holders during dust loading experiments.

5.3.2 Effects of different levels of air flow humidity on the dynamic resistance of clean media

H14 glass fiber media were also used in dust loading experiments conducted in the study presented in this Sub-section. For comparing the dynamic resistances of clean fibrous media under different air flow RH, polydisperse SiO_2 aerosol and polydisperse KCl aerosol were respectively used in these experiments.

Fig 5.8 illustrates the resistances of two H14 media during dust loading under two RH levels of 26.5% and 76.4%, respectively, using polydisperse SiO_2 aerosol. As seen, the differences in RH levels had almost no effect on the dynamic resistance of H14 media when loaded with SiO_2 aerosol.

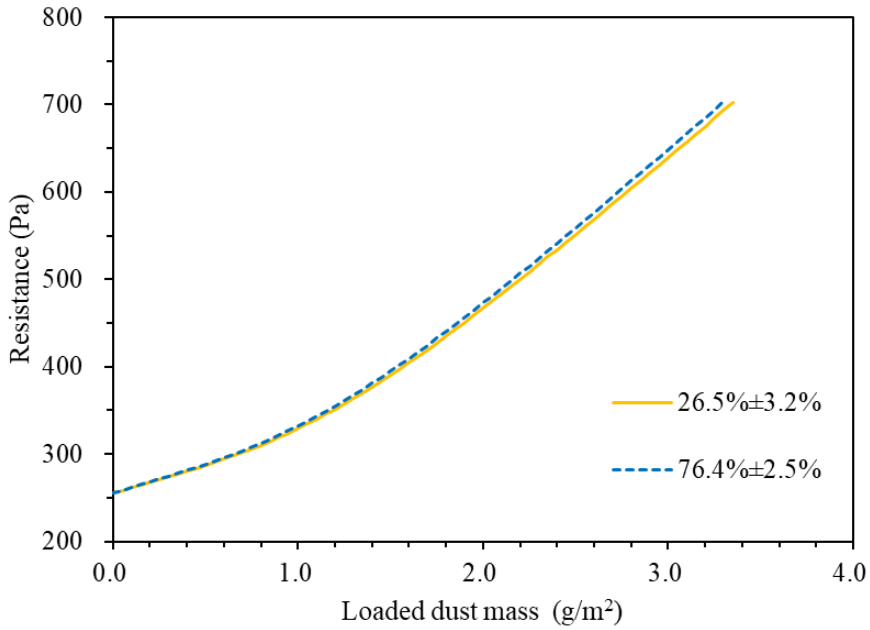

Fig 5.8 Resistance curves for two H14 glass fiber media loading with SiO_2 aerosol under different RH levels

Fig 5.9 shows the resistances for three H14 media during dust loading under the RH levels of 27.1%, 55.7% and 76.2%, respectively, using polydisperse KCl aerosol. It can be seen from Fig 5.9 that, a higher air flow RH caused a smaller increase in medium resistance at the same loaded dust mass. However, under air flow RH of 76.2%, when loaded dust mass exceeded 7 g/m^2, the rate of increase in medium resistance became more noticeable.

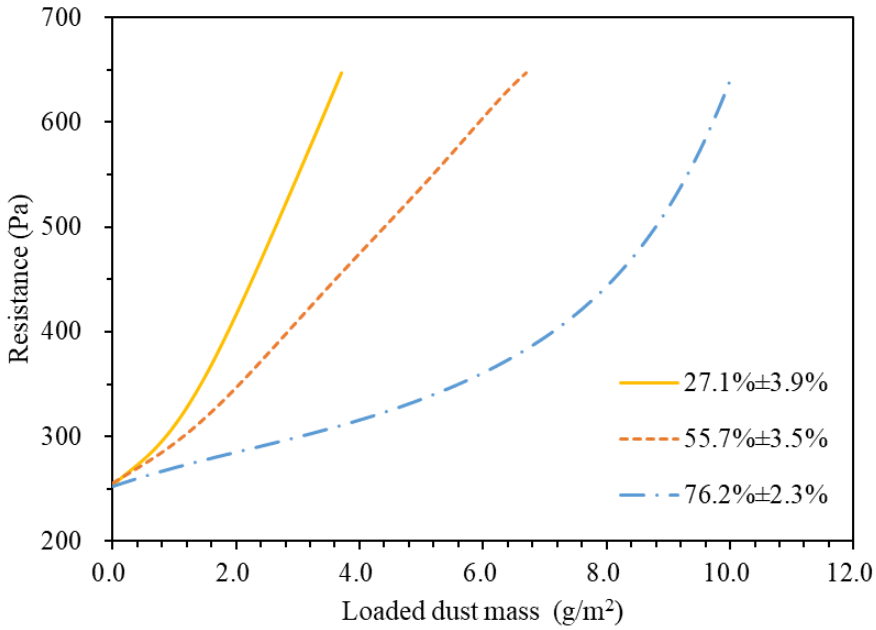

Fig 5.9 Resistances of three H14 glass fiber media loading with KCl aerosol under different air flow RH level

It was necessary to compare the growth rates for three resistance curves in Fig 5.9. In Novick's semi-empirical model for HEPA fibrous media resistance, i.e., Equation (2-11), K_2 was defined as a resistance coefficient to represent the relationship between medium resistance increase and loaded dust mass [Novick et al. 1992]. However, the use of K_2 cannot reflect the instantaneous resistance growth rate for a fibrous medium. Actually, the instantaneous growth coefficient of dynamic resistance for fibrous media at a fixed loaded dust mass, k_2, was defined by Zhang et al. [2018] as $\frac{(\Delta P_2 - \Delta P_0)A}{M_2 V}$, as shown in Fig 5.10.

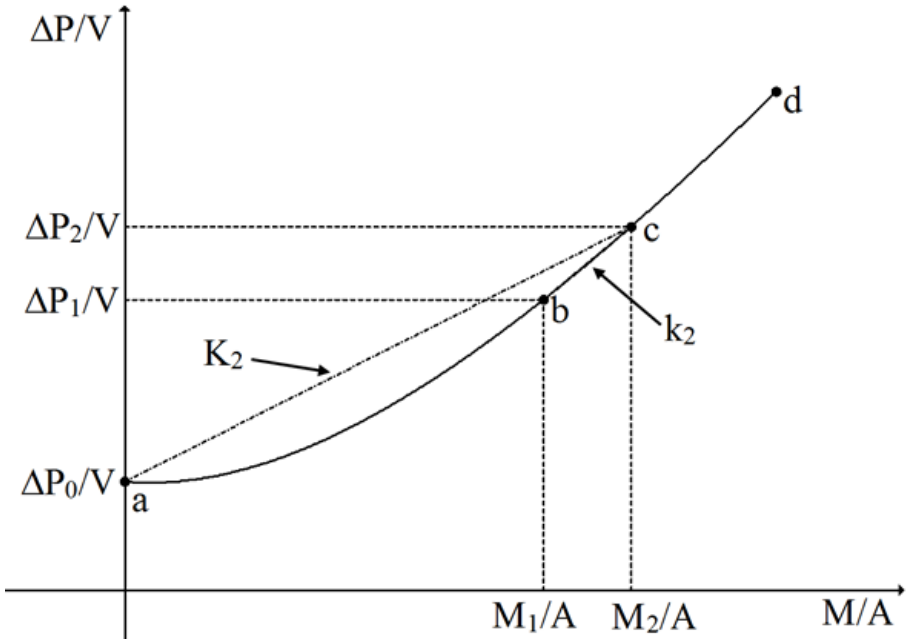

Fig 5.10 Schematic definition of k_2, the instantaneous resistance growth rate for a fibrous medium [Zhang et al. 2018]

In order to compare the influences of air flow RH on the instantaneous growth rate for H14 medium resistance when loaded with KCl aerosol, k_2 values for the three curves shown in Fig 5.9 were calculated and are illustrated in Fig 5.11. It can be seen that, at two relatively low air flow RH levels, i.e., 27.1% and 55.7%, k_2 values for H14 medium loaded with KCl aerosol were firstly increased with an increase in loaded dust mass, then remained relatively stable, but finally dropped slightly. However, at a higher air flow RH at 76.2%, k_2 values were increased steadily at the initial stage and were much lower than those at air flow RH of 27.1%, but was increased sharply when the loaded dust mass exceeded 7 g/m^2. The variation trends in k_2 values for the medium

loaded with KCl aerosol at high RH levels were similar to that of the medium loaded with liquid aerosol.

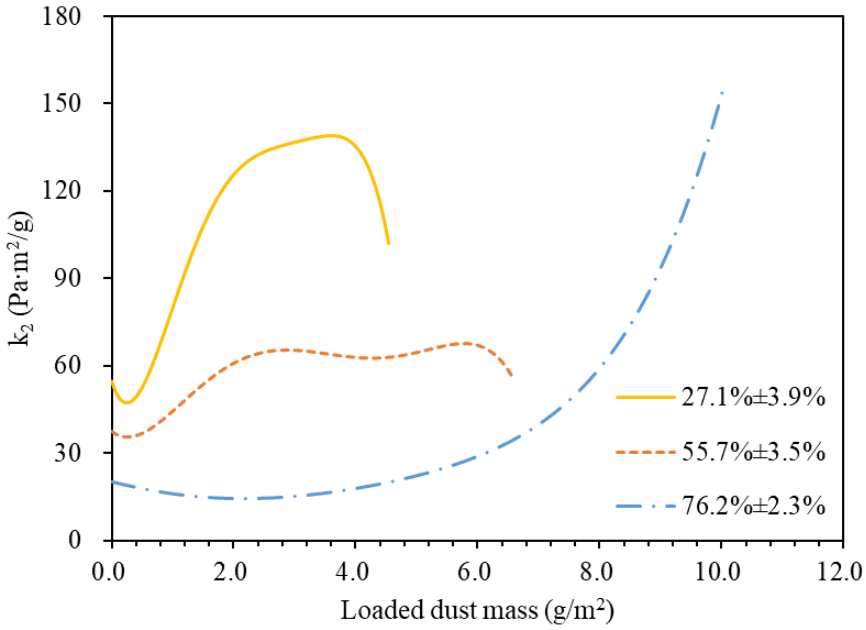

Fig 5.11 k_2 values for three H14 glass fiber media loading with KCl aerosol under different RH levels

When liquid aerosol was loaded into a fibrous medium, deposited liquid particles would firstly wrap fibers to form a liquid film. This type of deposition could only increase the fiber diameter at an initial stage of dust loading, leading to a lower resistance growth rate than the dendric deposition of solid particles. However, in the later stages of dust loading, the connection of the liquid film between fibers would directly block the microporous structure inside a fibrous medium, resulting in a sharp rise in its resistance, as reflected by the curve marked with "76.2%±2.3%" in Fig 5.11.

According to relevant experimental results, KCl crystal would deliquesce at an environmental RH of about 85% at room temperature [Ye and Chen 2013]. The deliquescent RH for KCl crystal was lowered when in particle shape. Accordingly, it may be deduced that the KCl particles generated in the experimental work reported in this Chapter at air flow RH level of 76.2% were in the liquid state before reaching the fibrous medium, resulting in a similar resistance growth trend to that for a medium loaded with liquid aerosols.

In summary, the effects of air flow humidity on both the resistance of loaded media and dynamic resistance of clean media were through the interaction between the water vapor in moist air and hygroscopic aerosol particles. Special attention should hence be paid when using hygroscopic aerosol like KCl to avoid errors due to the changes in air flow RH and the high RH environment in subsequent experiments presented in Chapters 6 to 8.

5.4 Aerosol concentration

In the Standards of performance test for air filters and fibrous media, long-term performances of filters and media, i.e., their resistance and filtration efficiency in their life cycle, were tested under laboratory conditions using experimental aerosols instead

of ambient aerosols. Much higher concentrations for experimental aerosols than those of ambient aerosols were generally applied in standard tests to reduce dust loading time. This is also to be adopted in the research work reported in this Thesis. At present, there seemed no consensus on the effects of aerosol concentration on the dynamic resistance of fibrous media in existing literature. In this Section, hence, such effects were studied experimentally.

Polydisperse KCl aerosol was used as the experimental aerosol. Its concentration was adjusted through changing dry air flow rate, since changing the pressure of compressed air and mass concentration of KCl solution for aerosol generation may influence the aerosol particle size distribution. Four dust loading experiments for H14 glass fiber media were conducted at a filtration velocity of 3.0 cm/s and 5.3 cm/s and using two mass concentration KCl aerosols, respectively. The final resistance was set at 900 Pa. During dust loading, the upstream aerosol mass concentration was basically kept constant and real-time monitored.

Fig 5.12 and Fig 5.13 show the resistance curves for H14 glass fiber media during dust loading using different concentration KCl aerosols at a filtration velocity of 3.0 cm/s and 5.3 cm/s, respectively. In the two figures, at the same filtration velocity, the medium resistances corresponding to the same loaded dust mass using different concentration KCl aerosols was almost the same, suggesting that the aerosol

concentration had no significant effects on the dynamic resistance of fibrous media, within the range of aerosol concentration involved in the experiments presented in this Section.

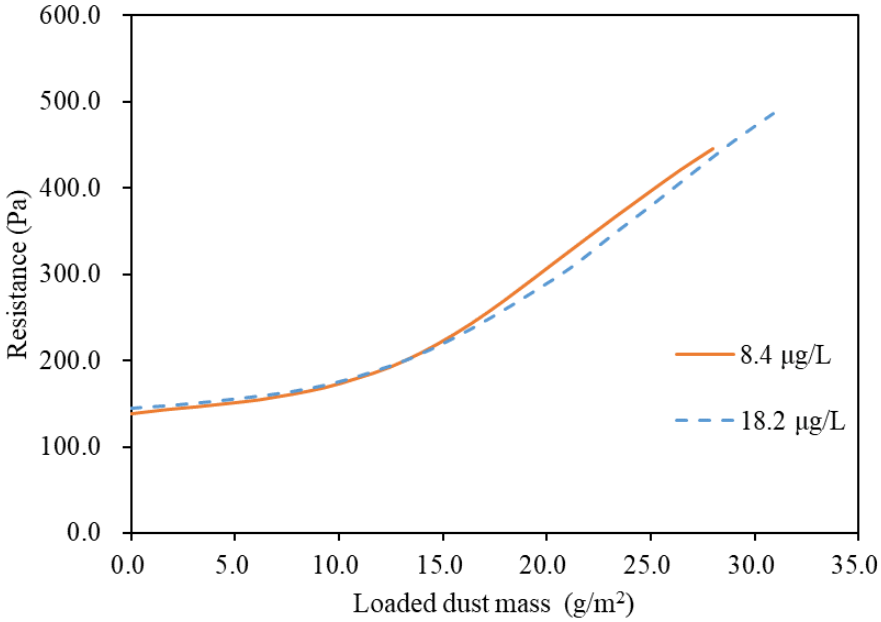

Fig 5.12 Resistance curves for two fibrous media loading with different concentration KCl aerosols at a filtration velocity of 3.0 cm/s

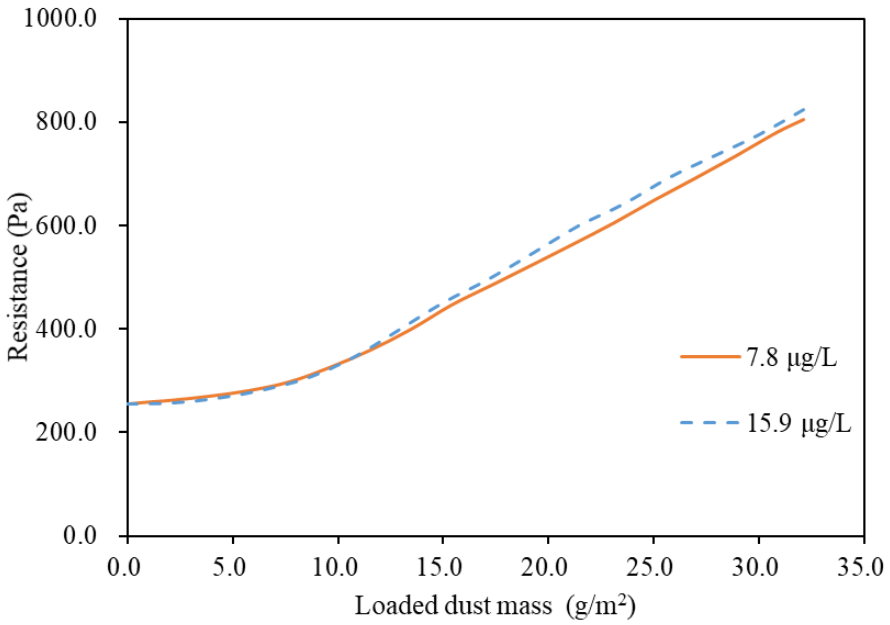

Fig 5.13 Resistance curves for two fibrous media loading with different concentration KCl aerosols at a filtration velocity of 5.33 cm/s

In the limited existing studies on the effects of aerosol concentration on the dynamic resistance of fibrous media, Thomas et al. [2001] and Zhang et al. [2018] considered that changes in aerosol concentration within a certain range had no effect on the growth of dynamic resistance of fibrous media. This was similar to the observations from Fig 5.13 and Fig 5.14. On the other hand, the experimental results of Wang et al. [2016] indicated that the aerosol concentration had a noticeable influence on the resistance curve of the tested filter media as shown in Fig 5.14. However, the results were obtained from the dust loading experiments for glass fiber media using ISO 12103-1 A1 dust.

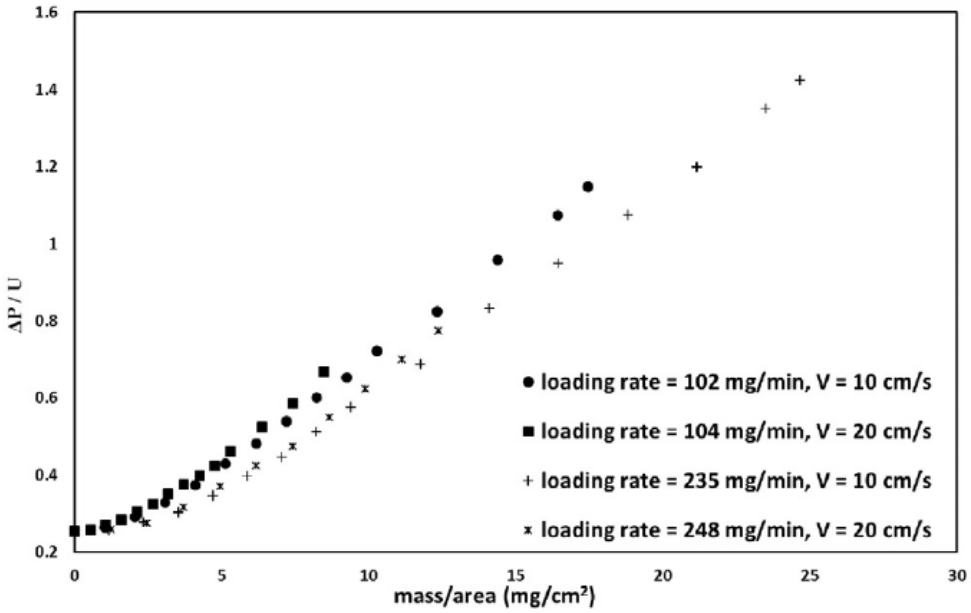

Fig 5.14 The experimental results on effects of the aerosol concentration on glass fiber medium dynamic resistance [Wang et al. 2016]

As seen in Fig 5.14, there were only minor differences among the resistance curves for media during dust loading under different aerosol concentrations. On the other hand, the effects of aerosol concentration on the dynamic resistance were demonstrated to become less significant at the smaller average particle size of the experimental aerosol. However, the aerosols involved in general ventilation applications and hence the experimental aerosols to be used in the research work reported in this Thesis would have much smaller average particle sizes than the ISO A1 dust used. Hence, the fact that aerosol concentration had almost no effect on the dynamic resistance of fibrous media was not in conflict with the conclusions made by Wang et al. [2016] due to the difference in particle size. Therefore, the aerosol

concentration in subsequent experiments reported in Chapters 6 to 8 can be appropriately increased to shorten the duration of a dust loading experiment.

5.5 Conclusions

The influences of filtration velocity, air flow humidity and aerosol concentration on the dynamic resistance of fibrous filter media were studied experimentally and the study results are presented in this Chapter. The experimental results showed that, in the filtration velocity range of 2~10 cm/s which was commonly used for general ventilation, although an increase in filtration velocity resulted in a decrease in the filtration efficiency of a fibrous medium and caused a change in the deposition form of the particles on the surface of medium fibers, its influence on the dynamic resistance of fibrous filter media was overall not significant.

The experimental results also showed that, an increase of over 5% in relative humidity of passing air flow would lead to a significant decrease in resistance over a short time period when the media was loaded with polydisperse KCl aerosols. The resistance growth trend for a medium loaded with KCl aerosols at an air relative humidity close to the deliquescence point of the KCl aerosol was similar to that loaded with a liquid aerosol. But polydisperse SiO_2 aerosols loaded into the media were not sensitive to the changes in air flow relative humidity.

Moreover, it was demonstrated through dust loading experiments under different aerosol concentrations and the comparison with a previous study that, the aerosol concentration had no significant influence on the dynamic resistance of a filter medium at the same filtration velocity.

The above experimental results can therefore be referenced when selecting appropriate operating parameters for the experiments reported in Chapters 6 to 8.

Chapter 6

Depth filtration resistance of fibrous media

6.1 Introduction

As shown in Fig 6.1, if a clean fibrous medium was divided into four layers of the same thickness, each layer would have the same packing density, filtration efficiency and resistance. However, when the medium was used to filtrate particles, a layer close to the windward side of the medium would capture more particles than that close to the leeward side because the concentration of particles was higher, leading to an uneven distribution of deposited particles. As deposited particles were able to enhance the mechanical filtration efficiency of a fibrous medium, uneven distribution of deposited particles would be further enhanced during the filtration process.

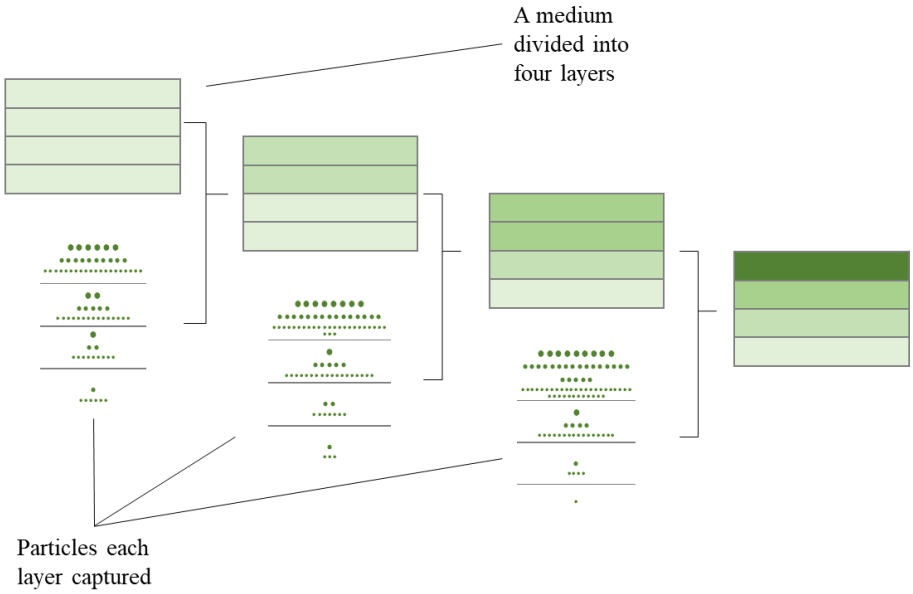

Fig 6.1 Schematic diagram of depth filtration for a fibrous medium

Fig 6.2 shows the photos of both the windward and leeward sides of a loaded V-Bank filter. As seen, the windward side was completely filled with captured dust and its color was black. However, the color of the leeward side was gray, implying a lower loaded dust concentration than that on the windward side. The difference in loaded dust concentration between the two sides of a loaded filter also demonstrated the uneven distribution of deposited particles for a fibrous medium during depth filtration.

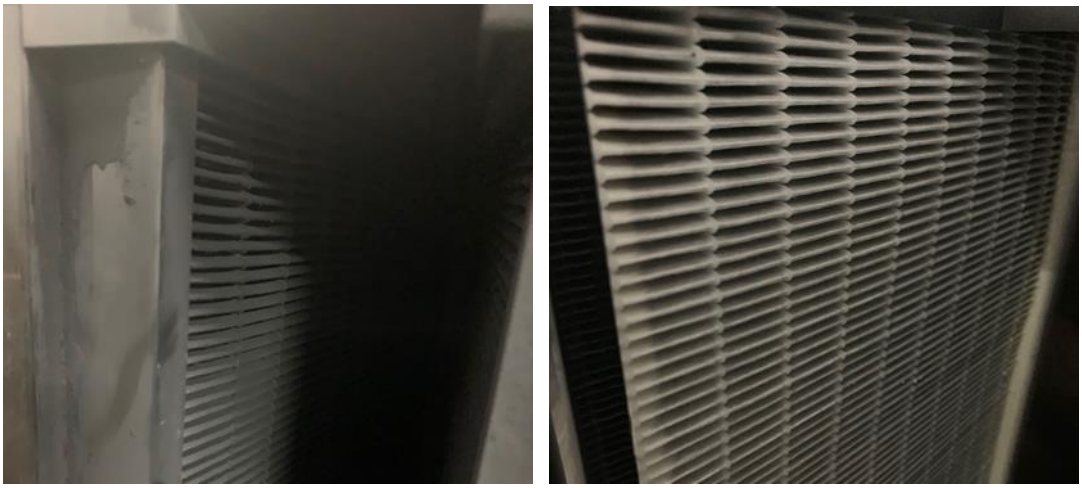

Fig 6.2 Photos of windward (left) and leeward (right) sides of a loaded V-Bank filter

According to the literature review presented in Chapter 2, Bergman et al. [1978] proposed a model to evaluate the depth filtration resistance by regarding deposited particles as “particle fibers” and applying the Davies model to a loaded medium. However, Bergman model did not consider the uneven distribution of deposited particles along the thickness of a medium during depth filtration. The air flow resistance of a deposited particles was influenced by its local porosity and velocity, which were directly determined by the distribution of deposited particles in the medium. Therefore, it became necessary to investigate the distribution of deposited particle in a fibrous medium during depth filtration, and it may also be a better method to evaluate the depth filtration resistance of a fibrous medium by incorporating the distribution of deposited particles into Bergman model.

Although there were previous studies on the distribution of deposited particles inside a fibrous medium [Letourneau et al. 1991, Thomas et al. 2001], no theoretical models have been established. On the other hand, certain experimental results were reported in existing literature for the distribution of deposited particles, but their accuracies may be in doubt due to the potential errors in measuring operations. For example, an adhesive tape was used to distinguish the deposited particle mass in the different thickness range of a loaded medium [Thomas et al. 2001].

Therefore, to study the depth filtration resistance of fibrous filter media, dust loading experiments for five-stacked glass fiber media were conducted firstly to obtain the distribution of deposited particles and the resistance of the five-stacked media. Secondly, the Bergman model was combined with the experimentally obtained distribution of deposited particles to evaluate the depth filtration resistance of fibrous media. The effect of particle size on depth filtration resistance was also discussed. Finally, a new model, or D-model, for the mass concentration distribution of deposited particles inside a loaded medium was theoretically established and numerically solved. The growth coefficient of single fiber efficiency, an important parameter of the D-model, was also evaluated based on the experimental results and the D-model. In this Chapter, the results of both theoretical modeling and dust loading experiments for depth filtration resistance are presented.

6.2 Dust loading experiments for five-stacked media

6.2.1 Method of the dust loading experiments

Dust loading experiments were required for experimentally investigating the depth filtration resistance of fibrous media and the distribution of deposited particles, i.e., the loaded dust mass in different thickness ranges of the loaded media. Considering that the deposition of particles in a loaded media was fragile and easy to be damaged, therefore, the measuring operations previously used such as dividing a medium using an adhesive tape [Thomas et al. 2001] and solidifying it using the resin [Aguiar and Coury 1996] may not be appropriate.

It was considered that instead of cutting a fibrous medium into several pieces, stacking several media and measuring their respective parameters before and after a dust loading experiment could be realized more easily. In this way, a five-stacked media were regarded as one “thickened” fibrous medium and each medium in the five-stacked media occupied a certain thickness range of the “thickened” medium. Therefore, an experimental method for dust loading experiments as schematically shown in Fig 6.3 was proposed. By using this method, the resistance, filtration

efficiency and loaded dust mass for each fibrous medium could be measured and recorded independently.

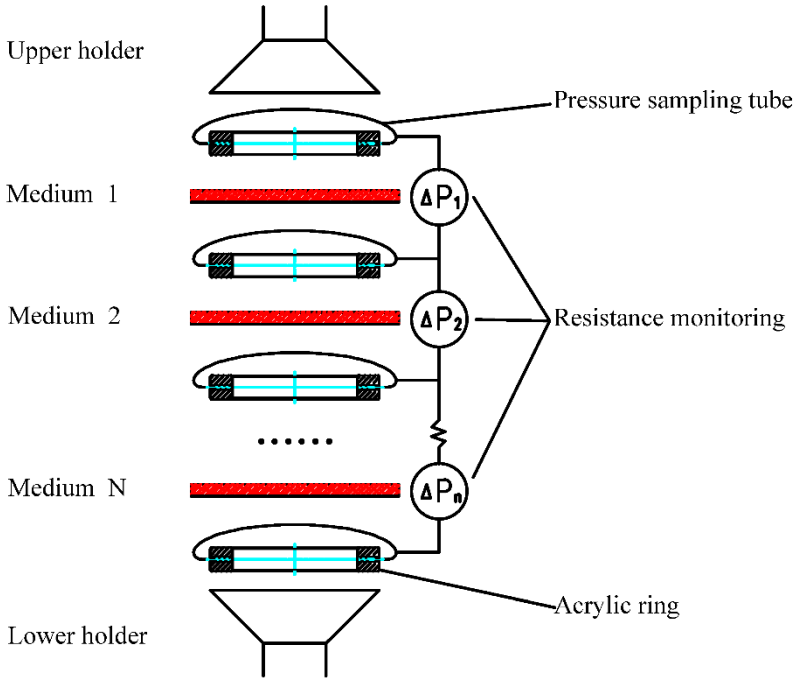

Fig 6.3 Experimental method of dust loading for multi-stacked fibrous media

Holders of the experimental setup may be opened to measure the loaded dust mass for each medium during the dust loading experiments. Therefore, to avoid the effect of the changes in air humidity on the resistance of loaded media, SiO_2 aerosols were used in the experiments. Furthermore, four monodisperse SiO_2 aerosols and a polydisperse one were employed to investigate the influence of particle size distribution on the depth filtration resistance of fibrous media.

Table 6.1 shows the particle size distributions of experimental aerosols.

Table 6.1 Particle size distributions of experimental monodisperse/polydisperse SiO_2 aerosols

	Particle diameter (manufacturers), μm	Geometric mean diameter (SEM), μm	Geometric standard deviation (SEM)
Monodisperse	0.30	0.305	1.13
	0.40	0.412	1.10
	0.55	0.548	1.14
	1.0	1.06	1.08
Polydisperse	-	0.283	1.29

On the other hand, using too few stacked media was not able to provide enough useful data, but using too many may also be counter-productive because the mass concentration of deposited particles for the downstream media would be small and then no significant changes in the concentration may be observed. According to the results from preliminary experiments, the number of stacked media was hence determined at five. Glass fiber media with classes of both M6 and M7 were used in the experiments. Their parameters are listed in Table 6.2.

Table 6.2 Parameters of two experimental fibrous media

Class	Basic weight, g/m^2	Thickness, mm	Packing density	Average fiber diameter, μm	Initial filtration efficiency at 0.4 μm
M6	61.3	0.595	0.0406	2.67	34.2 %
F7	60.0	0.431	0.0548	2.05	52.9 %

Two dust loading experiments for the five-stacked M6 media and M7 media using the polydisperse SiO_2 aerosol, and four experiments for five-stacked M6 media using four monodisperse SiO_2 aerosols were conducted, respectively, at a filtration velocity of 5.33 cm/s. The following parameters including resistance, filtration efficiency and mass of each clean medium were measured before a dust loading experiment. During dust loading, the same parameters would be measured several times at a regular time interval. The final resistance to terminate an experiment was set at 3 times the initial resistance of the five-stacked media.

6.2.2 Experimental results of dust loading experiments

Figs 6.4 to 6.6 show the experimental results for loaded dust mass, filtration efficiency for 0.4 μm particles and resistance of each M6 medium during dust loading for the five-stacked media using the polydisperse SiO_2 aerosol.

It can be seen from Fig 6.4 that, the loaded dust mass for Medium 1 was much greater than that of the other media at the end of dust loading, and increased almost linearly with an increase in dust loading time after 4000 s. The loaded dust mass for Medium 2 was increased significantly prior to 4000 s, but was increased slightly thereafter, with an increase in dust loading time. In addition, the increases in loaded dust mass for the other three media were not obvious during the whole process of dust loading.

In Fig 6.5, the filtration efficiency for 0.4 μm particles for Medium 1 was increased from 60% at the beginning of dust loading to nearly 100%, 6000 s after dust loading time. This variation trend in filtration efficiency was affected by loaded dust mass, and determined the variation trend of loaded dust mass at the same time.

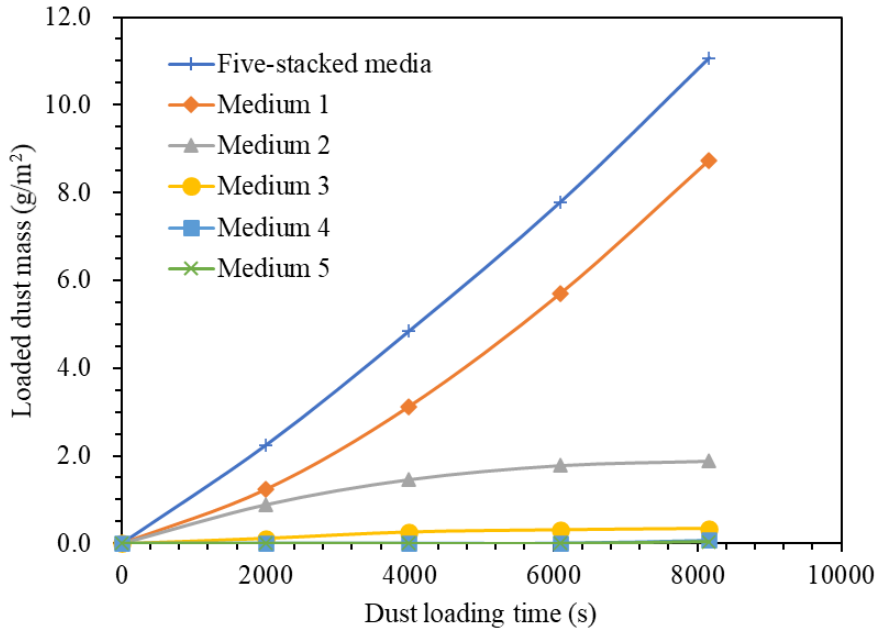

Fig 6.4 Loaded dust masses for each M6 medium and the corresponding five-stacked media during dust loading

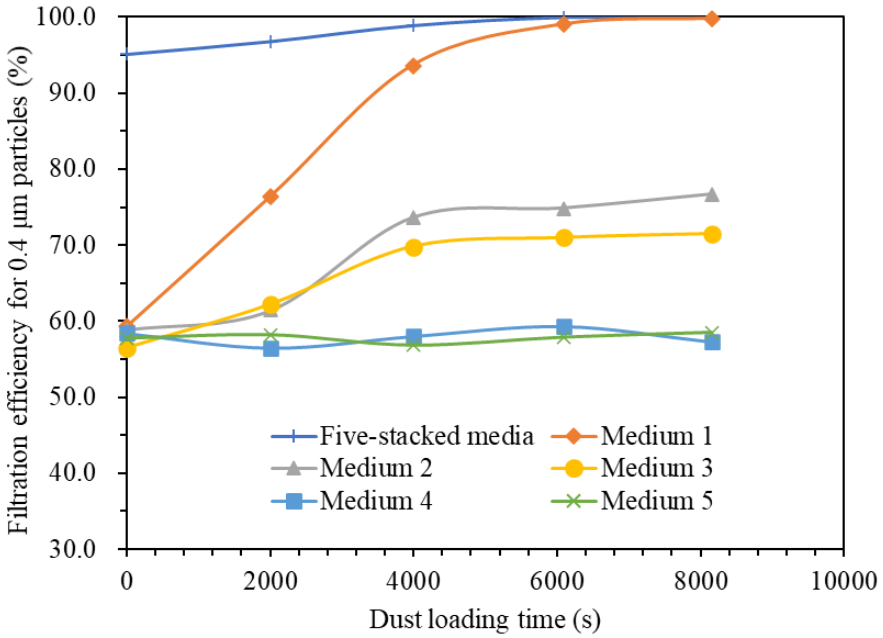

Fig 6.5 Filtration efficiencies for 0.4 μm particles for each M6 medium and the corresponding five-stacked media during dust loading

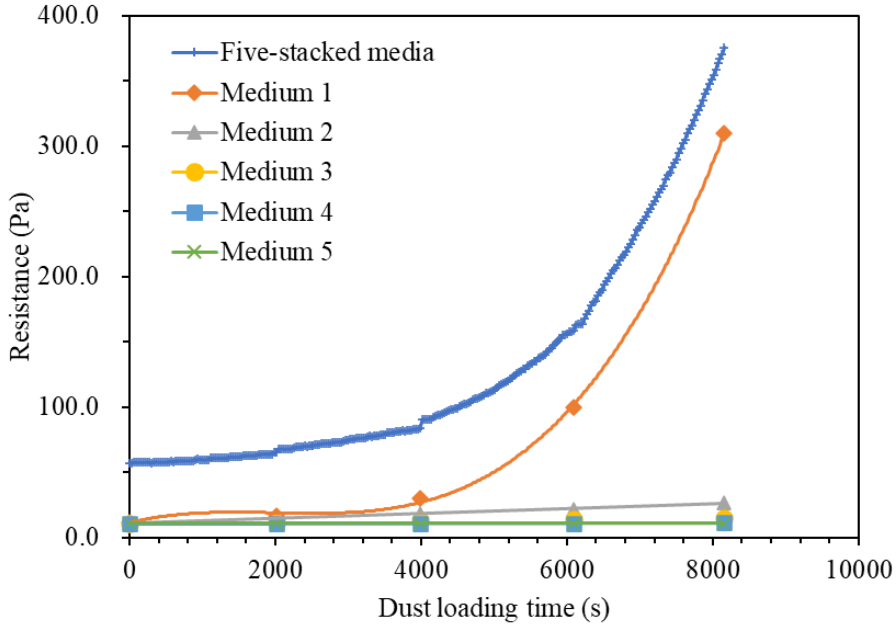

Fig 6.6 Resistance curves for each M6 medium and the corresponding five-stacked media

Fig 6.6 illustrates resistance curves for each M6 medium and the corresponding five-stacked media. As seen, the variation trend of the resistance for Medium 1 was similar to that of loaded dust mass shown in Fig 6.4. However, at the same dust loading time, the ratio of the resistance for Medium 2 to that for Medium 1 was significantly less than the ratio of loaded dust mass for Medium 2 to that for Medium 1. This might reflect the difference in size distributions of particles captured by Medium 1 and Medium 2, respectively.

It should be noticed, however, that the five-stacked M6 fibrous media was thicker than the single M6 fibrous medium. The performance and distribution of deposited particles of five-stacked M6 fibrous media belonged to the stacked media which was

regarded as a new medium rather than the M6 medium. On the other hand, the five-stacked M6 fibrous media has a relatively even structure in its thickness direction, while some commercial fibrous media that have gradient structures for better dust holding capacity. Therefore, the experimental results of the five-stacked M6 fibrous media may be different from those of the commercial fibrous media.

Fig 6.7 shows the changes in loaded dust mass for each M7 medium and the corresponding five-stacked media during dust loading using the polydisperse SiO_2 aerosol. As seen, the trend of increase in loaded dust mass was more significant than that for the five-stacked M6 media due to the higher initial filtration efficiency for the M7 medium.

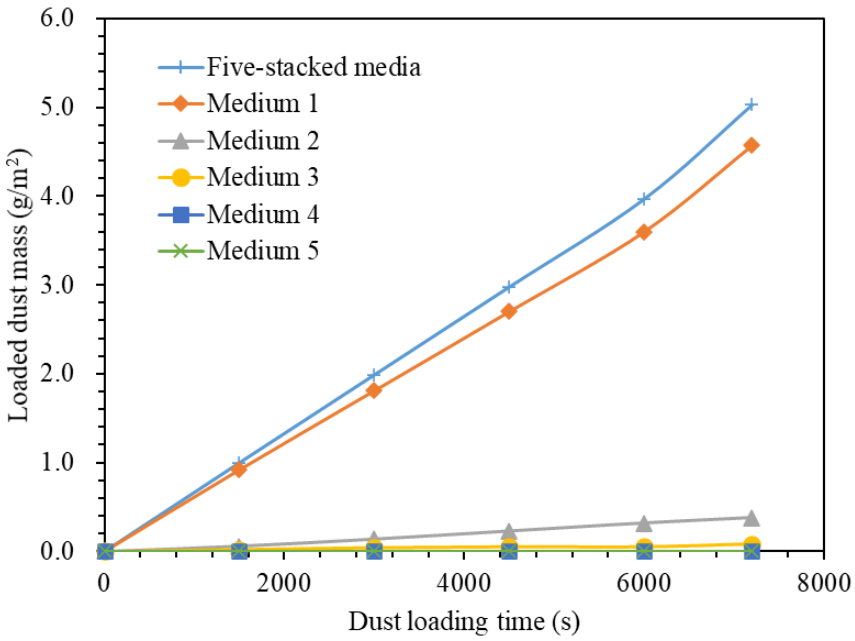

Fig 6.7 Loaded dust masses of each F7 medium and the corresponding five-stacked media

The variation trends for results of dust loading experiments using respectively the four monodisperse SiO_2 aerosols were overall similar to those using the polydisperse SiO_2 aerosol. These results are not shown in the current Section but would be used in the subsequent Section for the evaluation of depth filtration resistance.

6.3 Resistance of fibrous media during depth filtration

6.3.1 Layered resistance model for depth filtration

Since the deposited particle masses in different layers of loaded five-stacked media were experimentally obtained, the depth filtration resistance of the five-stacked media may therefore be evaluated by incorporating the experimental data into Bergman model. A layered resistance model for depth filtration was then established as follows,

$$\Delta P = 64\mu_a V Z_i \sum_{i=1}^{i=n} \left(\frac{\alpha_f}{{d_f}^2} + \frac{\alpha_{pf,i}}{{d_{pf}}^2}\right)^{1/2} \left(\frac{\alpha_f}{d_f} + \frac{\alpha_{pf,i}}{d_{pf}}\right) \quad (6\text{-}1)$$

where Z_i and $\alpha_{pf,i}$ are respectively the thickness and packing density for layer i.

6.3.2 Comparison between the layered resistance model and Bergman model

An increase in packing density of fibrous media caused by dust loading was not significant when compared to the packing density of clean media. Therefore, this had little effect on air flow velocity and its influence on the resistance of clean medium fibers can be ignored. Furthermore, to compare directly the predictions using the layered model and Bergman model for depth filtration resistance, the comparison was based on the resistances of particle fibers rather than those of loaded media.

Fig 6.8 shows the experimental and the predicted resistances of particle fibers for each M6 medium for the five-stacked M6 media loaded with the monodisperse aerosol with an average diameter of 0.412 μm. In this figure, "0" represents the five-stacked M6 media. It can be seen from Fig 6.8 that, all the resistances obtained using the layered model were significantly greater than those from experiments. According to experimental results, certain growth in loaded dust mass for Medium 3 to 5 were measured, however, there was almost no resistance growth caused by loaded dust being observed for these media.

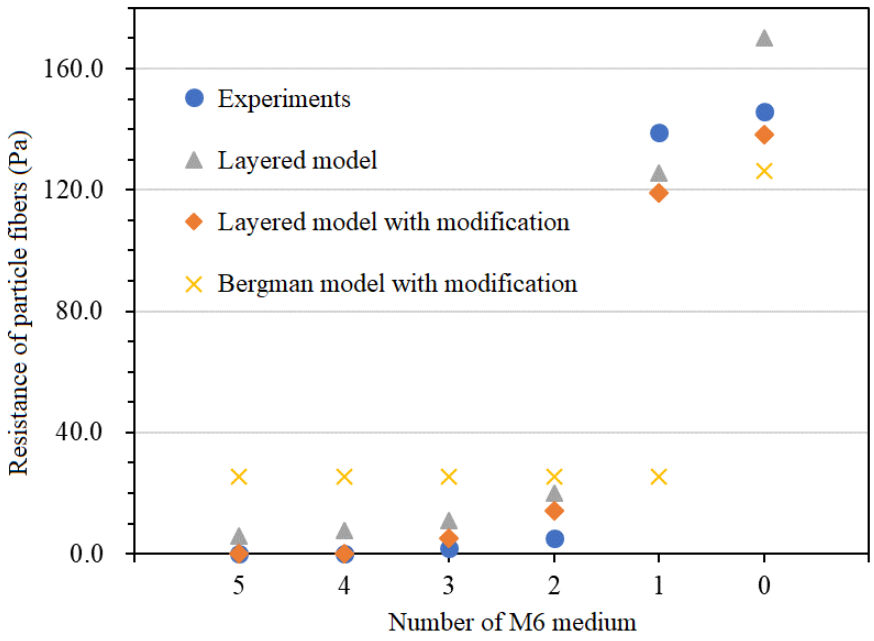

Fig 6.8 Resistance comparison between experiments and models for five-stacked M6 media loaded with 0.412 μm monodisperse aerosol

Furthermore, Fig 6.9 shows an SEM photo for medium fibers in the initial stage of dust loading. As seen, under a smaller loaded dust mass condition, deposited particles were only attached to the fiber surface but not formed particle fibers that can cause a significant growth in medium resistance. This implied that there existed a critical loaded dust mass for a loaded medium, below which the dust loading cannot cause a significant resistance increase.

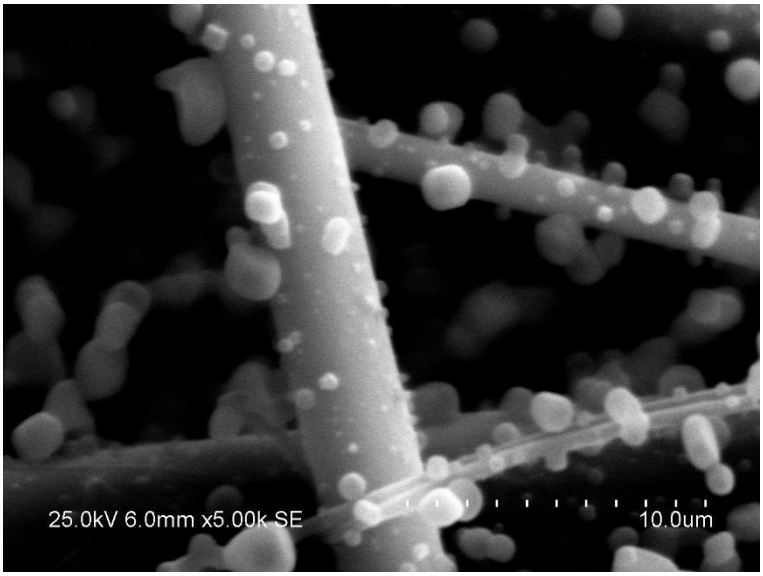

Fig 6.9 SEM photo for medium fibers in the initial stage of dust loading

In the current study, the critical loaded dust mass was defined as the 50% of average loaded dust masses corresponding to a resistance increase of 1 Pa for the loaded M6 media. The modification was therefore made by subtracting the critical loaded dust mass from the original loaded dust mass when it was used to evaluate the depth filtration resistance. The resistance growths predicted by the layered model with the modification were evaluated and are shown in Fig 6.8, as marked by "Layered model with modification". As seen, the predicted values by the layered model with modification were closer to experimental values than those without modification.

On the other hand, Bergman model can be directly used to predict the resistance growth for each M6 medium and five-stacked M6 media when the uneven distribution of loaded dust mass was ignored. Hence, the Bergman model was also modified by

the critical loaded dust mass. As shown in Fig 6.8, the predicted total growth of resistance values by Bergman model with modification were significantly smaller than those obtained from experiments. The distribution of resistance growth in different media cannot be predicted as well. Therefore, the layered model established by incorporating the distribution of deposited particles into the Bergman model was considered more appropriate for evaluating the depth filtration resistance of fibrous media.

6.3.3 Effects of aerosol particle size on depth filtration resistance of fibrous media

The resistance curves for particle fibers respectively made of four monodisperse SiO_2 aerosols are shown in Fig 6.10. As seen, the resistance was higher for particle fibers made of the monodisperse aerosol with a smaller average diameter at the same loaded dust mass. This agreed well with the predictions made by the layered model, Equation (6-1). On the other hand, a smaller diameter of particles was able to cause a greater growth coefficient of single fiber efficiency according to the experimental results shown in Table 6.5. Therefore, the gathering trend of the increase in loaded dust mass and resistance toward the windward side for a fibrous medium would be more significant when loaded with smaller particles, which would also cause a greater resistance growth.

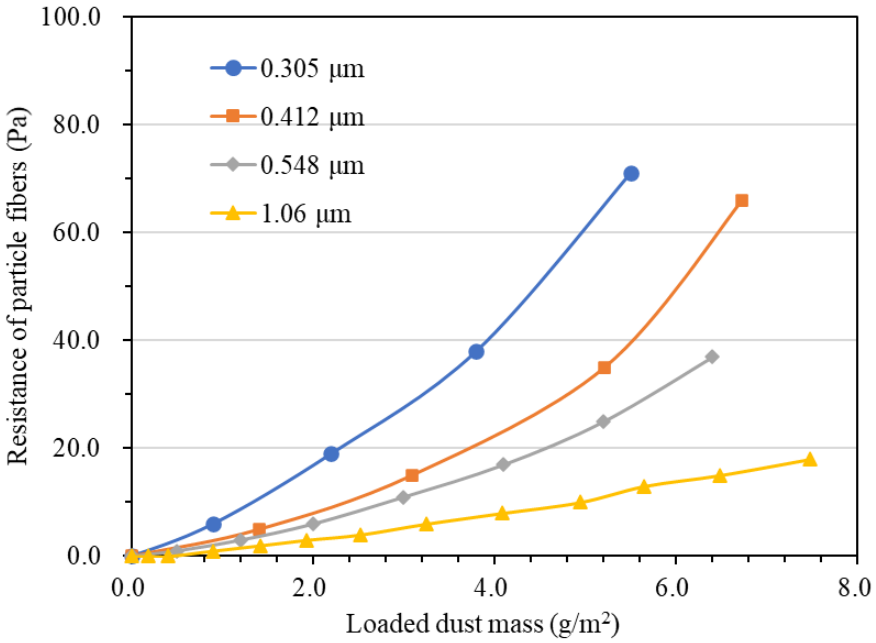

Fig 6.10 Resistance curves for particle fibers respectively made of four monodisperse SiO_2 aerosols

Although Equation (6-1) showed satisfactory applicability when predicting the resistance growth of a fibrous medium loaded with monodisperse aerosols, it may not appropriate when polydisperse aerosols were adopted. For a polydisperse aerosol, its average diameter can be expressed in different types, like geometric mean diameter, surface area mean diameter and volume mean diameter. These three kinds of diameter differed greatly and would be changed during dust loading for deposited polydisperse SiO_2 particles. Therefore, different predictions would be made when applying the three kinds of diameter to Equation (6-1).

The geometric mean diameter, surface area mean diameter and volume mean diameter of deposited polydisperse particles for five-stacked M6 media were calculated and are

showed in Fig 6.11. As seen, the volume mean diameter and surface area mean diameter of deposited particles was decreased gradually while the geometric mean diameter remained almost unchanged during dust loading. The values of volume mean diameter and surface area mean diameter were mainly determined by t larger particles, which had smaller numbers and contributed less to resistance growth under the same loaded dust mass. Therefore, the geometric mean diameter may be more appropriate when evaluating the resistance growth of fibrous media loaded with polydisperse aerosols.

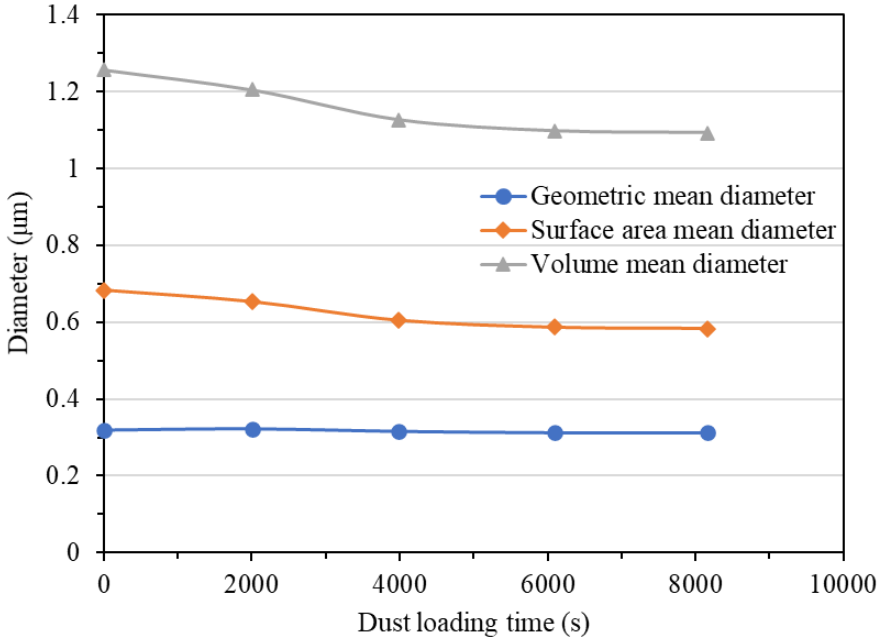

Fig 6.11 Variation trends for three kinds of average diameter for deposited polydisperse SiO_2 particles during dust loading

On the other hand, Table 6.3 lists the differences between the experimental resistance growth and the predicted using the layered model, using three kinds of the average

diameter. It can be seen that the predictions by using geometric mean diameter agreed better with the experimental results. Therefore, the geometric mean diameter was recommended as the representative diameter in evaluating the resistance growth of fibrous media during depth filtration in the studies presented in this Chapter.

Table 6.3 Differences between the experimental resistance growth and the predicted one using three kinds of average diameter

Kind of diameter	Geometric mean diameter	Surface area mean diameter	Volume mean diameter
Predicted resistance growth	357	113	40
Difference	19.4%	-61.8%	-86.6%

6.4 Modeling the mass concentration distribution of deposited particles inside fibrous media

Although the layered model, i.e., Equation (6-1), can be used to evaluate the depth filtration resistance for fibrous media, the distribution of deposited particles was required in the model. In Sections 6.2 and 6.3, the distribution of deposited particles was obtained through the dust loading experiments for five-stacked media. To enable the practical use of the layered model, it was considered necessary that the distribution

of deposited particles of fibrous media should be theoretically modeled. Hence, in this Section, modeling the distribution of deposited particles of fibrous media is reported.

6.4.1 An established D-model for the mass concentration distribution of deposited particles

It can be seen from Fig 6.1 that when filtration time, $t > 0$, both the deposited particle mass and the filtration efficiency would be uneven along the thickness of a loaded medium. During a filtration process, filtration efficiency at the current time point would determine the mass distribution of deposited particles at the next time point, and vice versa.

A model for the mass concentration distribution of deposited particles, or D-model, was established based on the following assumptions:

1) A fibrous medium was uniform, isotropic and can be divided into thin layers along the thickness with fixed filtration efficiency;

2) The filtration velocity inside the medium was one-dimensional and perpendicular to the medium surface, and air flow was laminar due to low filtration velocity;

3) An experimental aerosol was uniform and stable upstream of the medium. The hydrodynamic characteristics of aerosol particles remained unchanged when passing through each layer of the medium. The effects of air molecular diffusion and turbulence on suspended particles in the medium were neglected;

4) Single fiber efficiency was increased linearly with an increase in local deposited particle concentration. The effect of deposited particles on medium porosity was considered but that on clean fiber length was not;

5) Particles would not be detached from medium fibers after being captured.

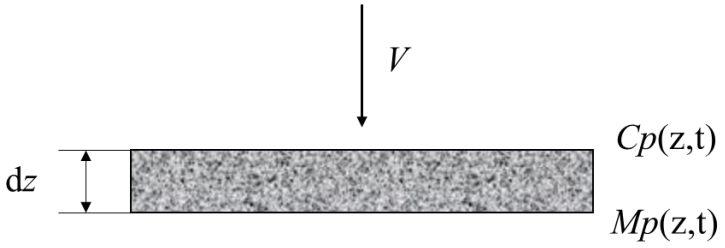

Fig 6.12 A unit layer in a loaded medium

A unit layer with a thickness of dz and a surface area of S in a loaded fibrous medium is schematically shown in Fig 6.12. The mass concentration for deposited particles inside the loaded medium was termed as M_p and that for suspended particles as C_p.

The total length of the clean fiber, l, inside the unit layer was evaluated as follows,

$$l = \frac{4\alpha_f S \mathrm{d}z}{\pi {d_f}^2} \tag{6-2}$$

where α_f is the initial packing density of the unit layer, d_f the average fiber diameter.

The local average air velocity around medium fibers, V', was influenced by medium fibers and deposited particles, expressed as

$$V' = \frac{V}{1-\alpha} \tag{6-3}$$

where V is the face velocity of loaded medium, α the local packing density taking into account the deposited particles, which may be evaluated as follows,

$$\alpha = \alpha_f + \frac{M_p}{\rho_p} \tag{6-4}$$

where α_f is the packing density of a clean medium and ρ_p the density of deposited particles.

The local single fiber efficiency was increased linearly with an increase in the mass concentration of loaded dust, expressed as

$$\frac{\eta_{fp}}{\eta_f} = 1 + \lambda M_p \tag{6-5}$$

where η_{fp} is the local single fiber efficiency of the loaded medium, η_f the single fiber efficiency of a clean medium, λ the growth coefficient of single fiber efficiency.

According to the definition of single fiber efficiency [Xu and Zhou 2014], for the unit layer, an increase in the mass concentration of deposited particles with an increase in dust loading time can be evaluated as,

$$\frac{\mathrm{d}M_p}{\mathrm{d}t} = \frac{\eta_{fp} d_f V' C_p l}{S \mathrm{d}z} \tag{6-6}$$

where t is the dust loading time.

Integrating Equation (6-6) with Equations (6-2) to (6-5), $\frac{\mathrm{d}M_p}{\mathrm{d}t}$ can be expressed as

$$\frac{\mathrm{d}M_p}{\mathrm{d}t} = V C_p \frac{4\alpha_f \eta_f}{\pi d_f} \cdot \frac{1 + \lambda M_p}{1 - \alpha_0 - \frac{M_p}{\rho_p}} \tag{6-7}$$

On the other hand, the change in the mass concentration of suspended particles, $\frac{\partial C_p}{\partial t}$, was equal to the sum of an increase in the mass concentration of deposited particles and the particle transportation caused by the passing aerosol, expressed as

$$-\frac{\partial C_p}{\partial t} = V\frac{\partial C_p}{\partial z} + \frac{\mathrm{d}M_p}{\mathrm{d}t} \tag{6-8}$$

Equation (6-8) can be re-arranged as:

$$\frac{\partial C_p}{\partial t} + V\frac{\partial C_p}{\partial z} + \frac{\mathrm{d}M_p}{\mathrm{d}t} = 0 \tag{6-9}$$

Then the equations for the mass concentration of deposited particles and suspended particles inside a loaded medium during depth filtration were obtained and combined as the D-model for the mass concentration of deposited particles, shown as Equation (6-10).

$$\begin{cases} \dfrac{\mathrm{d}M_p}{\mathrm{d}t} = VC_p\dfrac{4\alpha_0\eta_f}{\pi d_f}\cdot\dfrac{1+\lambda M_p}{1-\alpha_0-\dfrac{M_p}{\rho_p}} \\ \dfrac{\partial C_p}{\partial t} + V\dfrac{\partial C_p}{\partial z} + \dfrac{\mathrm{d}M_p}{\mathrm{d}t} = 0 \end{cases} \tag{6-10}$$

The boundary conditions for Equation (6-10) were

$$\begin{cases} C_p(0,t) = C_0 \\ C_p(z,0) = 0 \ (z \neq 0) \\ M_p(0,t) = 0 \\ M_p(z,0) = 0 \end{cases} \tag{6-11}$$

where C_0 is the aerosol mass concentration upstream of the loaded medium.

In the D-model, or Equation (6-10), all the parameters except for the growth coefficient of single fiber efficiency, λ, can be easily obtained based on the initial and boundary conditions of a medium before dust loading. However, the values of λ at different dust loading conditions were still to be determined. Furthermore, since it was generally impossible to obtain analytical solutions for a partial differential equation, numerical approaches to solve Equation (6-10) were therefore adopted based on a given λ value.

6.4.2 Numerical solutions for the D-model for mass concentration distribution of deposited particles

To numerically solve the D-model for mass concentration distribution of deposited particles, i.e., Equation (6-10), continuous variables, z and t, should be discretized firstly so that the continuous equations for $C_p(z,t)$ and $M_p(z,t)$ can be transformed into discrete sequences. The two terms, h and τ, were used to represent the step length

in medium thickness and dust loading time, respectively. $C_p(i,j)$ was the discrete value of mass concentration for suspended particle and $M_p(i,j)$ that for deposited particles in a loaded fibrous medium at point (i,j), where i and j are for the thickness axis and time axis, respectively.

Then, Equation (6-7) was transformed into

$$\begin{aligned}\frac{\mathrm{d}M_p}{\mathrm{d}t} &= \frac{M_p(i,j)-M_p(i,j-1)}{\tau} \\ &= VC_p(i,j-1)\frac{4\alpha_0\eta_f}{\pi d_f}\cdot\frac{1+\lambda M_p(i,j-1)}{1-\alpha_0-\frac{M_p(i,j-1)}{\rho_p}}\end{aligned} \tag{6-12}$$

and further re-arranged as

$$\begin{aligned}M_p(i,j) = M_p(i,j-1) &+ \tau VC_p(i,j-1)\frac{4\alpha_0\eta_f}{\pi d_f} \\ &\cdot\frac{1+\lambda M_p(i,j-1)}{1-\alpha_0-\frac{M_p(i,j-1)}{\rho_p}}\end{aligned} \tag{6-13}$$

$\frac{\partial C_p}{\partial t}$ and $\frac{\partial C_p}{\partial z}$ were discretized in Equation (6-14) and (6-15), respectively.

$$\frac{\partial C_p}{\partial t} = \frac{C_p(i,j)-C_p(i,j-1)}{\tau} \tag{6-14}$$

$$\frac{\partial C_p}{\partial z} = \frac{C_p(i,j)-C_p(i-1,j)}{h} \tag{6-15}$$

Therefore, Equation (6-9) can be transformed into

$$\frac{C_p(i,j)-C_p(i,j-1)}{\tau}+V\frac{C_p(i,j)-C_p(i-1,j)}{h}+VC_p(i,j)\frac{4\alpha_0\eta_f}{\pi d_f}\cdot\frac{1+\lambda M_p(i,j)}{1-\alpha_0-\frac{M_p(i,j)}{\rho_p}}=0 \tag{6-16}$$

and further re-arranged as

$$C_p(i,j)=\frac{\frac{C_p(i,j-1)}{\tau}+V\frac{C_p(i-1,j)}{h}}{\frac{1}{\tau}+\frac{V}{h}+V\frac{4\alpha_0\eta_f}{\pi d_f}\cdot\frac{1+\lambda M_p(i,j)}{1-\alpha_0-\frac{M_p(i,j)}{\rho_p}}} \tag{6-17}$$

Accordingly, based on the initial and boundary conditions, the mass concentration distribution of deposited particles and suspended particles in a loaded fibrous medium at different dust loading times can be numerically obtained.

Fig 6.13 schematically illustrates the calculation procedures for Equations (6-13) and (6-17). The black dots in Fig 6.13 represent boundary conditions, i.e., known values and black circles unknown values for M_p and C_p. According to Equation (6-13), the value of M_p at (1,1) can be calculated using the values of M_p and C_p at (1,0). Then the value of C_p at (1,1) can be obtained using the value of M_p at (1,1) and C_p

values at (1,0) and (0,1) based on Equation (6-17). The values of M_p and C_p at any time points and any thickness can therefore be obtained by repeating these calculation procedures.

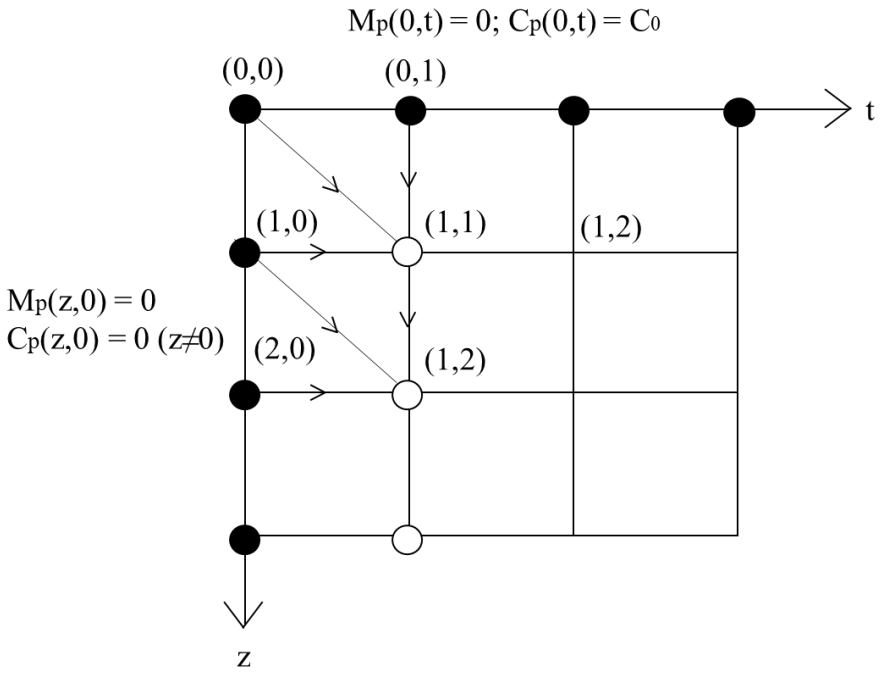

Fig 6.13 Schematic diagram of numerical calculation procedures for Equations (6-13) and (6-17)

A python program was constructed based on the calculation procedures shown in Fig 6.13 to numerically solve Equation (6-10). Fig 6.14 shows the flow chart of python program design. Python 3.7 was used and the libraries of Numpy and Matplotlib were applied to designing and executing the program. Program coding is listed in Appendix A.

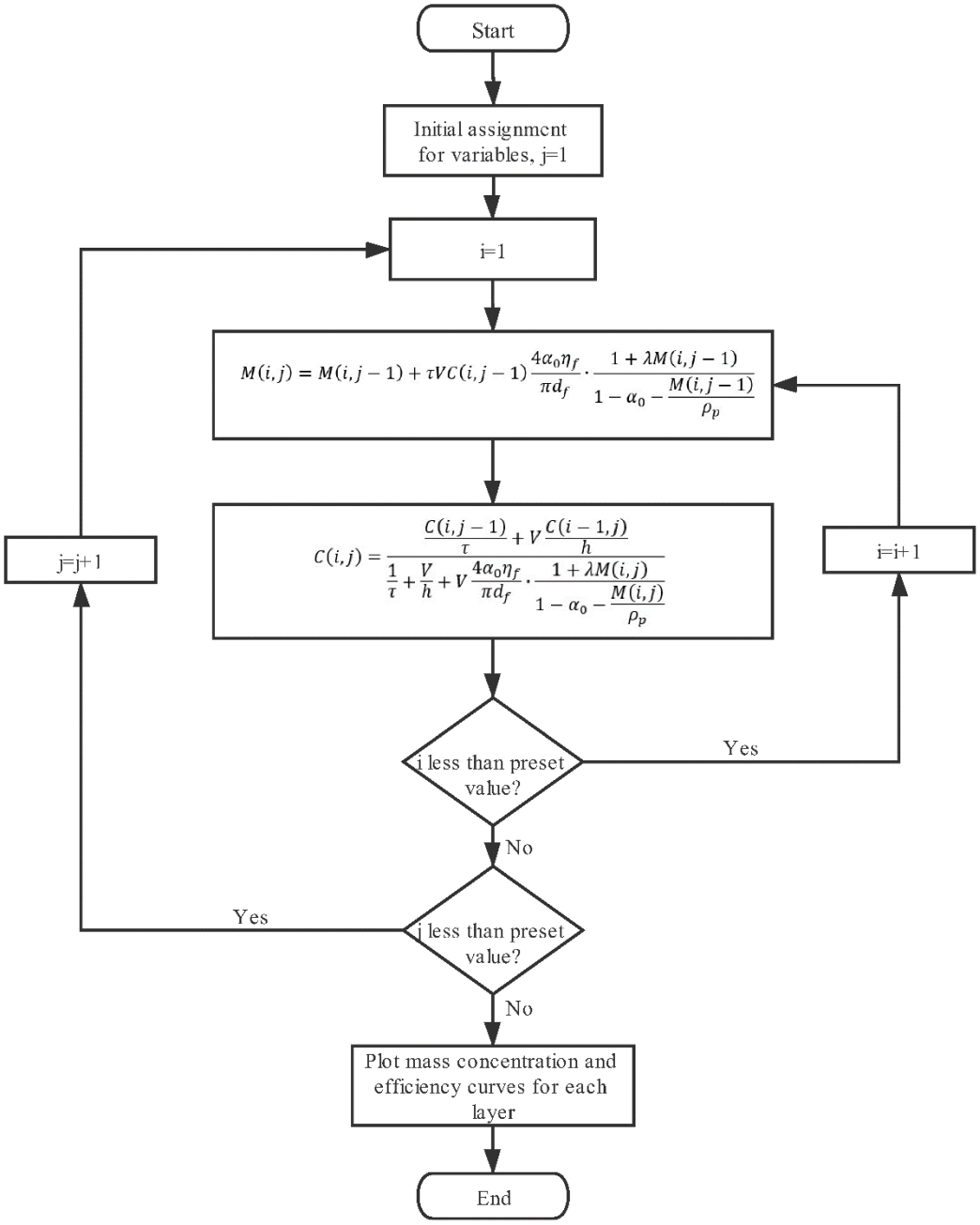

Fig 6.14 A program flow chart

The initial values for the parameters used in the program are shown in Table 6.4. These values were basically the same as those in the dust loading experiments presented in Section 6.2.

Table 6.4 The initial values of the parameters for the program used for the aerosol mass concentration calculation in a loaded medium

Parameter	Value	Unit
Time step length	0.1	s
Time step number	1×10^{5}	-
Thickness step length	8×10^{-5}	m
Thickness step number	25	-
Filtration velocity	0.0533	m/s
Packing density of clean medium	0.3	-
Single fiber efficiency of clean medium	0.4	-
Average fiber diameter of clean filter material	5.0×10^{-6}	m
Growth coefficient of single fiber efficiency	5.0×10^{-6}	m^3/mg
Particle density	2.2×10^{9}	mg/m^3
Initial aerosol mass concentration	10	mg/m^3

Fig 6.15 and Fig 6.16 respectively show the numerical results of the mass concentrations of suspended particles in different medium thicknesses and the loaded dust masses within different medium thickness ranges. The parameter of mass concentration was used in Equation (6-10) to represent the distribution of deposited particles. However, the loaded dust mass would be easier to be obtained than the mass concentration in a dust loading experiment. Therefore, the loaded dust mass instead of

the mass concentration was applied in Fig 6.16, so as to compare directly the results between numerical solutions and the dust loading experiments.

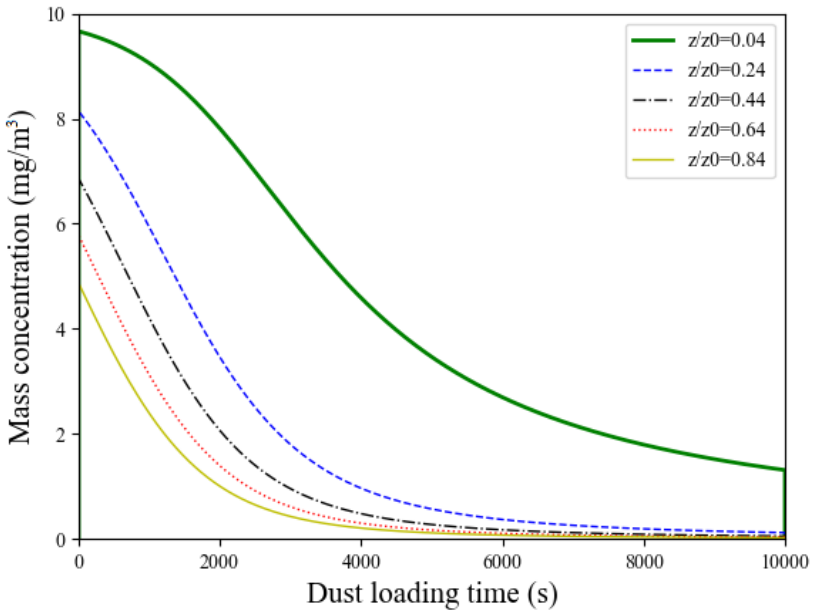

Fig 6.15 Numerical results for the mass concentrations of suspended particles in different medium thicknesses

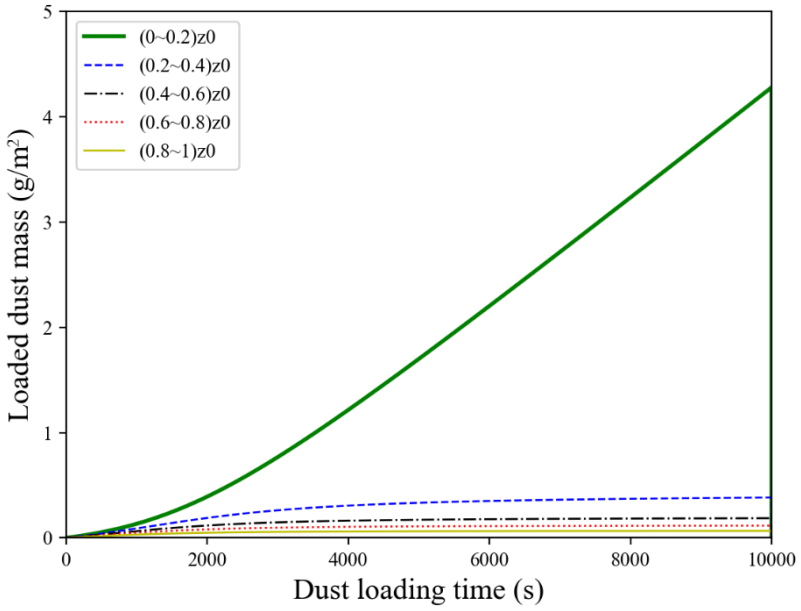

Fig 6.16 Numerical results for the loaded dust masses within different medium thickness ranges

As seen from Fig 6.15, the mass concentration of suspended particles was higher at a lower thickness at a fixed dust loading time due to the filtration of the medium. With an increase in dust loading time, the mass concentration of suspended particles was decreased rapidly. Moreover, except for the mass concentrations at the thickness adjacent to the windward side of the loaded medium, shown by the curve marked with "z/z0=0.04" in Fig 6.15, the mass concentrations at the other four thicknesses were all decreased to nearly 0 when ~ 6000 seconds in dust loading time elapsed. This indicated that the increase in filtration efficiency tended to be mainly near the windward side of the loaded medium.

In Fig 6.16, although the loaded dust mass in all the five thickness ranges was increased with an increase in dust loading time prior to 4000 s, a much greater loaded dust mass in the range of (0~0.2)z0 than that in the other four ranges after 2000 s was resulted in because of increased filtration efficiency near the windward side. Besides, the loaded dust mass in the thickness range of (0~0.2)z0 was increased almost linearly with an increase in dust loading time after 4000 s, which implied that the gravimetric efficiency, i.e., the filtration efficiency evaluated by the particle mass was increased to around 100% during this period.

The growth trends of loaded dust mass for all the five thickness ranges shown in Fig 6.16 were similar to those obtained from the dust loading experiments. This suggested that the established D-model can predict well the distribution of deposited particles when an appropriate growth coefficient of single fiber efficiency was adopted.

6.4.3 Evaluation of the growth coefficient of single fiber efficiency

In Equation (6-10), the single fiber efficiency of a clean medium, η_f, can be evaluated using the logarithmic penetration law, which was proposed by combining the single fiber efficiency and filtration efficiency of a clean medium [Xu and Zhou 2014]. However, the growth coefficient of single fiber efficiency, λ, was difficult to determine. In open literature, Huang et al. [2006] observed the deposition of particles

on a single fiber using a microscope, but no information about single fiber efficiency was provided. There were also two other studies modeling the deposition of particles on medium fibers [Kanaoka et al. 1983, Hosseini and Vahedi Tafreshi 2012]. However, the modeling results were only described qualitatively and cannot be used to evaluate the growth coefficient.

The growth coefficient of single fiber efficiency for a medium during dust loading may be determined by the particle size distribution and medium fiber diameter. In the current study, the growth coefficient of single fiber efficiency for experimental media could be evaluated by combining the numerical results presented in Sub-section 6.4.2 and the experimental results of dust loading for five-stacked media using monodisperse SiO_2 aerosols.

Although the variation trends for the experimental results of dust loading for five-stacked M6 media using polydisperse SiO_2 were similar to those predicted by the D-model, they were not appropriate for evaluating the growth coefficient of single fiber efficiency. This was because the filtration efficiency evaluated by particle mass, i.e., the arrestance, was adopted in Equation (6-10) and would be determined by the size distribution of experimental aerosol. However, the filtration efficiencies of a medium evaluated by either particle mass or particle number for monodisperse aerosols were the same. Therefore, the growth coefficient of single fiber efficiency could be

evaluated based on the results of dust loading experiments using monodisperse SiO_2 aerosols.

Therefore, the experimental results of dust loading experiments for five-stacked M6 media using the monodisperse SiO_2 aerosol with an average diameter of 0.412 μm were used to evaluate the growth coefficient of single fiber efficiency. On the other hand, a numerical study following the method illustrated in Sub-section 6.4.2 was also performed using the same parameters as those in dust loading experiments, except that variable growth coefficients of single fiber efficiency were applied. The experimental and numerical simulation results on the increases in loaded dust mass for the five M6 media were compared and are shown in Fig 6.17 (a). As seen, the predicted mass concentration distribution of deposited particles by the established D-model presented in this Chapter agreed very well with the experimental results when a suitable growth coefficient of single fiber efficiency was applied.

Considering that the majority of the increase in loaded dust mass and resistance for the five-stacked media was distributed in Medium 1 and Medium 2, the determined growth coefficient of single fiber efficiency should predict the best the loaded dust mass for Medium 1 and Medium 2. The differences between the experimental and simulated loaded dust mass for both Medium 1 and Medium 2 were calculated and are plotted in Fig 6.17 (b). Also, the sum of the absolute value for the difference for

Medium 1 and that for Medium 2 at a fixed growth coefficient was obtained. Then the growth coefficient was determined when the sum reached its minimum value. As shown in Fig 6.17 (b), the growth coefficient of single fiber efficiency for 0.4 μm particles for the experimental M6 medium was determined at 1.0×10^{-6} m^3/mg.

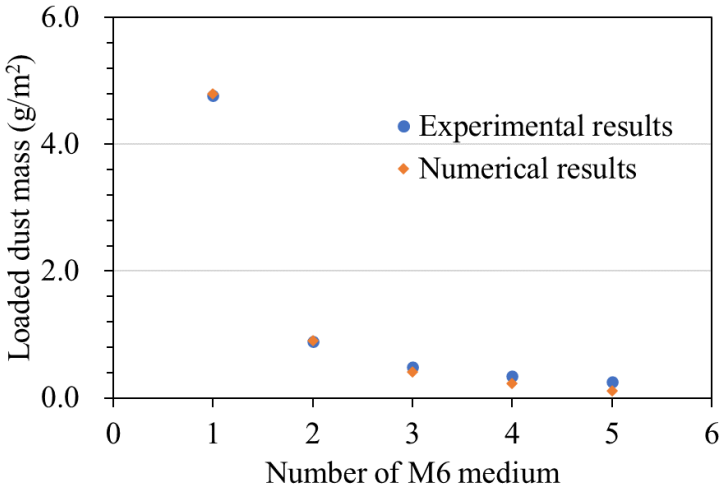

(a) The comparison between experimental results and simulated loaded dust mass

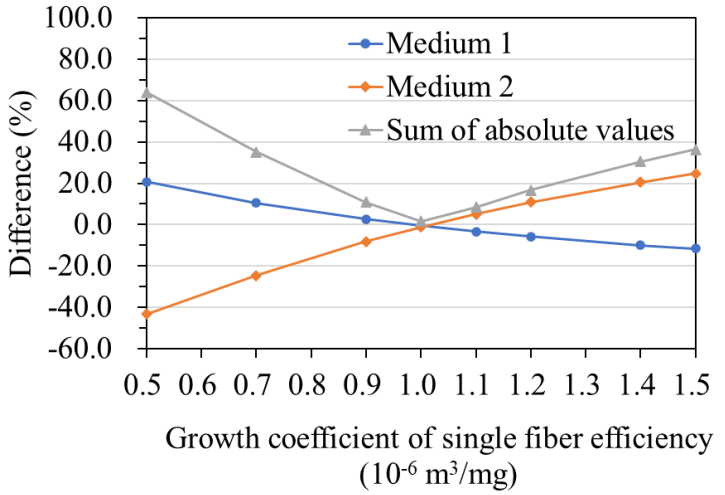

(b) Differences between experimental results and numerical results for Medium 1 and Medium 2 at different growth coefficients of single fiber efficiency

Fig 6.17 Evaluation of the growth coefficient of single fiber efficiency

On the other hand, it seemed that the growth coefficient of single fiber efficiency may also be evaluated using the logarithmic penetration law. Fig 6.18 (a) shows all the measured filtration efficiencies for each M6 medium at different loaded dust mass. By

applying the logarithmic penetration law to each measured filtration efficiency, the corresponding single fiber efficiencies at different loaded dust concentrations were obtained and are plotted in Fig 6.18 (b). By applying a linear fitting to these single fiber efficiencies, the growth coefficient of single fiber efficiency was determined at 2.55×10^{-8} m^3/mg.

It can therefore be seen that the growth coefficient obtained using the logarithmic penetration law was much smaller than that obtained from the numerical results. However, the logarithmic penetration law was established based on the assumption that a fibrous medium was always uniform. Once the medium was loaded with particles, the assumption was no longer applicable. Therefore, combining the D-model and a numerical solution proposed in this Chapter shall provide a better way to evaluate the growth coefficient of single fiber efficiency for a fibrous medium.

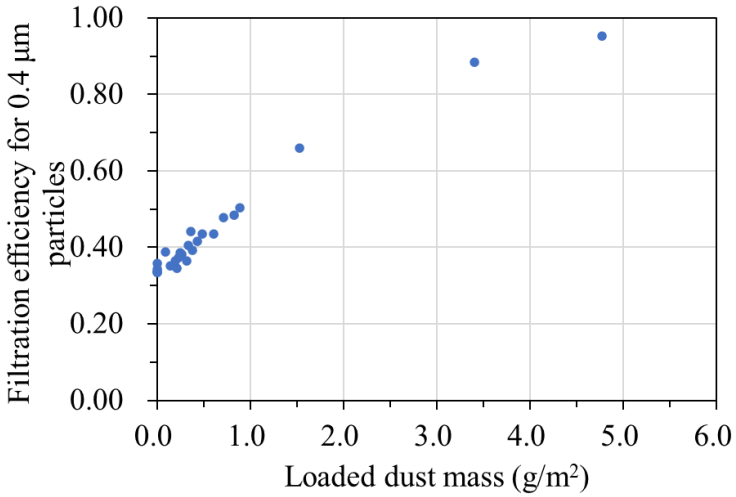

(a) Filtration efficiencies for 0.4 μm particles at different loaded dust masses

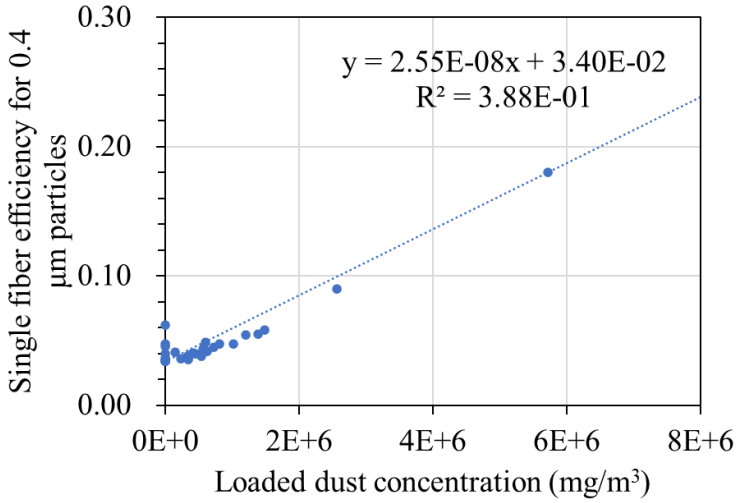

(b) Single fiber efficiencies for 0.4 μm particles

Fig 6.18 Evaluation of the growth coefficient of single fiber efficiency using the logarithmic penetration law

The growth coefficients of single fiber efficiency for the other three monodisperse SiO_2 aerosols for the experimental M6 medium were also obtained based on the numerical solutions. Table 6.5 lists the obtained coefficients. As seen, a larger particle

had a less significant effect on the growth of single fiber efficiency at the same loaded dust mass concentration.

Table 6.5 The growth coefficients of single fiber efficiency for four experimental monodisperse SiO_2 aerosols for experimental M6 medium

Particle size (μm)	0.305	0.412	0.548	1.06
Growth coefficient of single fiber efficiency ($\times 10^{-6}$ m^3/mg)	1.4	1.0	0.7	0.2

6.5 Conclusions

To investigate the distribution of deposited particles, experiments for five-stacked glass fiber media loading respectively with four monodispersed SiO_2 aerosols and a polydisperse SiO_2 aerosol were firstly designed and conducted. Then, a layered model by incorporating the distribution of deposited particles into Bergman model was proposed to predict the depth filtration resistance for fibrous media. The resistance growths obtained respectively from experiments and model prediction showed good agreement when the modification of critical loaded dust mass was applied. In terms of the effect of particle size on depth filtration resistance for fibrous media, loading with smaller particles led to a greater rate of growth in filter media resistance. According

to comparative analysis and calculation, it was recommended to use the geometric average diameter as the representative particle size to evaluate the resistance increase for filter media loaded with polydisperse particles.

On the other hand, to theoretically evaluate the distribution of deposited particles inside a loaded medium, the D-model was established by dividing a filter medium into unit layers and applying the definition of single fiber efficiency to calculate the mass of particles captured by each layer. The variation trends in loaded dust mass predicted using the numerical solutions for the D-model agreed well with those obtained from the dust loading experiments. In addition, the D-model may also be used to evaluate the growth coefficient of single fiber efficiency for the experimental M6 medium.

Chapter 7

Surface filtration resistance of fibrous media

7.1 Introduction

From the literature review presented in Chapter 2, it can be seen that experimental and theoretical studies on the resistance of a dust cake formed during surface filtration for HEPA media under different dust loading conditions have been carried out [Novick et al. 1992, Gupta et al. 1993, Endo et al. 1998, Penicot et al. 1999, Endo et al. 2002, Thomas et al. 2014]. Among these studies, the Endo model [Endo et al. 1998] and Thomas model [Thomas et al. 2014] were the representative two theoretical models for surface filtration resistance. However, it may be difficult to directly evaluate the surface filtration resistance using Endo model because an empirical correction was still required in the model. Error may also result in when using Thomas model, because the resistance of the fibers parallel to flow direction in real applications was obviously different from that of the fibers perpendicular to flow direction assumed in the model.

On the other hand, for traditional glass fiber HEPA media, a filtration process would gradually change from depth filtration to transition stage, and then to surface filtration

[Thomas 2017]. However, for a PTFE HEPA medium, most of captured particles directly deposited on the surface of the PTFE membrane because the base material on windward side had a very low efficiency [Zhang et al. 2018]. Hence, it could be considered that only the surface filtration took place in PTFE media. Therefore, it would be more appropriate to study the surface filtration resistance using PTFE HEPA media than using glass fiber HEPA media which were generally used in previous relevant studies.

In addition, although various methods have been applied to dust cake porosity measurements [Aguiar and Coury 1996, Ito and Aguiar 2009, Elmøe et al. 2011, Liu et al. 2013], the measuring accuracy was still limited by the number of points measured, in particular when the thickness of a dust cake made of submicron/nanoparticles was less than 100 μm and the dust cake had a non-negligible surface roughness because of the rough surface of medium underneath. Moreover, in previous literatures, it was considered that the porosity of a dust cake remained unchanged during its formation, so only one measurement after loading dust was required. The changes in the thickness and porosity of a dust cake have been rarely studied during dust loading.

Therefore, to quantitively investigate the surface filtration resistance in the study reported in this Chapter, firstly resistance models for dust cakes made of monodisperse and polydisperse particles were respectively established based on the kinetic theory.

Secondly, a laser scanning porosity measuring system was set up to accurately monitor the changes in the thickness and porosity of a dust cake during its formation. Finally, dust loading experiments for PTFE media were conducted using monodisperse and polydisperse SiO_2 aerosols, when the changes in dust cake thickness and porosity were monitored and analyzed, and the models developed were validated using the experimental data with both monodisperse and polydisperse SiO_2 aerosols.

7.2 Theoretical models

Instead of using Stokes Law that cannot calculate the forces exerted on a specific area of a particle surface, the drag force of particles and shielding effects among neighboring particles in a dust cake were therefore evaluated using the kinetic theory. Fig 7.1 illustrates the shielding effect in a particle chain paralleled to flow direction in a dust cake formed during surface filtration.

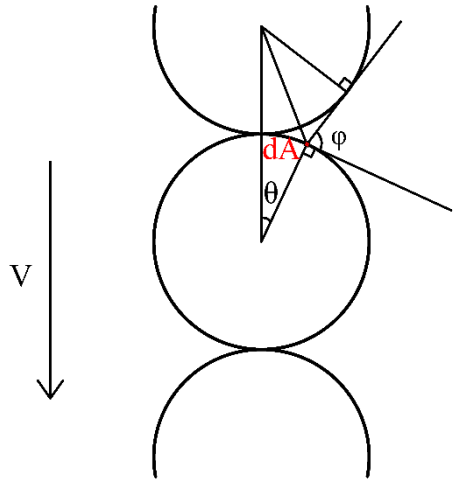

Fig 7.1 Schematic diagram of shielding effect in a particle chain

According to the rigid-body specular reflection hypothesis in the kinetic theory applied to evaluate molecules collisions on a surface [Bernardo et al. 2013], the impact force, dF_p, acting on a unit area of a particle, dA, at an angle of θ with the air flow direction can be expressed by

$$\mathrm{d}F_p = 2\rho_a V\sqrt{V^2 + \bar{c}^2}\cos\theta \mathrm{d}A \tag{7-1}$$

where ρ_a is air density, $\bar{c} = \sqrt{\frac{8k_B T_a}{\pi \bar{m}_a}}$ the average velocity of air molecules, k_B the Boltzmann constant, T_a the thermodynamic temperature of air, $\bar{m}_a$ the average mass of air molecules.

The impact force, dF_p, in Equation (7-1) was the sum of molecular collision from a normal semi-free space of dA. When the shielding effect between neighboring

particles was considered, the ratio between an effective corresponding space for dA and the semi-free space can be expressed as $\frac{\varphi}{\pi}$, which should also be taken as a correcting coefficient for dF_p, calculated as follows,

$$\frac{\varphi}{\pi} = \frac{3}{2} - \frac{1}{\pi}\left(\arccos\left(\frac{1-2\cos\theta}{\sqrt{5-4\cos\theta}}\right) + \arcsin\left(\frac{1}{\sqrt{5-4\cos\theta}}\right)\right) \tag{7-2}$$

As seen, $\frac{\varphi}{\pi} = 0$ when $\theta = 0$ and $\frac{\varphi}{\pi} = 1$ when $\theta = \frac{\pi}{2}$.

Then dF_p was corrected for the shielding effect as

$$\mathrm{d}F_p = 2\rho_a V\sqrt{V^2 + \bar{c}^2}\cos\theta\,\frac{\varphi}{\pi}\mathrm{d}A \tag{7-3}$$

For a single particle shielded by neighboring particles, its drag force, F_p, only came from the air flow direction since the horizontal drag forces were mutually canceled out. Then F_p can be obtained by integrating Equation (7-3):

$$\begin{aligned} F_p &= \int \mathrm{d}F_p\cos\theta \\ &= 2\rho_a {r_p}^2 V\sqrt{V^2 + \bar{c}^2}\int_0^{2\pi}\int_0^{\frac{\pi}{2}}\cos^2\theta\sin\theta\left(\frac{3}{2} - \frac{1}{\pi}\left(\frac{1-2\cos\theta}{\sqrt{5-4\cos\theta}}\right.\right. \\ &\qquad \left.\left. + \arcsin\left(\frac{1}{\sqrt{5-4cos\theta}}\right)\right)\right)\mathrm{d}\theta\mathrm{d}\psi \\ &= 0.788\pi\rho_a {r_p}^2 V\sqrt{V^2 + \bar{c}^2} \end{aligned} \tag{7-4}$$

In Equation (7-4), since V is far less than $\bar{c}$, so $\sqrt{V^2+\bar{c}^2}$ can be replaced by $\bar{c}$. Considering that the air velocity inside the dust cake can be increased to V/ε_c because the particles occupied some space but the air flow rate remained the same as that at cake inlet, and substituting r_p with d_p, the drag force was then evaluated by

$$F_p = \frac{0.197\pi\rho_a {d_p}^2 V\bar{c}}{\varepsilon_c} \tag{7-5}$$

The polydisperse particles making up the dust cake were assumed to have a lognormal distribution,

$$f(d_p) = \frac{1}{\sqrt{2\pi}\ln\sigma_g}\exp\left[-\frac{(\ln d_p - \ln d_{pg})^2}{2\ln^2\sigma_g}\right] \tag{7-6}$$

where d_{pg} is the geometric mean diameter, σ_g the geometric standard deviation.

Furthermore, assuming all the shielding effects caused by the contacts among particles in the dust cake were averaged as Equation (7-5), the sum of the drag forces on these particles was

$$F_c = \int_{\frac{1}{\infty}}^{\infty} \frac{0.197\pi\rho_a {d_p}^2 V\bar{c}}{\varepsilon_c} N_p f(d_p)\mathrm{d}(d_p) \tag{7-7}$$

where N_p is the number of particles in the dust cake.

Then a model for evaluating the resistance of the dust cake made of polydisperse particles was established as

$$\Delta P_c = \frac{F_c}{A} = \frac{0.197\pi\rho_a V\bar{c}N_p}{\varepsilon_c A}\int_{\frac{1}{\infty}}^{\infty} {d_p}^2 \frac{\exp\left[-\frac{\left(\ln d_p - \ln d_{pg}\right)^2}{2\ln^2\sigma_g}\right]}{\sqrt{2\pi}\ln\sigma_g}\mathrm{d}(d_p) \tag{7-8}$$

For a simplified case that the dust cake made of monodisperse particles, the relationship between particle number and dust cake mass, M_c, was

$$M_c = \frac{\pi}{6}N_p\rho_p {d_p}^3 \tag{7-9}$$

Therefore, a model for evaluating the resistance of a dust cake made of monodisperse particles was established as

$$\begin{aligned}\Delta P_c &= \frac{0.197\pi\rho_a {d_p}^2 V\bar{c}}{\varepsilon_c A}\cdot N_p \\ &= \frac{0.197\pi\rho_a {d_p}^2 V\bar{c}}{\varepsilon_c A}\cdot\frac{6M_c}{\pi\rho_p {d_p}^3} \\ &= \frac{1.182\rho_a\bar{c}}{\rho_p}\cdot\frac{VM_c}{\varepsilon_c d_p A}\end{aligned} \tag{7-10}$$

7.3 Experimentation methods

7.3.1 Size distributions of experimental aerosols

Table 7.1 shows the distributions of experimental aerosols. Three polydisperse aerosols were constructed using monodisperse aerosol SiO_2 of different particle sizes. For monodisperse aerosols, instead of using directly the technical specifications provided by their manufacturers, their distributions were calculated based on scanning electron microscope (SEM) photographs. As seen, SiO_2 aerosols used for monodisperse dust loading experiments had the geometric standard deviations of less than 1.25, which satisfied the required monodispersity [Japuntich et al. 1994].

Table 7.1 Particle size distributions of experimental monodisperse/polydisperse SiO_2 aerosols

	Particle diameter (manufacturers), nm	Geometric mean diameter (SEM), nm	Geometric standard deviation (SEM)
Monodisperse aerosol	50	52	1.13
	100	103	1.15
	300	310	1.19
	550	553	1.10
Polydisperse aerosol	-	305	1.25
	-	297	1.44
	-	314	1.65

7.3.2 Laser scanning porosity measuring system for dust cake

Considering that the accuracy for dust cake porosity measurement was inadequate due to limited measuring points used in previous studies [Cheng and Tsai 1998, Kim et al. 2009, Liu et al. 2013], a laser scanning porosity measuring system as shown in Fig 7.2 was developed to monitor the thickness and porosity of a dust cake during its formation. As seen, the measuring system consisted of a constant speed slider driven

by a stepper motor and a laser distance sensor having a resolution of 0.1 μm. During the back and forth movement of the slider along the diameter of the filter medium, the sensor monitored its distance from the filter medium, and the distance data were collected and recorded by a computer. For each medium, the number of distance data was around 1850 along the diameter. By comparing the distance data before and after a dust loading period, the changes in thickness along the filter medium diameter were determined and dust cake porosity calculated based on thickness distribution.

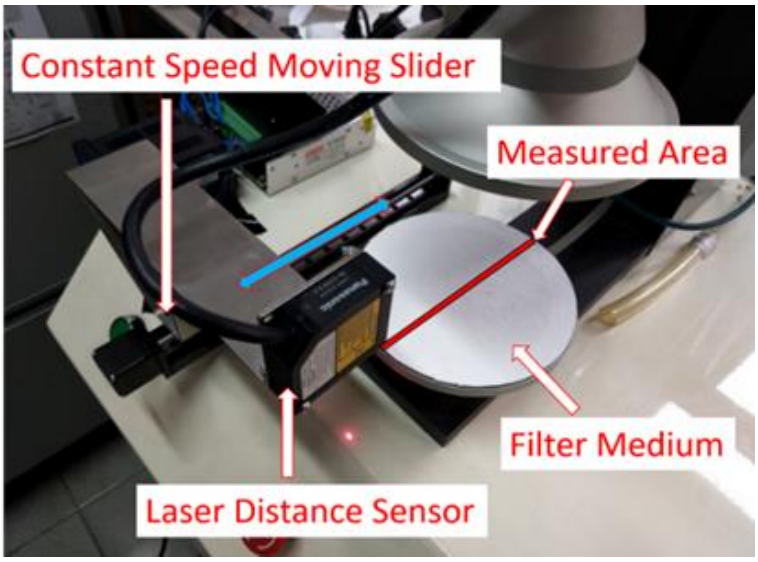

Fig 7.2 Laser scanning porosity measuring system

Furthermore, as shown in Fig 7.3, a metal gauze was placed on the lower holder and its air flow resistance may be considered as close to zero even at a very high face velocity. The filter medium was tightly sucked onto the metal gauze when the fan was operated and the thickness measured, avoiding the measuring error caused by the crimp or deformation of the filter medium.

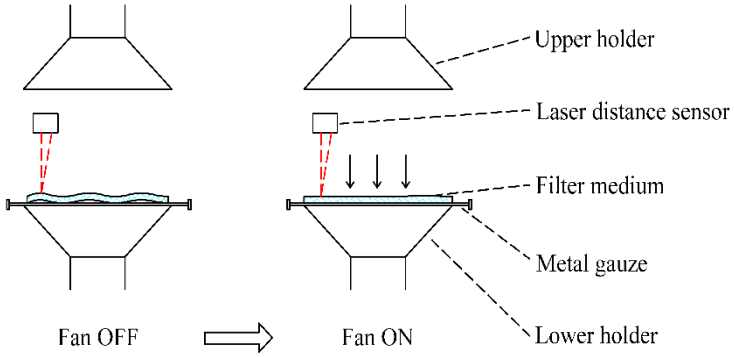

Fig 7.3 The metal gauze prevents deformation of filter media

In addition, Fig 7.4 illustrates an assumed thickness distribution for a dust cake. The dust cake was cut into two halves perpendicular to the measured area. In each half, the same thickness at the same radius distance as those on the measured area was assumed. Then, the area-weighted average thickness for each of half cakes may be calculated by taking each thickness data as the height of the half-ring area along the diameter.

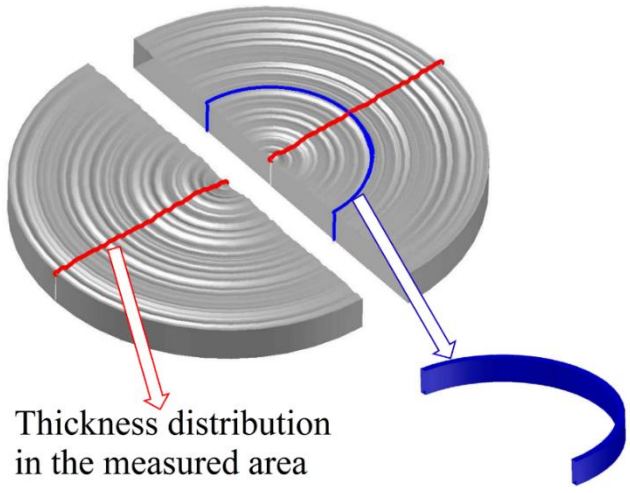

Fig 7.4 Diagram of a dust cake

Lastly, Fig 7.5 shows the thickness measurement results for an H14 glass fiber HEPA medium and an H14 PTFE HEPA medium, respectively. For each thickness measurement, over 1800 distance data were collected to area-weighted calculate the average thickness. Good reproducibility was demonstrated, ensuring the accuracy of porosity measurement.

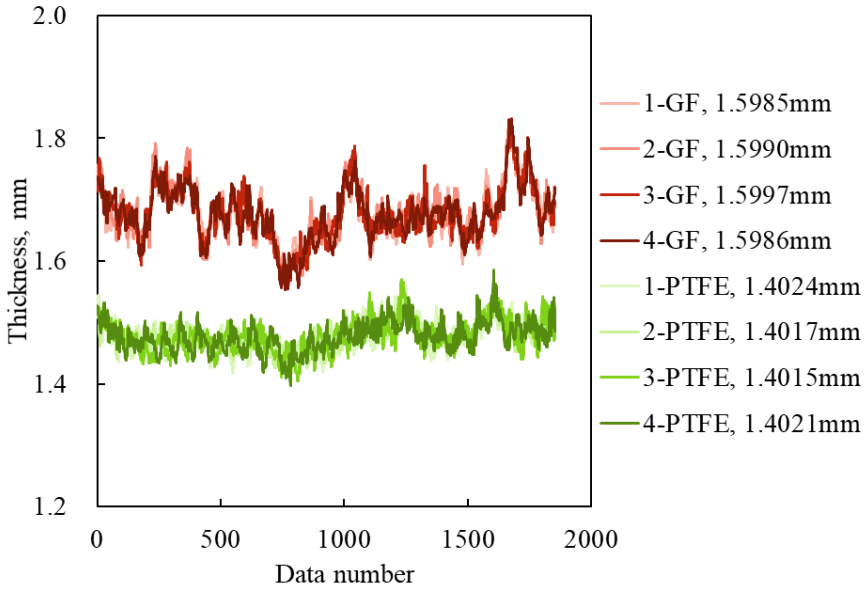

Fig 7.5 Thickness measurement results of two HEPA media

7.3.3 Experimental procedures

In some earlier studies, surface filtration was not distinguished from the whole filtration process [Aguiar and Coury 1996, Song et al. 2006], leading to considerable errors in studying dust cakes. Hence, the windward base materials of experimental

H14 PTFE HEPA media were removed to avoid its influence on dust cake porosity measurement.

The experimental air flow rate was set at 32 L/min, and the corresponding filtration face velocity at 5.33 cm/s. The relative humidity of the air flow was controlled at about 50%. The aerosol concentration was controlled at a level to allow that an experiment can be finished in 12 hours.

The initial air flow resistance and thickness distribution were measured before a filter medium was loaded with experimental aerosol. During a dust loading experiment, the resistance of the filter medium was real-time monitored and recorded. After each period of dust loading, the thickness distribution for the loaded filter medium was measured four times using the laser scanning porosity measuring system shown in Fig 7.2, when the filter medium remained stationary.

Prior to measuring the thickness distribution at each period, the air flow rate was adjusted so as to maintain the pressure drop at a set point for half an hour before and after opening the holders, to eliminate the influence of pressure drop changes during different dust loading period on the filter media thickness. The resistance of the loaded filter medium was found to remain unchanged before and after thickness measurement

during the experiments, suggesting that the dust cake structure was not affected by measurement operations.

Moreover, it was found that different pressures on a dust cake would not cause any changes in its thickness, so there was no dust cake compression mentioned in other studies [Aguiar and Coury 1996, Cheng and Tsai 1998]. The loaded dust mass was obtained after a dust loading experiment was ended. The gravimetric efficiency of HEPA media tended to be 100%. Hence, the loaded dust mass was directly proportional to the dust loading time duration at a stable aerosol concentration.

7.4 Results and discussions

7.4.1 Thickness and porosity of dust cakes

The laser scanning porosity measuring system was used to exam the thickness changes of dust cakes due to the deposit of monodisperse aerosols of different diameters of 52 nm, 103 nm, 310 nm and 553 nm, respectively, on the surface of PTFE membranes under the filtration velocity of 5.3 cm/s. The results are shown in Fig 7.6. To demonstrate the reliability of the porosity measuring system, a further baseline test without loading any dust was undertaken to exam the thickness changes for a PTFE

membrane under different resistances, which were realized through adjusting experimental air flow rate. As indicated in Fig 7.6 by the curve labeled “Without loading dust”, the pressure drop changes across the filter medium had no significant impact on the measurement results of its thickness.

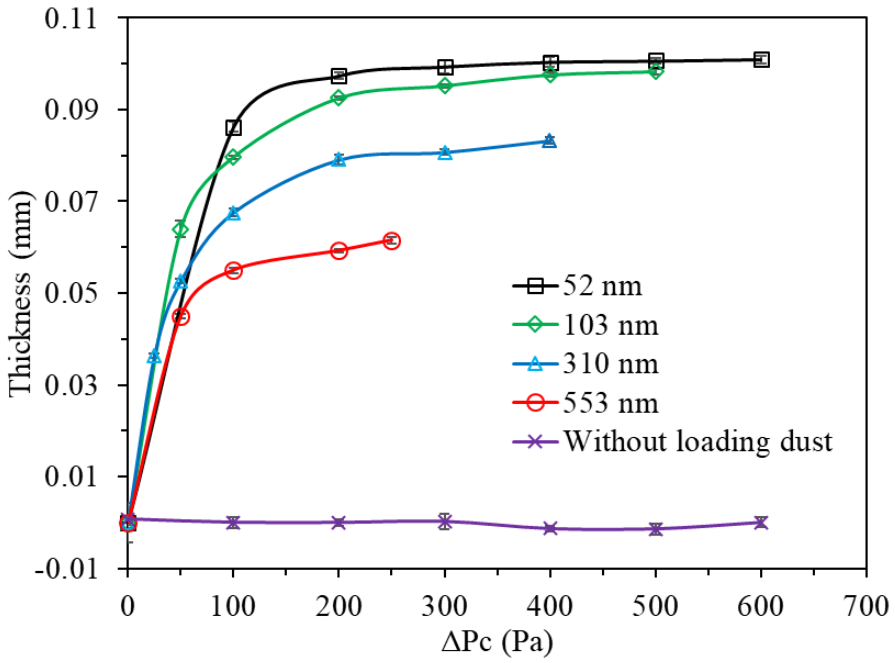

Fig 7.6 Thickness changes of dust cakes during the monodisperse aerosol loading process

As shown in Fig 7.6, the thickness of a dust cake grew non-linearly with the increase in loaded dust mass, but the rate of growth was gradually decreased and finally leveled as its resistance was increased. During dust loading, certain particles captured by the PTFE membrane deposited on top of the dust cake to promote thickness growth but the others went inside the cake. Initially, there were more particles on top of the dust

cake according to thickness measurement results and the dust cake structure was loose and thus easy to penetrate through. Later, the number of particles deposited inside the dust cake was increased gradually and that contributed to the thickness growth reduced. Finally, a balance between the number of particles deposited on top of the dust cake and that inside the cake was reached, to achieve stable micro growth in dust cake thickness.

This thickness growth speed slowing down can also be explained based on the study of Kasper et al. on the morphology and packing density of particles deposited on thin steel fibers using confocal microscopy [Kasper et al. 2010]. In their study, β was defined as the ratio of particle inertia to interception and used to distinguish the dust cake growth pattern. It was found that when β was increased (corresponding to the decrease in interception efficiency of dust cake top structures in the research work reported in this Thesis), the dendritic growth pattern of dust cakes was gradually changed to the compact growth one, i.e. the thickness growth speed was slowed down.

From Fig 7.6, it can also be seen that at the same increase in resistance, the dust cake formed with smaller particles had a greater thickness. This was because smaller particles had smaller inertia and stronger diffusion, and were therefore easily caught by the particle chains on top of a dust cake to promote thickness growth.

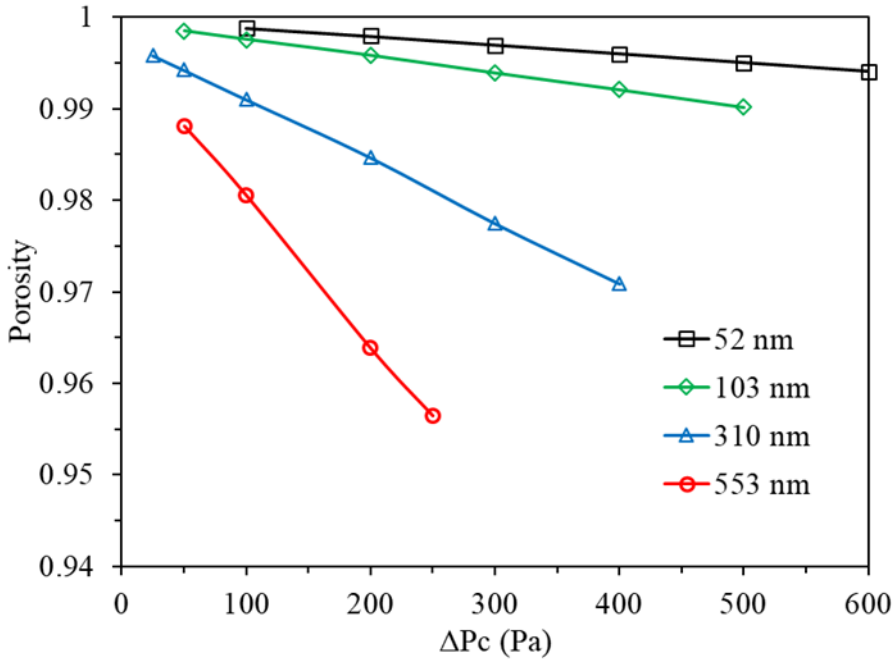

Fig 7.7 Porosities of dust cakes made of monodisperse aerosols of different diameters

The changes in dust cake porosities due to thickness changes were calculated using Equation (2-18) and are plotted in Fig 7.7. As seen, a dust cake formed by smaller particles had a larger porosity due to its greater thickness and smaller mass at the same increase in resistance. The porosities were decreased almost linearly with the resistance increase, which was easy to understand because as shown in Fig 7.6, the thickness growth rate for a dust cake slowed down and tended to be stable, while the loaded dust mass was increased linearly at a stable experimental aerosol concentration. Therefore, the decline trend in porosities of dust cakes should be linear according to Equation (2-18). In previous studies on the surface filtration, the thickness or porosity

of a dust cake was measured only once after a complete dust loading process, so the changes in its thickness and porosity were not investigated.

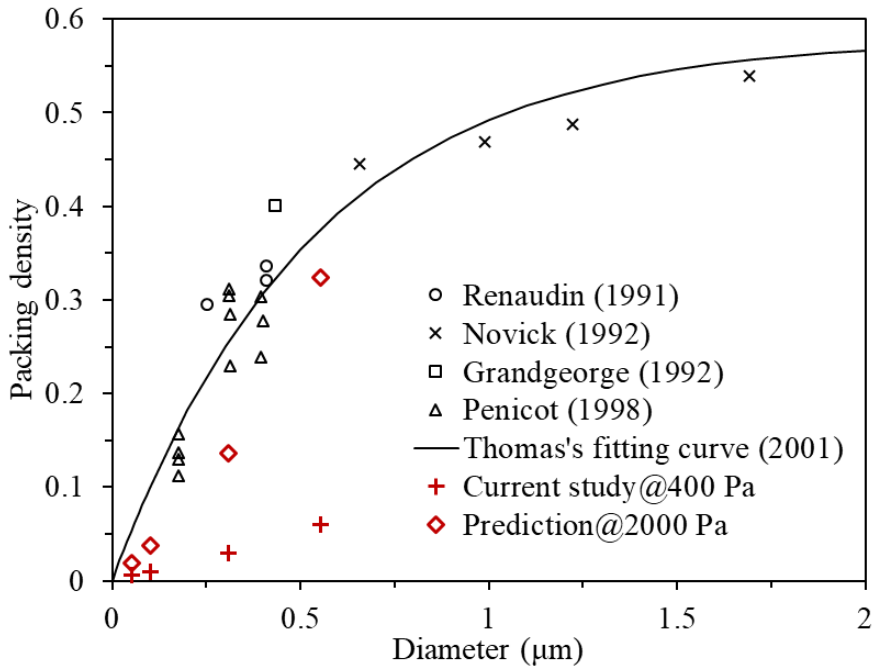

Fig 7.8 Packing densities of dust cakes and the comparisons with previous literatures

With reference to the previous experimental results by others, Thomas et al. presented a fitting curve relating the change in packing density to particle size [Thomas et al. 2001]. Fig 7.8 shows the experimental packing densities of dust cakes with different size particles at the resistance increase of 400 Pa and a face velocity of 5.33 cm/s in the research work. Fitting curve by Thomas and the packing densities obtained in previous studies are also shown in Fig 7.8. As seen, the experimental packing densities at different particle sizes obtained in the research work were far lower than those in

previous studies. However, it should be noted that the resistance growth in previous studies usually reached 2000 Pa or even to over 5000 Pa at 5.33 cm/s. As the change in porosity was related to an increase in dust cake resistance, a low load application as reflected by a low resistance would result in higher porosities and lower packing densities than a high load application. Therefore, if the porosity curves in Fig 7.7 may be linearly fitted, the packing densities of dust cakes with different particle sizes at 2000 Pa may be predicted.

In Fig 7.8, the predicted values and variation trend of the packing densities using the fitted linear relationship as marked by "Prediction @ 2000 Pa" were similar to the results from previous researches by others. Therefore, it can be concluded that the porosity and packing density of a dust cake formed during surface filtration were determined by dust loads, which should be taken into account when comparing and analyzing the porosity of a dust cake as well as building surface filtration resistance models.

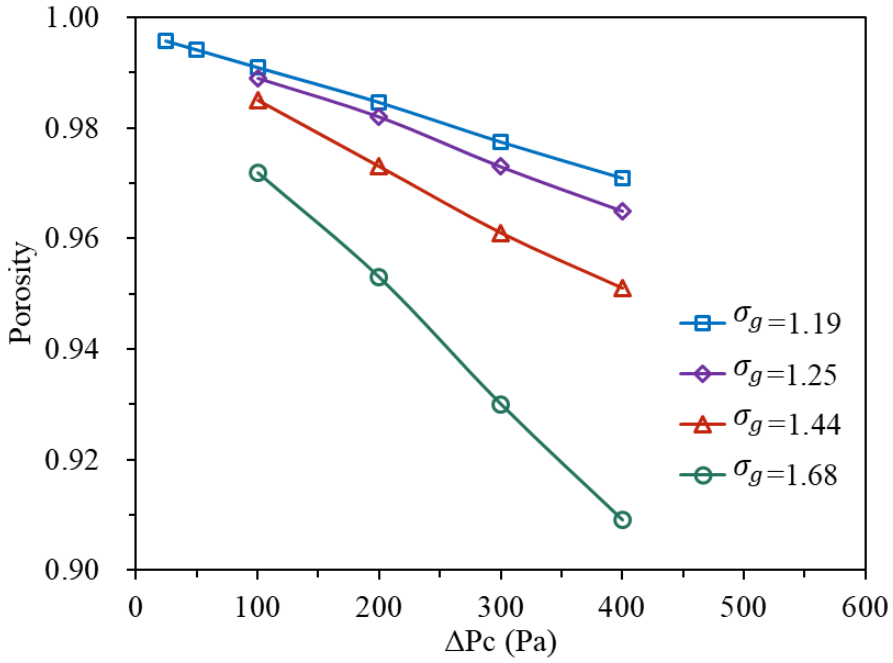

Fig 7.9 Porosities of dust cakes made of polydisperse aerosols with a geometric mean diameter of around 300 nm and different geometric standard deviations

The porosities were also evaluated for dust cakes formed from polydisperse aerosols with a geometric mean diameter of about 300 nm but with different geometric standard deviations. As seen from Fig 7.9, porosities of the dust cakes made of polydisperse particles showed an approximate linear decrease with the increase in resistance, which was the same as that for monodisperse aerosols.

The porosities of the dust cake with a greater geometric standard deviation, σ_g, were lower, but with a higher decline rate at the same level of resistance increase. This difference in porosity can be explained by the agglomeration effect. An increase in geometric standard deviation for aerosols led to an increase in particle size diversity

and more larger particles tended to deposit inside the dust cake and filled some gaps because of greater inertia, thus the agglomeration effect became more significant. This suggested that under the same loaded dust mass, a dust cake made of the aerosol of a larger geometric standard deviation had a smaller thickness and a larger packing density.

7.4.2 Evaluation of resistance for dust cakes made of monodisperse aerosols

The experimental surface filtration resistance curves of PTFE media loaded with monodisperse aerosols of different diameters are shown in Fig 7.10. As a parameter in the surface filtration resistance models, i.e., Equation (7-8) and Equation (7-10), the dust cake porosity was decreased with an increase in resistance according to the results shown in Fig 7.7, which further meant it was also decreased with an increase in loaded dust mass that was directly proportional to the resistance as shown in Fig 7.10. Therefore, formulas linking dust cake porosities with loaded dust mass were fitted and applied to the surface filtration resistance model for monodisperse aerosols, i.e., Equation (7-8). The pressure drops calculated based on the monodisperse model are also given in Fig 7.10.

As seen, the experimental resistances of dust cakes made of four monodisperse aerosols were increased almost linearly with an increase in loaded dust mass. A larger

particle size led to lower growth rates of resistance, which was consistent with the results from a previous study on monodisperse dust loading experiments [Song et al. 2006].

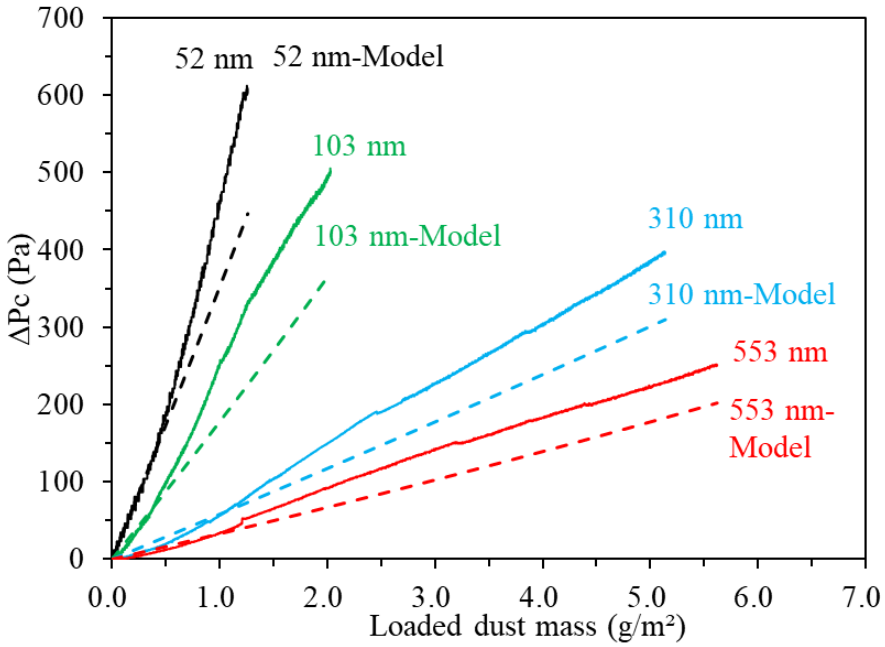

Fig 7.10 Experimental resistances for dust cakes made of monodisperse particles and its comparison with the monodisperse theoretical model

The calculation results for surface filtration resistances using monodisperse aerosols also showed linear variation trends with an increase in loaded dust mass. However, according to Equation (7-8), both a decrease in porosity and an increase in loaded dust mass would result in an increase in resistance, and the porosity was negatively correlated to the loaded dust mass. Consequently, a non-linear growth in resistance with an increase in loaded dust mass should be demonstrated, which was inconsistent with the linear variation trends in Fig 7.10. Nevertheless, as seen in Fig 7.7, the

porosities of dust cakes for the four monodisperse aerosols remained at > 0.9, thus the effect of the changes in porosity on the calculated results using the models for surface filtration resistance in this Chapter was not significant, and the linear trends can be adopted.

Table 7.2 Comparison between the dust cake resistances loaded with monodisperse aerosol and the model calculation

	Linear fitting coefficient for dust loading experiments, Pa/(g/m^2)	Linear fitting coefficient for model calculation, Pa/(g/m^2)	Ratio, experiment/model
52 nm	448.76	351.83	1.27
103 nm	249.26	180.16	1.38
310 nm	75.72	59.61	1.27
553 nm	45.22	34.97	1.29

According to Fig 7.10, the experimental resistances for the dust cakes made of four monodisperse aerosols were significantly greater than those calculated using the monodisperse model. The linear fitting coefficients for all eight curves shown in Fig 7.10 are listed in Table 7.2. As seen, the differences between the coefficients for experiments and those for model calculations were ranged between 27% and 38%.

It should be noticed that the resistance models in this Chapter were developed based on the rigid-body specular reflection hypothesis, which may not fully reflect the actual situation. According to a study on particle drag force for large Knudsen number situations [Li and Wang 2003], the specular reflection drag force should be corrected by a factor of $1+\pi/8$ if the diffuse reflection hypothesis was adopted, to bring the differences shown in Table 7.2 to within 10%. This suggested that after applying the correction factor, the diffuse reflection hypothesis may be better applied better to particle drag force evaluation in a dust cake. Consequently, the resistance models developed for the dust cake composed of both monodisperse and polydisperse particles were modified as Equation (7-11) and Equation (7-12), respectively, as follows,

$$\Delta P_c = \frac{1.595\rho_a \bar{c}}{\rho_p} \cdot \frac{VM_c}{\varepsilon_c d_p A} \tag{7-11}$$

$$\Delta P_c = \frac{0.266\pi\rho_a V\bar{c}N_p}{\varepsilon_c A} \int_{\frac{1}{\infty}}^{\infty} {d_p}^2 \frac{\exp\left[-\frac{\left(\ln d_p - \ln d_{pg}\right)^2}{2\ln^2\sigma_g}\right]}{\sqrt{2\pi}\ln\sigma_g} \mathrm{d}\left(d_p\right) \tag{7-12}$$

7.4.3 Evaluation of resistance for dust cakes made of polydisperse aerosols

For an aerosol with the lognormal size distribution, the relationship among its mass mean diameter, the geometric mean diameter and the geometric standard deviation was as follows[Xu 2014],

$$\lg {d_{pm}}^3 = \lg {d_{pg}}^3 + 10.362\lg^2\sigma_g \tag{7-13}$$

Therefore, the total number of particles in a dust cake, N_p, can be calculated using the cake mass and mass mean diameter of particles, and the polydisperse resistance model can be converted from Equation (7-12) to

$$\begin{aligned}\Delta P_c &= \frac{0.197\pi\rho_a V\bar{c}}{\varepsilon_c A}\cdot\frac{6M_c}{\pi\rho_p {d_m}^3}\cdot\int_{\frac{1}{\infty}}^{\infty}{d_p}^2\frac{\exp\left[-\frac{\left(\ln d_p-\ln d_{pg}\right)^2}{2\ln^2\sigma_g}\right]}{\sqrt{2\pi}\ln\sigma_g}\mathrm{d}(d_p)\\ &= \frac{1.182\rho_a V\bar{c}}{\varepsilon_c A}\cdot\frac{M_c}{\rho_p}\cdot\frac{1}{{d_m}^3}\int_{\frac{1}{\infty}}^{\infty}{d_p}^2\frac{\exp\left[-\frac{\left(\ln d_p-\ln d_{pg}\right)^2}{2\ln^2\sigma_g}\right]}{\sqrt{2\pi}\ln\sigma_g}\mathrm{d}(d_p)\end{aligned} \tag{7-14}$$

A coefficient relating to particle size distribution parameters was proposed to reflect their influences on the resistance growth rate for a dust cake as

$$\zeta(d_{pg},\sigma_g)=\frac{1}{{d_m}^3}\int_{\frac{1}{\infty}}^{\infty}{d_p}^2\frac{\exp\left[-\frac{\left(\ln d_p-\ln d_{pg}\right)^2}{2\ln^2\sigma_g}\right]}{\sqrt{2\pi}\ln\sigma_g}\mathrm{d}(d_p) \tag{7-15}$$

For aerosols with geometric mean diameters of 100 nm, 300 nm and 550 nm, Equation (7-15) was used to calculate the coefficients of $\zeta(d_{pg},\sigma_g)$ with geometric standard deviations from 1.1 to 2.0, and the calculation results are shown in Fig 7.11. The three coefficients corresponding to the three dust loading experiments conducted using aerosols with a geometric mean diameter of about 300 nm but different geometric standard deviations are also shown on the graph.

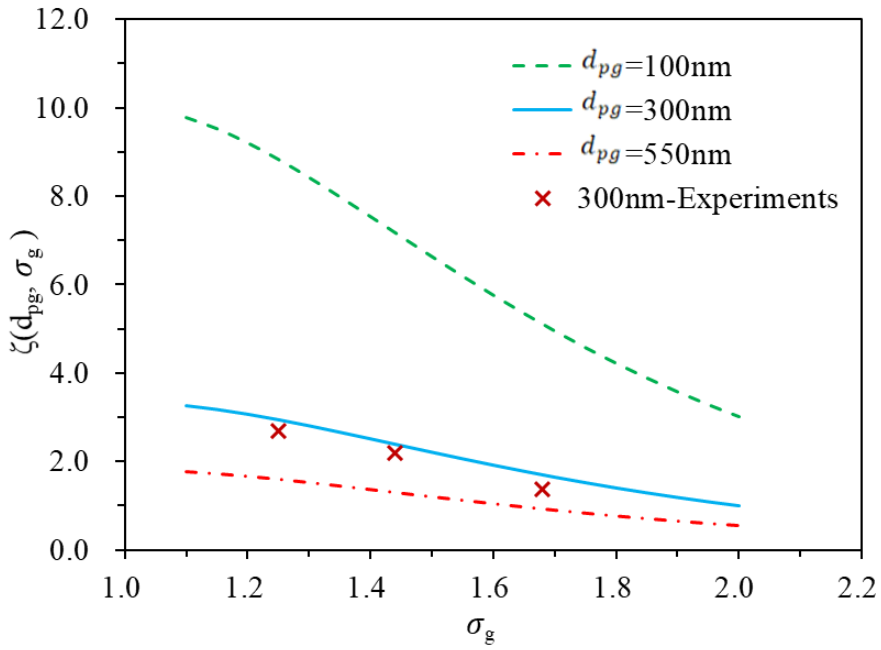

Fig 7.11 Influence of the polydispersity on the resistance of dust cakes -- theoretical calculation and experimental results

It can be seen from Fig 7.11 that for the aerosols with three different geometric mean diameters, the resistance growth rates were decreased dramatically with an increase in geometric standard deviation, indicating that aerosol polydispersity significantly impacted on the resistance growth rate of a dust cake. The coefficients based on the experimental results showed similar decreasing trends with an increase in the geometric standard deviation, but were lower than those calculated using Equation (7-15) for aerosols with a geometric mean diameter of about 300 nm. It seemed that with an increase in geometric standard deviation, the differences between the experimental and calculated coefficients were also increased. These differences may be determined by the agglomeration effect in the dust cake. It was assumed in the resistance models in this Chapter that each particle in a dust cake connected only two other particles upstream and downstream. However, the agglomeration of particles in a dust cake resulted in the shielding effect of some particles being far greater than that in the assumption. This meant that the actual effective drag force acting area for a particle was smaller than that used in assumption in the model, which was reflected in a macro way that the resistance for a dust cake was lower than that calculated by the models. The size diversity of particles was also increased with an increase in geometric standard deviation, leading to an increase in agglomeration effect. A similar pattern has been found in several previous dust cake simulation studies [Kim et al. 2009, Fu and Kang 2010].

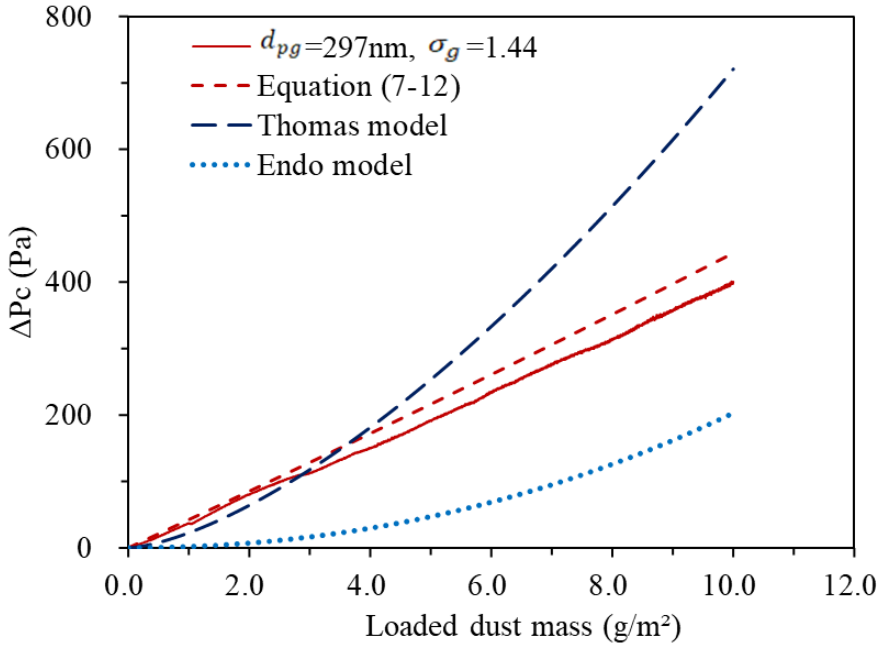

Fig 7.12 Comparison of dust cake resistances with different models for polydisperse aerosols

The experimental dust loading resistances for polydisperse aerosols with a geometric mean diameter of 297 nm and a geometric mean standard of 1.44 and the corresponding calculation results using Thomas model, Endo model and the polydisperse resistance model developed in this Chapter, i.e., Equation (7-12) are plotted in Fig 7.12. In the figure, C_o was taken as 0 for Thomas model, and $\varphi(\varepsilon) = 10(1-\varepsilon)/\varepsilon$ was assumed for Endo model.

As seen from Fig 7.12, the resistances calculated using the model for polydisperse aerosols developed in this Chapter demonstrated a linear growth with an increase in loaded dust mass and achieved the best agreement with the experimental results, as compared with the predictions by using other two models. The resistances calculated

using Endo model were significantly lower than the experimental results. According to Endo model, the calculation accuracy depended on the empirical coefficient $\varphi(\varepsilon)$ affected by the dust cake structure. Although Endo model showed good agreement with the experimental results when $\varphi(\varepsilon) = 10(1-\varepsilon)/\varepsilon$ was assumed for some applications [Elmøe et al. 2009], its practicability was inadequate for the research work reported in this Thesis.

Given 3.5^{th} power of porosity in Equation (2-17), Thomas model presented a much higher growth rate than a linear variation trend since the porosity of a dust cake was almost linearly decreased with an increase in dust loading mass. Furthermore, although the difference between the prediction by Thomas model and the experimental results was not significant initially, it was increased rapidly, with greater deviations from the experimental results when loaded dust mass was greater. It should be also noticed that Thomas model was built for the nanostructured dust cakes which were formed by nanoparticles and there may not be significant declines in the dust cake porosities as the dust load was much heavier, while the typical particle size for the general ventilation applications concerned in the research work reported in this Theis was submicron and varied from 0.05~0.5 μm.

In conclusion, as each resistance model has its applicability, for the surface filtration resistance in applications of general ventilation and clean air-conditioning, the model established in this Chapter demonstrated the best applicability.

7.5 Conclusions

The resistance performances for filter media during dust loading have received special attention because of its considerable influence on the energy consumption and life span of ventilation systems. In this Chapter, surface filtration resistance models were developed and experimentally validated. To monitor the changes in thickness and porosity for dust cakes during their formation, a laser scanning porosity measuring system was established and its accuracy and reproducibility demonstrated with over 1800 measuring points and the fact that the averaged values for HEPA media thickness in repeated tests were close one another. Using this system to monitor the formation process of a dust cake, it was found that an increase in the thickness of a dust cake was gradually decreased with an increase in loaded dust mass and finally leveled, and that the porosity was decreased linearly.

Moreover, the dust cake resistance models for both monodisperse aerosols and polydisperse aerosols were respectively developed by calculating the shielding effect of particles based on the kinetic theory. Experimental results using monodisperse

aerosol suggested the better applicability of using the rigid-body diffuse reflection hypothesis than the spectra reflection hypothesis in developing resistance models. The predictions by using the polydisperse model agreed better with the experimental results than that using the previous models by other researchers. The models developed in this Chapter provide a new approach to theoretically studying the filtration resistance, and could be applied to not only the surface filtration but also the complete process of filtration for fibrous filter media.

Chapter 8

Evaluation and optimization for the dust loading performance of PTFE HEPA media

8.1 Introduction

HEPA filters made of fibrous HEPA media have been used in many fields to maintain a super clean indoor air environment for various purposes, such as cleanrooms for producing semiconductor and LCD panels, nuclear power plants, bio-pharmacy and food processing and production facilities. During the service life of a HEPA medium, its filtration efficiency and resistance were simultaneously increased as dust was being loaded into the media. However, while little change in the filtration efficiency may be accepted due to its very high initial filtration efficiency at >99.95%, special attention should be paid to the increase in resistance which directly led to an increase in the energy consumption of a ventilation system and determined the lifespan of a HEPA filter.

Traditional glass fiber media has been commonly used as HEPA media. Recently, the PTFE HEPA media, which were usually applied to dedusting industry for the removal

of large particles in exhaust gas, have emerged as an alternative and gradually gained a certain percentage of market share because of their much lower initial resistance, as compared to that of glass fiber at the same efficiency class.

The dust loading performance of a HEPA medium referred to its dynamic resistance and energy consumption at a fixed amount of loaded dust mass. There have been a number of studies investigating the dust loading performance of glass fiber HEPA filters and HEPA media loaded with solid particles. However, there has been very limited research work reported in the open literature that focused on the dust loading performances of PTFE HEPA media. It is noted that the users of Fan Filter Unit (FFU) in the mainland China were always concerned about the experimental energy consumption comparison between PTFE HEPA media and glass fiber HEPA media and would expect a quantitative comparison result. But until now no tests for energy consumption and no developed evaluation methods for HEPA filters and media have been reported in the existing literature.

On the other hand, although PTFE HEPA media had a much lower initial resistance, their resistance growth rate may be higher than that of glass fiber HEPA media due to their sandwiched structure. Therefore, PTFE HEPA media can only be used in low dust load applications, where upstream air filters with a high efficiency were required. If the dust loading performance of PTFE HEPA media was improved, i.e., their

resistance growth rate was lowered, the energy consumption of PTFE HEPA media can be reduced and their applications expanded.

Therefore, the research work presented in this Chapter focused firstly on proposing an evaluation method for dust loading performance of HEPA media. A life span energy consumption model for HEPA media was built in the method. Secondly, the evaluation method was used to compare the dust loading performance between a glass fiber HEPA medium and a PTFE HEPA medium at the same filtration efficiency class. Lastly, composite PTFE HEPA media were developed for improving the dust loading performance of PTFE HEPA media.

8.2 Evaluation method for dust loading performance of HEPA media

Although the initial resistance and filtration efficiency of HEPA filter media have been extensively investigated, there were no standards and systematic research work on the evaluation method for the dust loading performance of HEPA filter media in the present literature. Therefore, based on the research work reported in Chapters 4~7, an evaluation method for the dust loading performance of HEPA media has been proposed from the following three aspects: the applicability of experimental aerosols, an experimental setup and procedures, and an energy consumption model for HEPA media.

8.2.1 Applicability of experimental aerosols

It has been reported in Chapter 5 that, an increase in air flow humidity would lead to an irreversible decrease in the resistance of a fibrous medium loaded with particles that were able to absorb moisture. On the other hand, due to the effect of particle diameter on the resistance of fibrous media, the loaded dust masses at the same final resistance could differ greatly for fibrous media loaded with particles of different average diameters. Therefore, the applicability of experimental aerosols including the humidity sensitivity and the size distribution should be specified and examined when evaluating dust loading performance of HEPA media.

The humidity sensitivity of an experimental aerosol can be examined by a pre-experiment. In the pre-experiment, the experimental aerosol was used to conduct dust loading for a HEPA medium at a fixed relative humidity of experimental air flow. When the resistance of the HEPA medium was increased to 150% of the initial value, the relative humidity of the experimental air flow was increased by about 10%. If the medium resistance was decreased significantly, the experimental aerosol was regarded as being humidity sensitive. When humidity-sensitive aerosols were used for dust loading of HEPA media, the relative humidity of experimental air flow should be controlled at a preset level, with a fluctuation of less than 3%.

The size distribution of experimental aerosols should refer to that of the challenge aerosol for HEPA media in the actual use environment[EN 2012]. Since a HEPA filter was commonly used with an upstream coarse filter and an upstream efficient filter, the size distribution of the atmospheric aerosol filtered firstly by a G3 medium and then an F7 medium was measured. The measurement began at 8:00 and ended at 17:00 and the aerosol concentration was averaged at each size range. Fig 8.1 shows the measured distributions. As seen, the filtered atmospheric aerosol was basically distributed in the size range of less than 1.0 μm and its concentration distribution was narrower than its mass distribution.

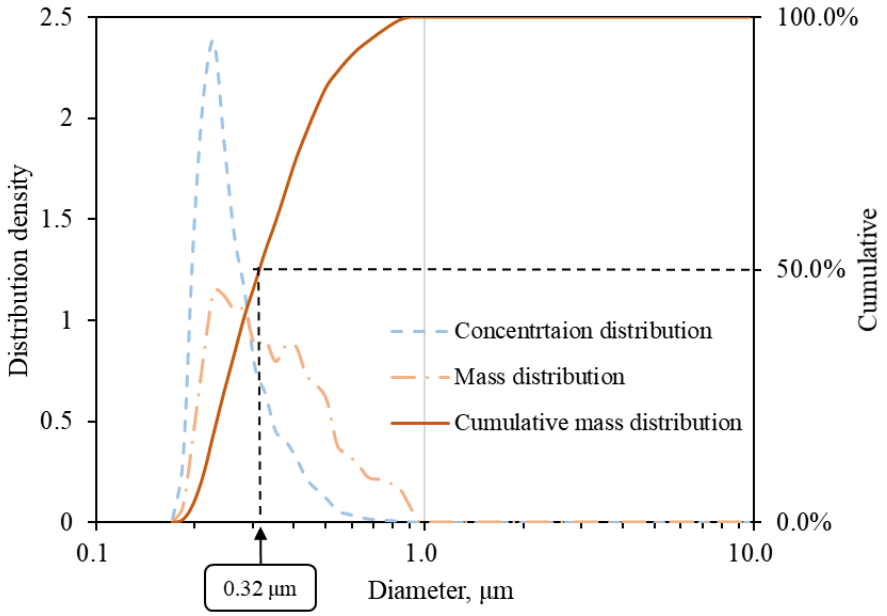

Fig 8.1 Size distribution of the atmospheric aerosol filtered by a G3 medium and an F7 medium

Since the MPPS of the efficient filter was about at 0.4 μm, in order to avoid the significant effect of large particles on the loaded dust mass of HEPA media, the experimental aerosol should have a mass median diameter, D_{50}^{V}, of less than 0.4 μm, which may be further used as a standard specification. In Fig 8.1, the value of D_{50}^{V} of the filtered atmospheric aerosol was at 0.32 μm, which was also consistent with the specification for the size distribution of the challenge aerosol.

When the pressure of compressed air in the aerosol generation bypass was set to 120 kPa and that in dry air bypass 20 kPa, the value of D_{50}^{V} of the experimental KCl aerosol generated using the aerosol generator of the experimental setup reported in Chapter 4 and the KCl solution with the mass concentration of 1% was at 0.38 μm. Then, this experimental KCl aerosol can be used in the evaluation for dust loading performance of HEPA media when the relative humidity of experimental air flow was controlled at a preset level with a fluctuation of less than 3%.

8.2.2 Experimental setup and procedures

The experimental setup reported in Chapter 4 was able to meet the experimental requirements for the desired evaluation, but the following procedures should be followed.

1) Getting ready the qualified experimental aerosol and the corresponding generator;

2) Opening the holders in experimental setup and examining the accuracy of resistance measurement for the setup;

3) Cutting the tested HEPA medium to the size suitable for the holders and measure its initial mass at the temperature and humidity of the experimental air flow, with an accuracy of 0.1mg;

4) Installing the tested HEPA medium in the experimental setup, adjusting the rate of experimental air flow to a preset value and recording the initial resistance of the HEPA medium, and adjusting the relative humidity of experimental air flow at a level of less than 65%. When the experimental aerosol was sensitive to the changes in relative humidity, the relative humidity should be more accurately controlled with a fluctuation of less than 3%;

5) Generating the experimental aerosol at a stable concentration to load the tested HEPA medium and recording real-time the medium resistance and aerosol concentration;

6) Shutting down the aerosol generator when the final resistance reached and measuring the final mass of the tested HEPA medium. The final resistance can be set at 2-3 times of the initial one according to the actual applications of the tested HEPA medium.

8.2.3 Energy consumption model of HEPA media

So far there have not been international or regional standards to evaluate the dust loading performances of HEPA filters. Manufacturers and end-users generally regarded loaded dust mass in actual use as a reference to describe the durability of a HEPA filter. However, dust loading capacity only reflected the dust mass containing by a HEPA filter at its final resistance under experimental conditions without taking the energy consumption performance into consideration. Therefore, it became worthwhile to study the energy consumption performances for HEPA filters.

The flow resistance of HEPA filters generally included both HEPA media resistance and structure resistance. The latter usually accounted for only a small percentage of the total resistance and remained unchanged during its entire service life. Hence, energy consumption comparison among HEPA filters based on their dynamic resistance should be acceptable.

The European Ventilation Association's Standard, EUROVENT 4/21: 2018 Energy efficiency evaluation of air filters for general ventilation purposes, provided a model for calculating the energy consumption of filters for general ventilation based on laboratory test results. This model was applied to evaluating the energy consumption performance of HEPA media presented in this Chapter.

The energy consumption of a HEPA medium can be evaluated as follows,

$$W_t = \frac{q_v \int_0^t \Delta P dt}{\eta \cdot 1000} = \frac{q_v t \overline{\Delta P_t}}{\eta \cdot 1000} = \frac{q_v m \overline{\Delta P_m}}{\eta \cdot 1000} \quad (8\text{-}1)$$

where W_t is the total energy consumption of a HEPA medium, q_v the rated air flow rate, ΔP the dynamic resistance, η the fan efficiency, t the run time, $\overline{\Delta P_t}$ the time averaged resistance, m the loaded dust mass, $\overline{\Delta P_m}$ the mass averaged resistance.

Since other parameters in Equation (8-1) were constant, the mass averaged resistance can be used to evaluate the energy consumption performance for HEPA media.

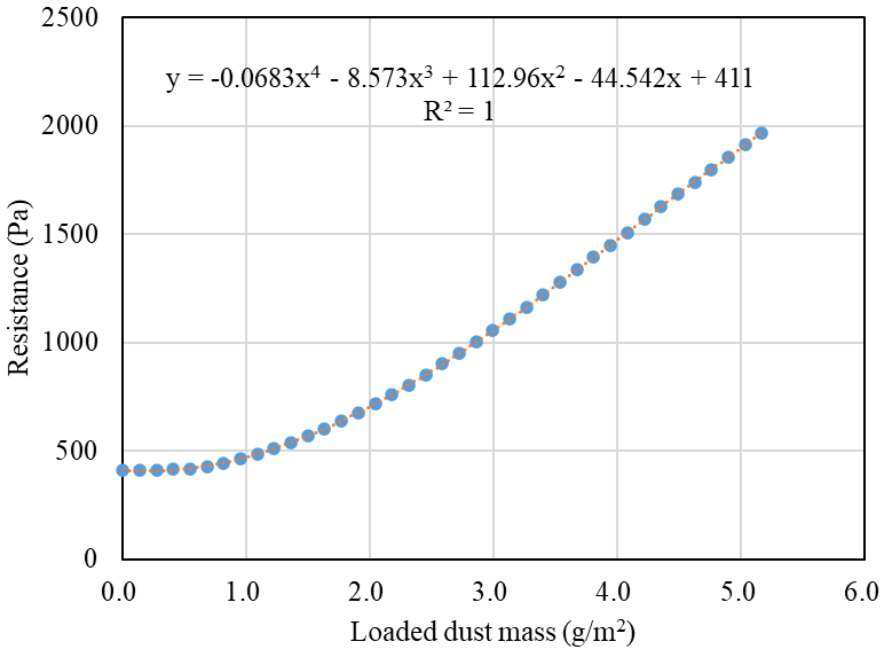

Fig 8.2 Resistance curve for a HEPA medium

In order to calculate the mass averaged resistance, a polynomial fitting can be made for the resistance curve of a HEPA medium during dust loading, as shown in Fig 8.2. The expression of the fitting was as follows,

$$\Delta P(m) = a \cdot m^4 + b \cdot m^3 + c \cdot m^2 + d \cdot m + \Delta P_0 \qquad (8\text{-}2)$$

where $\Delta P(m)$ is medium resistance at loaded mass m, a, b, c, d the fitting parameters.

Then the mass averaged resistance of a HEPA medium can be evaluated as follows.

$$\overline{\Delta P_m} = \frac{1}{M_f}\int_0^{M_f} \Delta P(m)dm = \frac{1}{5}a \cdot {M_f}^4 + \frac{1}{4}b \cdot {M_f}^3 + \frac{1}{3}c \cdot {M_f}^2 + \frac{1}{2}d \cdot M_f + \Delta P_0 \quad (8\text{-}3)$$

where M_f is the final loaded dust mass of the medium.

In summary, an evaluation method for dust loading performance of HEPA media was developed, based on the research work reported in Chapters 4~7 from three aspects: the applicability of experimental aerosol, experimental setups and procedures, and the evaluation method of energy consumption. It was considered in this method that the particle size distribution of experimental aerosols and the sensitivity of aerosols to the change in relative humidity of experimental air flow to eliminate the possible errors caused by the experimental aerosols. In addition, using energy consumption to reflect the dust loading performance for HEPA media would be better than using the dust loading capacity.

8.3 Dust loading performance comparison between PTFE HEPA media and glass fiber HEPA media

8.3.1 Resistance curves and filtration stage comparison

The evaluation method presented in Section 8.2 was used to evaluate and compare the dust loading performance between a glass HEPA medium and a PTFE HEPA medium, and the comparison results are presented in this Section. Dust loading experiments for an H14 glass fiber medium and an H14 PTFE medium were conducted at 5.3 cm/s filtration velocity and the final resistance was set at 900 Pa. In Fig 8.3, the SEM photos for loaded H14 glass fiber medium and H14 PTFE medium are compared, and in Fig 8.4, the obtained resistance curves for the two HEPA media illustrated.

Earlier studies indicated that in the preliminary dust loading stage for a glass fiber HEPA medium, part of particles may deposit on the surface of medium while others can easily penetrate the surface into the depth of the medium due to the porous structure of the glass fiber medium. However, as the growing dendritic particle fibers gradually filled up the space among fibers, it became harder for particles to arrive at the further depth of the medium. Then depth filtration turned into surface filtration and a dense dust cake can be formed. As shown in the SEM photos for the loaded glass

fiber medium in Fig 8.3 (a), Fig 8.3 (c) and Fig 8.3(e), after a long-time deposition, the dust particles captured by the glass fiber medium formed dendritic dust fibers inside the medium and a dust cake on the medium surface.

By contrast, the dust loading process for the PTFE medium was very different from that for the glass fiber medium. In Fig 8.3(b), no dust cake can be found on the surface of the PTFE medium. However, with an enlarged view shown in Fig 8.3(d), it is seen that the upper coarse fibers of base material contributed little to filtrating particles because of their much larger diameter and lower packing density, so that most of the particles were deposited on the surface of PTFE membrane. Fig 8.3(f) shows a profile SEM photo of a loaded PTFE medium whose windward base material was removed. As seen, the PTFE membrane was extremely thin and effective so that particles were deposited directly on the membrane rather than into it.

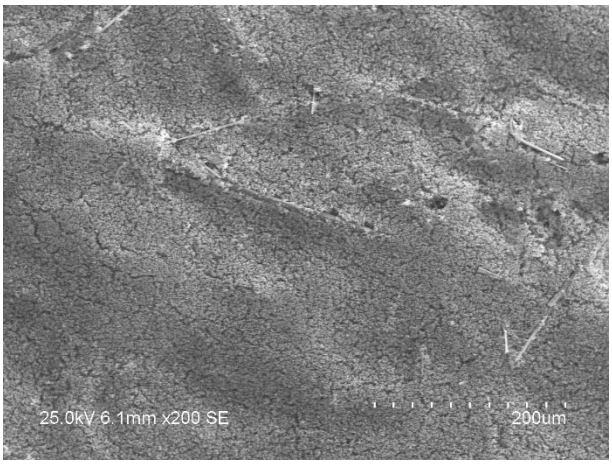

(a) Surface of the loaded glass fiber medium

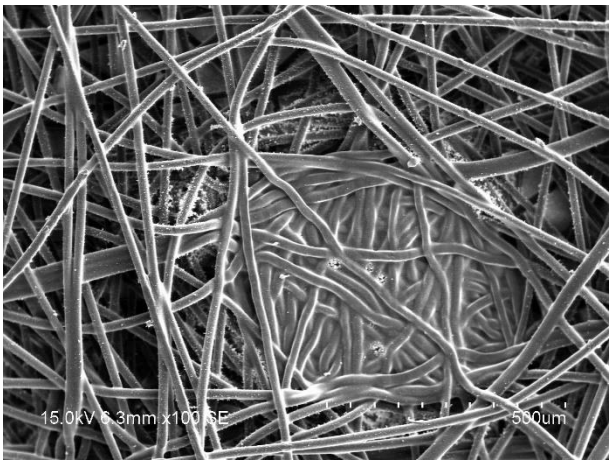

(b) Surface of the PTFE fiber medium

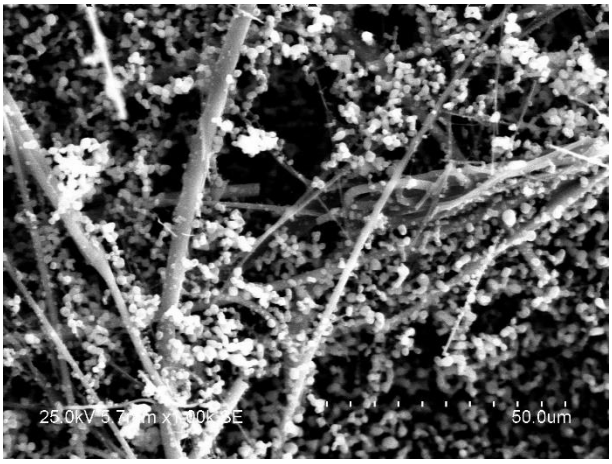

(c) Depth of the loaded glass fiber medium

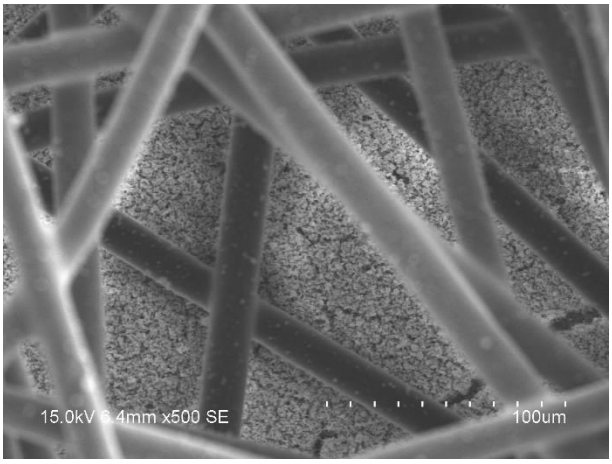

(d) Depth of the loaded PTFE medium

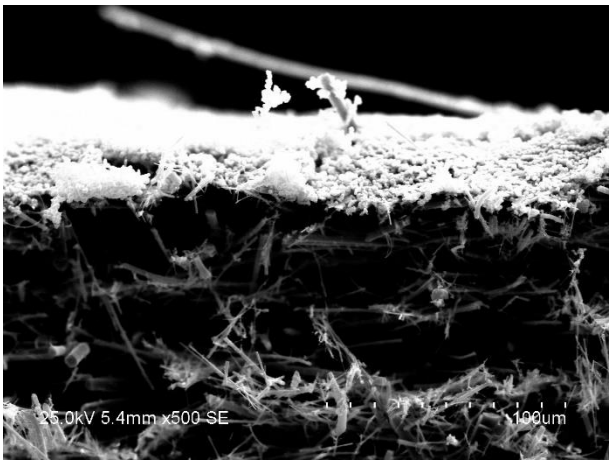

(e) Profile of the loaded glass fiber medium

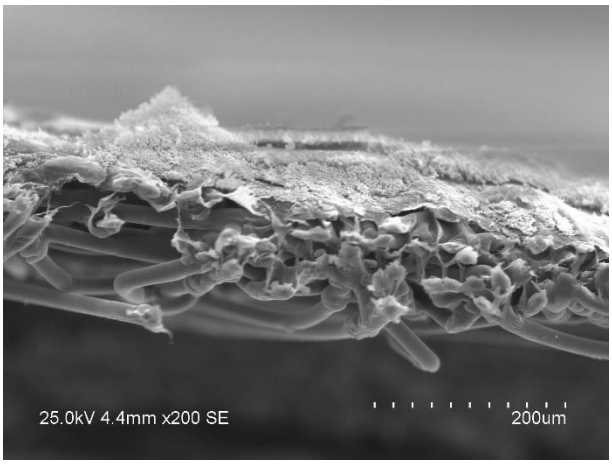

(f) Profile of the loaded PTFE medium

Fig 8.3 SEM photos of H14 glass fiber/PTFE media after being loaded with KCl solid particles

It can be seen from the resistance curve for the H14 glass fiber medium shown in Fig 8.4 that, the resistance of the glass fiber medium was increased with an increase in the amount of particles deposited on it. The rate of increase was small initially, but became gradually great, which was also consistent with the results in earlier studies. However, the resistance curve for the PTFE medium was almost a straight line, which was different from that of the glass fiber HEPA medium. This suggested that the resistance of PTFE media was increased uniformly and the filtration stage remained unchanged during the whole process of dust loading. From the above micro-observation results for the loaded H14 PTFE medium, it can be inferred that only one filtration stage existed during dust loading for PTFE media, i.e., surface filtration.

The resistance of the H14 PTFE medium was increased linearly with an increase in the loaded dust mass, and its rate of resistance growth was always higher than that of the H14 glass fiber medium. Therefore, although the initial resistance of the H14 PTFE medium was far lower than that of the H14 glass fiber medium, the resistance of the H14 PTFE medium actually exceeded that of the H14 glass fiber medium when the loaded dust mass reached 3 g/m^2.

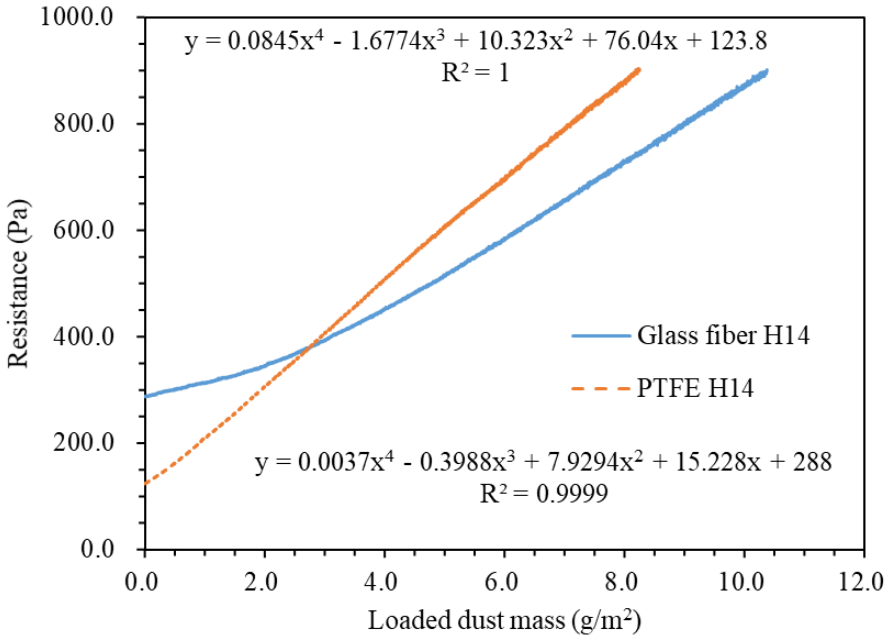

Fig 8.4 Resistance curves of H14 glass fiber medium and H14 PTFE medium

8.3.2 Average resistance comparison

Fig 8.5 shows the mass averaged resistance curves of the two tested H14 media under different loaded dust masses, where the mass averaged resistance was evaluated using Equation (8-3). It can be seen from Fig 8.5 that the growth rate for the mass averaged resistance of the H14 glass fiber medium was increased slowly but that of the H14 PTFE medium stayed almost constant. The mass averaged resistance of H14 PTFE medium was firstly less than, but finally greater than that of H14 glass fiber medium when the loaded dust mass exceeded 6 g/m^2 and the gap between them became wider thereafter. Thus, it can be concluded that the advantage of using H14 PTFE media for

low energy consumption was obvious at low dust loading or short-term use conditions, otherwise, the use of H14 glass fiber media would be more energy efficient.

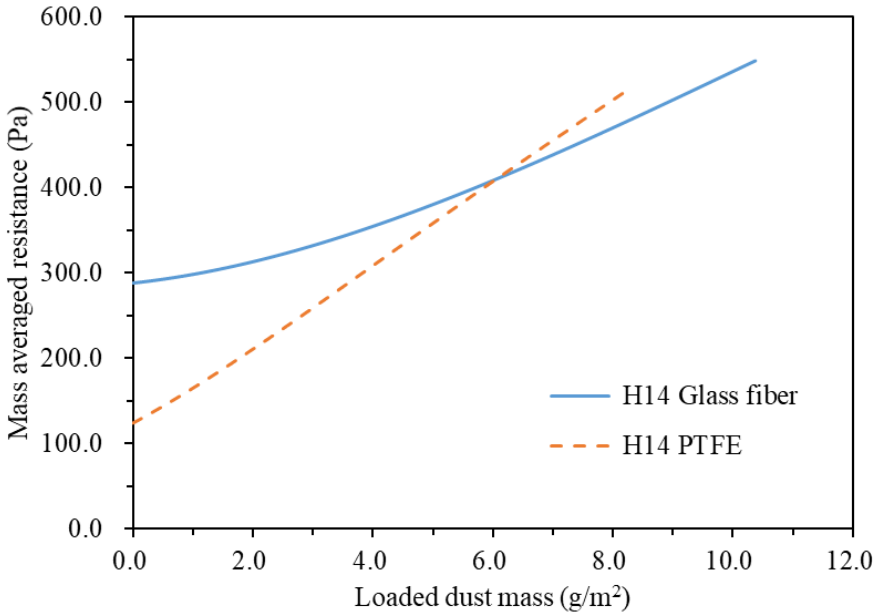

Fig 8.5 The mass averaged resistance curves for the tested H14 glass fiber medium and H14 PTFE medium

Although PTFE media had about 50% lower initial resistance than glass fiber HEPA media, the evaluation results for their mass averaged resistances revealed that, the use of PTFE HEPA media may not be more energy efficient than the use of glass fiber HEPA media as shown in Fig 8.5, due to the higher growth rate of resistance. If the dust loading performances of the PTFE media were improved, the applications of the PTFE medium can be significantly expended and the energy consumption by cleaning air-conditioning systems lowered.

8.4 Developing composite PTFE media

The composite filter media with gradient structures used in the mainland China were firstly designed by Shen [2006] and applied to the flue gas purification for coal-fired power plants. The filtration performances of these composite media were experimentally tested [Yan 2006, Liu and Xu 2009, Liang and Shen 2010] and their production methods investigated [Huangfu 2015, Zhang et al. 2016]. The composite media with gradient structures have also been used in the purification of indoor air [Zhou 2015]. However, these media were designed to filtrate large particles, and dust cakes were formed quickly, and the formed dust cakes used to filtrate particles. Therefore, the composite media with gradient structures cannot be applied to cleaning air-conditioning systems that were to having relatively small particles. However, the method of compositing media for the filtration performance optimization of fibrous media may be a good reference for enhancing the dust loading performance of PTFE media.

8.4.1 Windward base material for composite PTFE media

According to Section 8.3, the resistance growth rate of PTFE HEPA media was higher than that of glass fiber HEPA media at the same filtration efficiency class. Since the

windward base materials of PTFE HEPA media had almost no contribution to capturing particles, a composite PTFE medium could be constructed by using a medium with a fixed filtration efficiency as the windward material of a PTFE medium, so as to reduce the number of particles deposited on the PTFE membrane to form a dust cake. Glass fiber media and electret media may be considered as the windward base materials for composite PTFE media.

Electret media referred to the fibrous filter media made of fibers with static electricity inside or on the surface [Cao 2007], which had a relatively low initial resistance and high filtration efficiency. Although the filtration efficiency of electret media would be decreased due to the effect of deposited particles on fiber static electricity during dust loading, the filtration efficiency of a composite PTFE medium with a windward electret medium can also be guaranteed by the PTFE membrane.

Fig 8.6 shows the filtration efficiency curves for the original windward base material of an H14 PTFE medium, an electret medium and an F7 glass fiber medium, respectively, at a filtration velocity of 5.3 cm/s. As seen, the original windward base material had no significant filtration effects for particles, which was consistent with the SEM observation results shown in Fig 8.3. By contrast, the glass fiber medium had very high filtration efficiencies for particles within all relevant size ranges and

filtration efficiencies of the electret medium were overall higher than that of the glass fiber medium.

Fig 8.7 compares the initial resistance curves for the above mentioned three media. It can be seen that, the original windward base material had an initial resistance of only about 2 Pa at a filtration velocity of 5.3 cm/s, contributing little to the initial resistance of an H14 PTFE medium of about 120 Pa. Although the initial resistance of the electret medium was significantly higher than that of the original windward base material at the same filtration velocity, it was much lower than that of the glass fiber medium, suggesting that the electret media had lower initial resistances but higher filtration efficiencies than the glass fiber media. Therefore, the electret media were chosen as the windward base material of the composite PTFE media.

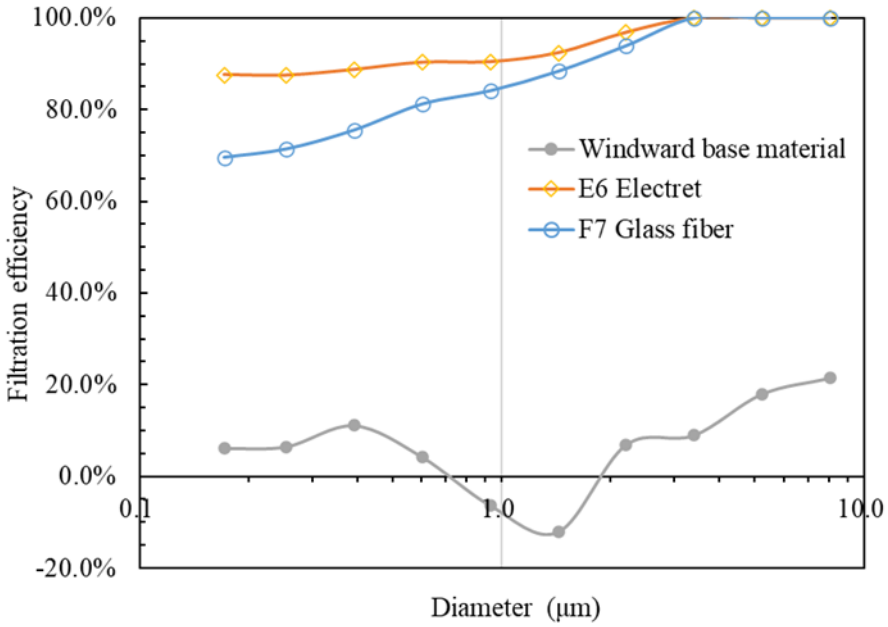

Fig 8.6 Filtration efficiency curves for the original base material of an H14 PTFE medium, an electret medium and an F7 glass fiber medium

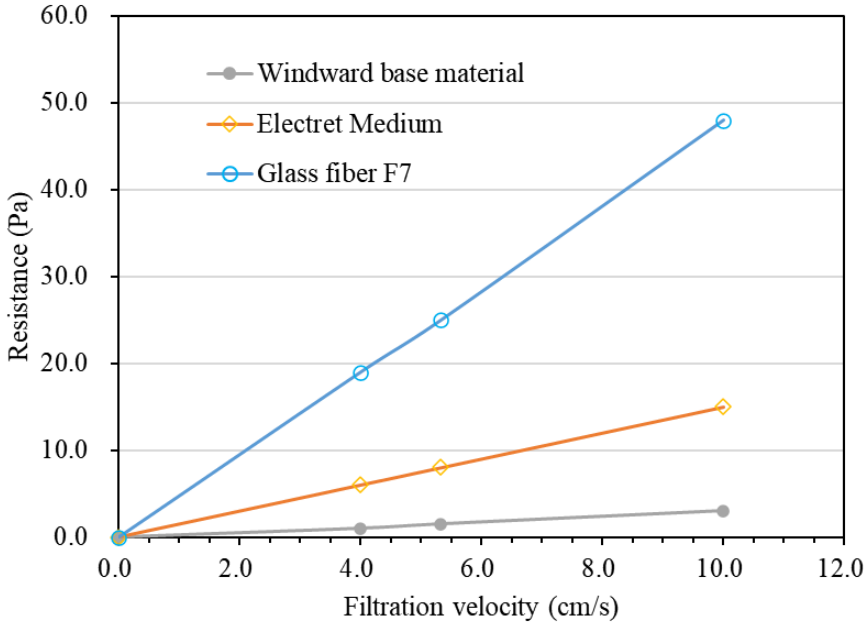

Fig 8.7 Initial resistance curves for the original base material of an H14 PTFE medium, an electret medium and an F7 glass fiber medium

8.4.2 Dust loading performance of composite PTFE media

The method proposed in Section 8.2 can also be used to evaluate the dust loading performance of the composite PTFE media. To investigate the initial filtration efficiency of the electret media on the dust loading performance of composite PTFE media, three electret media named “Electret Low”, “Electret Medium” and “Electret Efficient” were respectively used as the windward base material of composite PTFE media. The three media had their initial filtration efficiencies of over 65%, 90% and 95% for 0.4 μm particles, respectively. Fig 8.8 illustrates the resistance curves for three composite PTFE media during dust loading and also those for an H14 glass fiber medium and an H14 PTFE medium.

As seen, the loaded dust masses at the final resistance of 900 Pa for three composite PTFE media were all greater than that of the H14 PTFE media, meaning that the dust loading performances of PTFE media were significantly improved by being composited with the electret media. Moreover, the resistances of PTFE media composited respectively with the “Electret Medium” medium and the “Electret Efficient” medium were always less than that of the H14 glass fiber medium at the same amount of loaded dust mass. This implied that these two composite PTFE media could be always more energy efficient than the H14 glass fiber medium, thus removing the application limits for PTFE HEPA media.

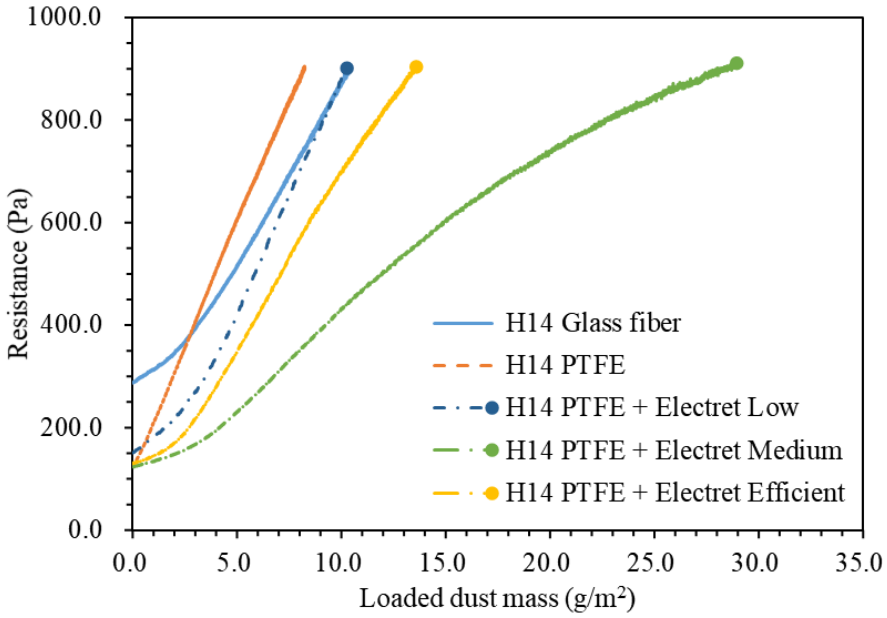

Fig 8.8 Resistance curves for three composite PTFE media, an H14 PTFE media and an H14 glass fiber media during dust loading

It can also be seen from Fig 8.8 that, although the resistances of PTFE media composited with the "Electret Low" medium or "Electret Efficient" medium were lower than that of the H14 PTFE media at a fixed loaded dust mass, they were higher than that of the PTFE composited with the "Electret Medium" medium. The filtration efficiency of an electret medium with a low filtration efficiency may be quickly weakened when its static electricity was eliminated. Hence, such an electret medium may not be able to provide effective protection for the PTFE membranes. However, an electret medium with a high filtration efficiency may be easily clogged by deposited particles and surface filtration would take place, leading to a higher growth rate of

resistance. Therefore, these two electret media would be less appropriate for compositing PTFE media than that named “Electret Medium”.

The resistance growth coefficients, k_2, for the five media shown in Fig 8.8 were evaluated and are plotted in Fig 8.9. The coefficients can be used to reflect the filtration stage (i.e., depth filtration, transition stage, or surface filtration) for the five media. As seen, firstly, except for the H14 PTFE media experiencing only surface filtration and with the highest k_2 value, the other four media had all experienced depth filtration, with smaller initial k_2 values.

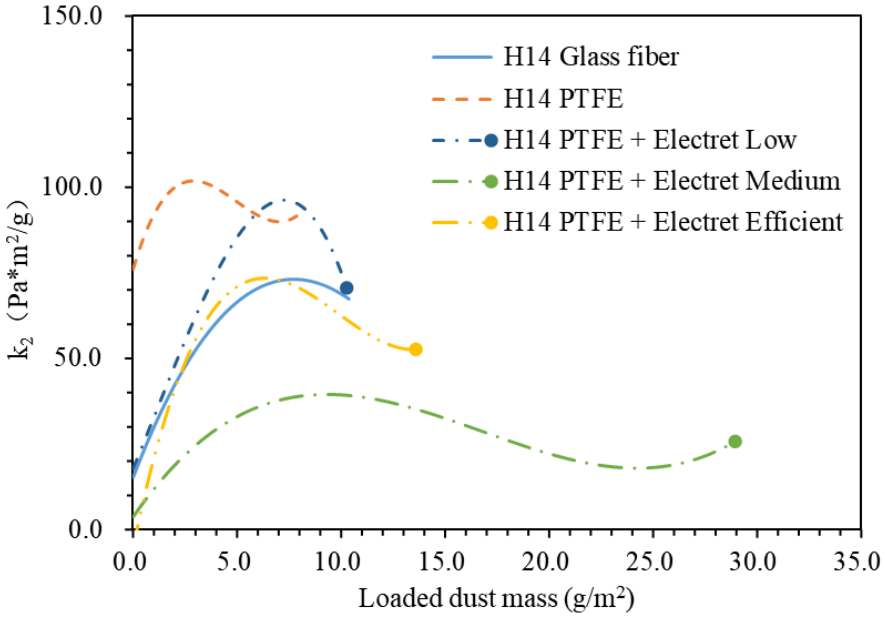

Fig 8.9 The resistance growth coefficients for three composite PTFE media, an H14 PTFE media and an H14 glass fiber media

Secondly, the k_2 values for the PTFE medium composited with the "Electret Low" medium at a loaded dust mass of 7 g/m^2 were as high as those of the H14 PTFE medium. This indicated that the "Electret Low" medium had little filtration efficiency under this loaded dust mass condition, and the composite PTFE media behaved as an H14 PTFE medium. Thirdly, the variation trend for the k_2 values of the PTFE medium composited with the "Electret Efficient" medium was similar to that of the H14 glass fiber medium, indicating a similar clogged filtration process. Lastly, the PTFE medium composited with the "Electret Medium" medium had always smaller k_2 values and correspondingly lower growth rates of resistance.

Fig 8.10 shows the mass averaged resistances for the five media, which can be used to directly compare their energy consumption performances. As seen, the mass averaged resistances for the three composite PTFE media at a fixed loaded dust mass were always lower than those of both the H14 glass fiber medium and H14 PTFE medium. Among the three composite PTFE media, the PTFE medium composited with the "Electret Medium" medium had the lowest mass averaged resistance under the same loaded dust mass and was therefore the most energy efficient composite PTFE media for the experimental aerosol.

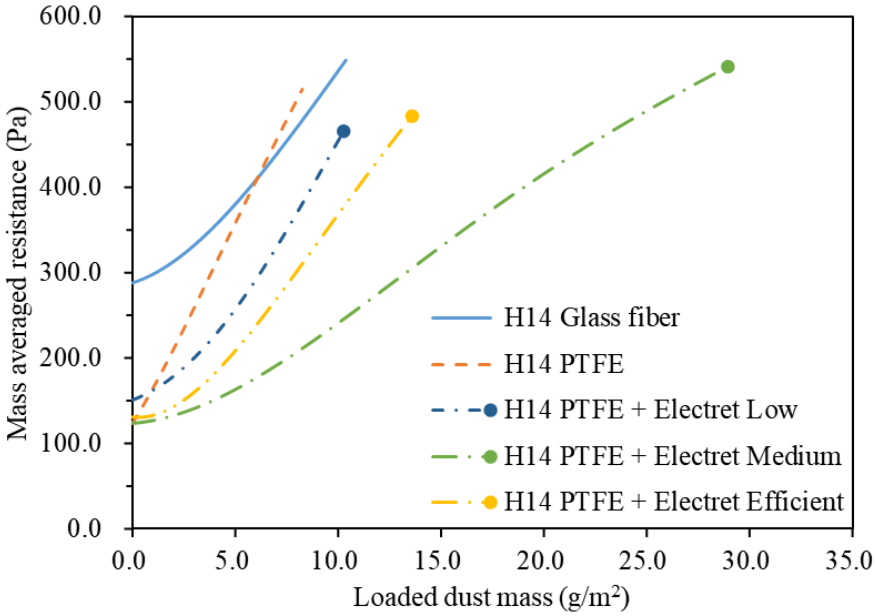

Fig 8.10 Mass averaged resistances for three composite PTFE media, an H14 PTFE media and an H14 glass fiber media

8.5 Conclusions

In this Chapter, firstly, the development of an experimental evaluation method for dust loading performances of HEPA filter media is presented. The method considered the following three aspects: the applicability of experimental aerosol in terms of particle size and humidity sensitivity, experimental setups and procedures, and the evaluation method of energy consumption. This method was used to compare the dust loading performances when using an H14 PTFE medium with those when using an H14 glass fiber medium. Scanning electronic microscope (SEM) photos were taken, when the resistance of the two media after being loaded reached 900 Pa at a filtration velocity

of 5.3 cm/s. The comparison results showed that although the PTFE HEPA medium had a 50% lower initial resistance, its resistance growth rate was far greater than that of the glass fiber HEPA medium.

Secondly, to remove the application limit of PTFE media due to their poorer dust loading performances, the development of composite PTFE media is reported in this Chapter. Composite PTFE media were developed by replacing the windward base materials of PTFE media, three electret filter media of three different efficiencies were used as the windward materials to make composite PTFE media. The mass averaged resistances during dust loading for these composite PTFE media were experimentally obtained and compared. The comparison results showed that the dust loading performances of the above three PTFE media were significantly improved after compositing, all being better than that of a glass fiber HEPA medium. Among them, the PTFE medium composited with the “Electret Medium” medium had the best energy consumption performance when using an eligible experimental aerosol. It should be noticed, however, that the best composite PTFE medium applied only to the experimental aerosol used in the research work reported in this Chapter. Since the size distribution of aerosols had a significant influence on the dust loading performance of fibrous media, the most energy efficient composite PTFE medium may still be determined according to the type of the challenge aerosols used.

Chapter 9

Conclusions and proposed future work

9.1 Conclusions

In this Thesis, the research work on the dynamic resistance of fibrous media used for general ventilation and clean air-conditioning is presented. The conclusions of the Thesis are:

1) An experimental setup has been specifically established for dust loading experiments of fibrous media. The construction of the setup, experimental air flow, experimental aerosols and the filter media are detailed in Chapter 4. The operating performances of the experimental setup were validated through resistance test, Zero% efficiency test, 100% efficiency test and aerosol concentration test, and the test results demonstrated that the setup can meet the needs of the experimental part of the research work reported in this Thesis.

2) An experimental study on the influences of filtration velocity, air flow humidity and aerosol concentration on the dynamic resistance of fibrous filter media was

carried out and is reported in Chapter 5. The experimental results showed that, at the filtration velocity range of 2~10 cm/s, the influence of an increase in filtration velocity on the dynamic resistance of fibrous filter media was not significant. However, an increase of over 5% in relative humidity of passing air flow would lead to a significant decrease in the dynamic resistance in a short time period when the media was loaded with polydisperse KCl aerosols. The resistance growth trend for a medium loaded with KCl aerosols at an air relative humidity close to the deliquescence point of the KCl aerosol was similar to that loaded with a liquid aerosol. By contrast, polydisperse SiO_2 aerosols loaded into the media were not sensitive to the changes in air flow relative humidity. Moreover, it was demonstrated that the aerosol concentration had no significant influence on the dynamic resistance of a filter medium at the same filtration velocity.

3) Chapter 6 reports on the study on the depth filtration resistance of fibrous filter media by combining the classical depth filtration resistance calculation formula with the mass concentration distribution for deposited particles. Firstly, experiments for five-stacked glass fiber media loaded with four monodisperse SiO_2 aerosols and polydisperse SiO_2 aerosols were conducted to investigate the distribution of deposited particles. Secondly, a layered model by incorporating the distribution of deposited particles into Bergman model was proposed to predict the depth filtration resistance for fibrous media. The resistance growths obtained

respectively from experiments and model prediction showed good agreement when the modification of critical loaded dust mass was applied. Lastly, to theoretically evaluate the distribution of deposited particles inside a loaded medium, the D-model was established by dividing a filter medium into unit layers and applying the definition of single fiber efficiency to calculating the mass of particles captured by each layer. The variation trends in loaded dust mass predicted using the numerical solutions for the D-model agreed well with those obtained from the dust loading experiments.

4) A study on the surface filtration resistance of fibrous media is presented in Chapter 7. Dust cake resistance models for both monodisperse aerosols and polydisperse aerosols were respectively developed by calculating the shielding effect of particles based on the kinetic theory. The predictions by using the polydisperse model agreed better with the experimental results than that using the previous models by others. To monitor the changes in the thickness and porosity of dust cakes during their formations, a laser scanning porosity measuring system was established and its accuracy and reproducibility demonstrated. When using this system to monitor the formation process of a dust cake, it was found that an increase in the thickness of a dust cake was gradually decreased with an increase in loaded dust mass and finally leveled, and that the porosity was decreased linearly.

5) Chapter 8 presents an experimental evaluation method for dust loading performances of HEPA filter media. The method was developed based on the considerations of i) the applicability of experimental aerosol in terms of particle size and humidity sensitivity; ii) experimental setups and procedures; and iii) the evaluation of energy consumption for loaded media. This evaluation method was used to compare the dust loading performances when using an H14 PTFE medium with those when using an H14 glass fiber medium. Composite PTFE media were also developed by replacing the windward base materials of PTFE media with electret media to improve the dust loading performances of PTFE media. The average resistances during dust loading for these composite PTFE media were experimentally obtained and compared. Results showed that the dust loading performances of the above three PTFE media were significantly improved after compositing, all being better than that of a glass fiber HEPA medium.

The research work reported in this Thesis has made important contributions to better understanding the mechanism and characteristics of the dynamic resistance of fibrous filter media used for general ventilation and clean air-conditioning. The research results have provided new theoretical bases for both the depth filtration and the surface filtration resistance modeling, which can be used to enhance significantly the filtration performances of existing air filters and media. Therefore, it is believed that the

research results reported in this Thesis can contribute significantly to advancing air filtration theories, developing more energy efficient ventilation and air-conditioning systems and finally sustaining the global long-term goal of carbon neutrality.

9.2 Proposed future work

Based on the research work presented in this Thesis, a number of future studies are proposed:

1) The SEM photos shown in Chapters 6~8 can only provide qualitative descriptions of clean or loaded fibrous media but not quantitative results, and thus cannot be used to describe the real-time interaction between particles and fibers. Therefore, microscopic real-time observation means shall be used to study the filtration processes for a single fiber or multiple fibers, so as to get a better understanding of the mechanism of aerosol filtration and to further improve the filtration performances of fibrous media.

2) The layered resistance model built and reported in Chapter 6 may be not of sufficient accuracy in predicting the depth filtration resistance of a fibrous medium, because the effect of size distribution of deposited particles on medium resistance was not considered in Bergman model. Therefore, the kinetic theory

used in Chapter 7 may be used to evaluate the depth filtration resistance for fibrous media at given mass concentration distribution and size distribution of deposited particles.

3) Electret fibrous media were chosen as the windward base materials of composite PTFE media, as reported in Chapter 8, due to their much lower resistance than that of glass fiber media at the same filtration efficiency class. However, there was no theoretical model describing the dynamic resistance of electret media. Therefore, further work to investigate the dynamic resistance of electret media based on the research results of depth filtration resistance obtained in Chapter 6 should be organized for further optimization of composite PTFE media.

4) As presented in Chapter 6, the uneven distribution of deposited particles in fibrous media has led to the acceleration in the growth rate of the medium resistance. In addition to the method of composite media applied reported in Chapter 8, it can also be considered to develop the fibrous medium with gradient packing density and distribution of fiber diameter along its thickness, so as to extend the life span of fibrous media made of single material.

Appendix A The python program for numerically solving Equation (6-10)

```
import numpy as np

import matplotlib.pyplot as plt


dt = 0.1 #set step length for dust loading time, s

m = 100000 #set the number of step for dust loading time

dz = 0.00008 # set step length for medium thickness, m

n = 25 # set the number of step for medium thickness


V = 0.0533 #filtration velocity, m/s

a0 = 0.3 #packing density of clean medium

nf = 0.004 #sigle fiber efficiency for clean medium

df = 0.000005 #average fiber diameter of clean medium, m

λ = 0.000005 #growth coefficient of single fiber efficiency, m^3/mg

ρ = 2.2e9 #density of particles, mg/m^3

C0 = 10.0 #aerosol concentration, mg/m^3

pi = 3.1415945


# Initial assignment

C = np.zeros([n+1, m+1]) # two-dimensional array for mass concentration of
```

```
suspended aerosol
M = np.zeros([n+1, m+1]) # two-dimensional array for mass concentration of deposited particles
for k in range(0, m+1):
    C[0, k] = C0

#Calculating M and C
for i in range(1, n):
    for j in range(1, m):
        M[i, j] = M[i, j-1]+dt*V*C[i, j-1]*4*a0*nf/pi/df*(1+ λ *M[i, j-1])/(1-a0-M[i, j-1]/ ρ )
        C[i, j] = (C[i, j-1]/dt+V*C[i-1, j]/dz)/(1/dt+V/dz+V*4*a0*nf/pi/df*(1+ λ *M[i, j-1])/(1-a0-M[i, j-1]/ ρ ))

#Plotting
Space = np.arange(0, (m+1)*dt, dt)

plt.figure(' Mass concentrations of suspended particles in different medium thicknesses', dpi=200)
plt.plot(Space, C[1, :], 'g-', label='z/z0=0.04', linewidth=2.0)
plt.plot(Space, C[6, :], 'b--', label='z/z0=0.24', linewidth=1.0)
```

```
plt.plot(Space, C[11, :], 'k-.', label='z/z0=0.44', linewidth=1.0)
plt.plot(Space, C[16, :], 'r:', label='z/z0=0.64', linewidth=1.0)
plt.plot(Space, C[21, :], 'y-', label='z/z0=0.84', linewidth=1.0)
plt.ylabel('Mass concentration (mg/m )', fontsize=15)
plt.xlabel('Dust loading time (s)', fontsize=15)
plt.xlim(0, dt*m)
plt.ylim(0, C0)
plt.legend(loc='upper right')

plt.figure(' Loaded dust masses within different medium thickness ranges ', dpi=200)
CM = np.zeros([n+1, m+1]) # two-dimensional array for loaded dust mass
for r in range(0, m):
    for s in range(1, 26, 5):
        CM[s, r] = dz/1000*(M[s, r] + M[s+1, r] + M[s+2, r] + M[s+3, r] + M[s+4,
r])
plt.plot(Space, CM[1, :], 'g-', label='(0~0.2)z0', linewidth=2.0)
plt.plot(Space, CM[6, :], 'b--', label='(0.2~0.4)z0', linewidth=1.0)
plt.plot(Space, CM[11, :], 'k-.', label='(0.4~0.6)z0', linewidth=1.0)
plt.plot(Space, CM[16, :], 'r:', label='(0.6~0.8)z0', linewidth=1.0)
plt.plot(Space, CM[21, :], 'y-', label='(0.8~1)z0', linewidth=1.0)
plt.ylabel('Loaded dust mass (g/m )', fontsize=15)
```

```
plt.xlabel('Dust loading time (s)', fontsize=15)

plt.xlim(0, dt*m)

plt.ylim(0, C0*5e-1)

plt.legend(loc='upper left')

plt.show()
```

References

1. Adam et al. 1992

   Adam, R., Lücke, T., Tittel, R. and Fissan, H.

   Investigation of structure of planar inhomogeneous filter media from glass fibers. Journal of Aerosol Science, 23. (1992): 737-740.

2. Aguiar and Coury 1996

   Aguiar, M. L. and Coury, J. R.

   Cake Formation in Fabric Filtration of Gases. Industrial & Engineering Chemistry Research, 35.10 (1996): 3673-3679.

3. Alonso et al. 1997

   Alonso, M., Kousaka, Y., Hashimoto, T. and Hashimoto, N.

   Penetration of nanometer-sized aerosol particles through wire screen and laminar flow tube. Aerosol Science and Technology, 27.4 (1997): 471-480.

4. Balazy 2005

   Balazy, A.

   Filtration of nanosized aerosol particles in fibrous filters: I Experimental Results. Europian Aerosol Conference, Balazy, 2005 (2005).

5. Bao et al. 1998

   Bao, L., Otani, Y., Namiki, N., Mori, J. and Emi, H.

   Prediction of HEPA filter collection efficiency with a bimodal fiber size distribution. Kagaku Kogaku Ronbunshu, 24.5 (1998): 766-771.

6. Becker et al. 2016

   Becker, J., Cheng, L., Kronsbein, C. and Wiegmann, A.

Simulation of Cake Filtration for Polydisperse Particles. Chemical Engineering & Technology, 39.3 (2016): 559 -566.

7. Bergman et al. 1978

Bergman, W., Taylor, R. D., Miller, H. H., Bierman, A. H., Hebard, H. D., Daroza, R. A. and Lum, B. Y.

Enhanced filtration program at LLL. A progress report. Environmentalences (1978).

8. Bernardo et al. 2013

Bernardo, B. D. L., Moraes, F. and Rosas, A.

Drag Force Experienced by a Body Moving through a Rarefied Gas. Chinese Journal of Physics, 51.2 (2013): 189-199.

9. Bian et al. 2020

Bian, Y., Wang, S. J., Zhang, L. and Chen, C.

Influence of fiber diameter, filter thickness, and packing density on PM2.5 removal efficiency of electrospun nanofiber air filters for indoor applications. Building and Environment, 170. (2020): 106628.

10. Billings 1966

Billings, C. E.

Effects of particle accumulation in aerosol filtration, California Institute of Technology (1966).

11. Biskos et al. 2006

Biskos, G., Russell, L. M., Buseck, P. R. and Martin, S. T.

Nanosize effect on the hygroscopic growth factor of aerosol particles. Geophysical Research Letters, 33.7 (2006).

12. Boskovic et al. 2008

Boskovic, L., Agranovski, I. E., Altman, I. S. and Braddock, R. D.

Filter efficiency as a function of nanoparticle velocity and shape. Journal of Aerosol Science, 39.7 (2008): 635-644.

13. Boskovic et al. 2007

Boskovic, L., Agranovski, I. E. and Braddock, R. D.

Filtration of nanosized particles with different shape on oil coated fibres. Journal of Aerosol Science, 38.12 (2007): 1220-1229.

14. Boskovic et al. 2005

Boskovic, L., Altman, I. S., Agranovski, I. E., Braddock, R. D., Myojo, T. and Choi, M.

Influence of particle shape on filtration processes. Aerosol Science and Technology, 39.12 (2005): 1184-1190.

15. Bourrous et al. 2016

Bourrous, S., Bouilloux, L., Ouf, F. X., Lemaitre, P., Nerisson, P., Thomas, D. and Appert-Collin, J. C.

Measurement and modeling of pressure drop of HEPA filters clogged with ultrafine particles. Powder Technology, 289. (2016): 109-117.

16. Brown 1993

Brown, R. C.

Air filtration: an integrated approach to the theory and applications of fibrous filters, Pergamon (1993).

17. Cai 1992

Cai, J.

Fibrous filters with non-ideal conditions. Stockholm, The Royal Institute of Technology. Doctor (1992).

18. Cao 2007

Cao, M.

Experimental study on fractional efficiency of electret filter for fine particulate matter, Donghua University (2007). (In Chinese)

19. Carman 1956

Carman, P. C.

Flow of gases through porous media, Butterworths Scientific Publications (1956).

20. Chen et al. 2019

Chen, C., Ji, W. J. and Zhao, B.

Size-dependent efficiencies of ultrafine particle removal of various filter media. Building and Environment, 160. (2019): 106171.

21. Chen 1955

Chen, C. Y.

Filtration of aerosols by fibrous media. Chemical Reviews, 55.3 (1955): 595-623.

22. Chen et al. 2015

Chen, X., Lin, Z. and Liu, H.

Influence of humidity on resistance of ePTFE high performance air filtration media. Building Energy & Environment, 34.03 (2015): 26-28+25.

23. Cheng and Tsai 1998

Cheng, Y.-H. and Tsai, C.-J.

Factors Influencing Pressure Drop through a Dust Cake during Filtration. Aerosol Science and Technology, 29.4 (1998): 315-328.

24. Cunningham 1910

Cunningham, E.

On the Velocity of Steady Fall of Spherical Particles through Fluid Medium. Proceedings of the Royal Society of London. Series A, Containing Papers of a Mathematical and Physical Character, 83.563 (1910): 357 -365.

25. Dahneke 1971

Dahneke, B.

The capture of aerosol particles by surfaces. Journal of Colloid and Interface Science, 37.2 (1971): 342-353.

26. Dahneke 1972

Dahneke, B.

The influence of flattening on the adhesion of particles. Journal of Colloid and Interface Science, 40.1 (1972): 1-13.

27. Dahneke 1973

Dahneke, B.

Measurements of bouncing of small latex spheres. Journal of Colloid and Interface Science, 45.3 (1973): 584-590.

28. Davies 1973

Davies, C. N.

Air filtration. (1973).

29. De Freitas et al. 2006

De Freitas, N. L., Gonçalves, J. A., Innocentini, M. D. and Coury, J. R.

Development of a double-layered ceramic filter for aerosol filtration at high-temperatures: The filter collection efficiency. Journal of Hazardous Materials, 136.3 (2006): 747-756.

30. Dennis and Dirgo 1981

Dennis, R. and Dirgo, J. A.

Comparison of laboratory and field derived K2 values for dust collected on fabric filters. Filtration and Separation, 18.5 (1981): 394-396+417.

31. Dhaniyala and Liu 2001

Dhaniyala, S. and Liu, B. Y. H.

Theoretical modeling of filtration by nonuniform fibrous filters. Aerosol Science and Technology, 34.2 (2001): 170-178.

32. Drummond and Tahir 1984

Drummond, J. E. and Tahir, M. I.

Laminar Viscous-Flow through Regular Arrays of Parallel Solid Cylinders. International Journal of Multiphase Flow, 10.5 (1984): 515-540.

33. Elmøe et al. 2011

Elmøe, T. D., Tricoli, A. and Grunwaldt, J.-D.

Characterization of highly porous nanoparticle deposits by permeance measurements. Powder Technology, 207.1-3 (2011): 279-289.

34. Elmøe et al. 2009

Elmøe, T. D., Tricoli, A., Grunwaldt, J.-D. and Pratsinis, S. E.

Filtration of nanoparticles: Evolution of cake structure and pressure-drop. Journal of Aerosol Science, 40.11 (2009): 965-981.

35. EN 2012

EN, B.

EN 779-2012 Particle air filters for generalventilation-determination of filtration performance. Brussels: CEN (2012).

36. Endo et al. 1998

Endo, Y., Chen, D.-R. and Pui, D. Y. H.

Effects of particle polydispersity and shape factor during dust cake loading on air filters. Powder Technology, 98.3 (1998): 241-249.

37. Endo et al. 2002

Endo, Y., Chen, D.-R. and Pui, D. Y. H.

Theoretical consideration of permeation resistance of fluid through a particle packed layer. Powder Technology, 124.1-2 (2002): 119-126.

38. Ergun 1952

Ergun, S.

Fluid flow through packed columns. Journal of Materials Science & Chemical Engineering, 48.2 (1952): 89-94.

39. Ergun and Orning 1949

Ergun, S. and Orning, A. A.

Fluid Flow through Randomly Packed Columns and Fluidized Beds. Industrial & Engineering Chemistry, 41.6 (1949): 1179-1184.

40. Ermak and Buckholz 1980

Ermak, D. L. and Buckholz, H.

Numerical integration of the Langevin equation: Monte Carlo simulation. Journal of Computational Physics, 35.2 (1980): 169-182.

41. Feng and Long 2016

Feng, Z. and Long, Z.

Modeling unsteady filtration performance of pleated filter. Aerosol Science and Technology, 50.6 (2016): 626 -637.

42. Fotovati et al. 2011

Fotovati, S., Hosseini, S. A., Vahedi Tafreshi, H. and Pourdeyhimi, B.

Modeling instantaneous pressure drop of pleated thin filter media during dust loading. Chemical Engineering Science, 66.18 (2011): 4036-4046.

43. Fotovati et al. 2012

Fotovati, S., Tafreshi, H. V. and Pourdeyhimi, B.

A macroscale model for simulating pressure drop and collection efficiency of pleated filters over time. Separation and Purification Technology, 98. (2012): 344-355.

44. Fu and Kang 2010

Fu, H.-m. and Kang, Y.-m.

Dust Cake Deposition Simulating On Fibrous Media Surface. International Conference on Bioinformatics and Biomedical Engineering. Chengdu, IEEE (2010): 1 -4.

45. Fu 2006

Fu, H.

Simulation and experimental study on purification performance of surface filtration materials used in bag type dust removal equipment, Donghua University (2006). (In Chinese)

46. Fu 2009

Fu, H.

Study on unsteady filtration pressure loss of fiber filter medium. Journal of Textile Research, 30.04 (2009): 15-18+23. (In Chinese)

47. Fu and Kang 2008

Fu, H. and Kang, Y.

Fractal study on filter cake structure formed by dust deposition. Journal of Filtration & Separation02 (2008): 4-7. (In Chinese)

48. Fu and Shen 2003

Fu, H. and Shen, H.

Research and development of air filtration theory. Journal of Filtration & Separation03 (2003): 20-24. (In Chinese)

49. Fu and Shen 2004

Fu, H. and Shen, H.

Study on the mathematical model of trapping efficiency of fiber filter Medium. Journal of Donghua University (Natural Science)03 (2004): 5-9. (In Chinese)

50. Fuchs and Stechkina 1963

Fuchs, N. A. and Stechkina, I. B.

A note on the theory of fibrous aerosol filters. Ann Occup Hyg, 6.1 (1963): 27-30.

51. Gupta et al. 1993

Gupta, A., Novick, V. J., Biswas, P. and Monson, P. R.

Effect of Humidity and Particle Hygroscopicity on the Mass Loading Capacity of High Efficiency Particulate Air (HEPA) Filters. Aerosol Science and Technology, 19.1 (1993): 94-107.

52. Happel 1959

Happel, J.

Viscous flow relative to arrays of cylinders. AIChE Journal, 5.2 (1959): 174-177.

53. Happel 1983

Happel, J.

Viscous flow in multiparticle systems: slow motion of fluids relative to beds of spherical particles. AIChE Journal9 (1983): 22-22.

54. Happel and Brenner 1983

Happel, J. and Brenner, H.

Low Reynolds Number Hydrodynamics, Distributed by Kluwer Boston (1983).

55. Hasimoto 1959

Hasimoto, H.

On the periodic fundamental solutions of the Stokes equations and their application to viscous flow past a cubic array of spheres. Journal of Fluid Mechanics, 5.2 (1959): 317-328.

56. Heidenreich et al. 1991

Heidenreich, E., Tittel, R., Neuber, A. and Adam, R.

Measuring the inhomogeneities of high efficient glass fibrefilter media. Journal of Aerosol Science, 22. (1991): S785-S788.

57. Henry and Ariman 1983

Henry, F. S. and Ariman, T.

An evaluation of the Kuwabara model. Particulate Science and Technology, 1.1 (1983): 1-20.

58. Hinds 1999

Hinds, W. C.

Aerosol technology: properties, behavior, and measurement of airborne particles, John Wiley & Sons (1999).

59. Hosseini and Tafreshi 2010

Hosseini, S. A. and Tafreshi, H. V.

3-D simulation of particle filtration in electrospun nanofibrous filters. Powder Technology, 201.2 (2010): 153-160.

60. Hosseini and Vahedi Tafreshi 2012

Hosseini, S. A. and Vahedi Tafreshi, H.

Modeling particle-loaded single fiber efficiency and fiber drag using ANSYS–Fluent CFD code. Computers & Fluids, 66. (2012): 157-166.

61. Hu et al. 2010

Hu, D., Qiao, L., Chen, J., Ye, X., Yang, X., Cheng, T. and Fang, W.

Hygroscopicity of inorganic aerosols: size and relative humidity effects on the growth factor. Aerosol and Air Quality Research, 10. (2010): 255-264.

62. Huang et al. 2006

Huang, B., Yao, Q., Li, S.-Q., Zhao, H.-L., Song, Q. and You, C.-F.

Experimental investigation on the particle capture by a single fiber using microscopic image technique. Powder Technology, 163.3 (2006): 125-133.

63. Huangfu 2015

Huangfu, C.

Preparation and properties of gradient structure composite filter, Jiangnan University (2015). (In Chinese)

64. Hung and Leung 2011

Hung, C. H. and Leung, W. W. F.

Filtration of nano-aerosol using nanofiber filter under low Peclet number and transitional flow regime. Separation and Purification Technology, 79.1 (2011): 34-42.

65. Iliev et al. 2018

Iliev, O., Kirsch, R. and Osterroth, S.

Combined Depth and Cake Filtration Model Coupled with Flow Simulation for Flat and Pleated Filters. Chemical Engineering & Technology, 41.1 (2018): 70 -78.

66. Ito and Aguiar 2009

Ito, L. X. and Aguiar, M. L.

A study of the porosity of gas filtration cakes. Brazilian Journal of Chemical Engineering, 26.2 (2009): 307-315.

67. Jackson and James 1986

Jackson, G. W. and James, D. F.

The Permeability of Fibrous Porous-Media. Canadian Journal of Chemical Engineering, 64.3 (1986): 364-374.

68. Japuntich et al. 1994

Japuntich, D. A., Stenhouse, J. I. T. and Liu, B. Y. H.

Experimental results of solid monodisperse particle clogging of fibrous filters. Journal of Aerosol Science, 25.2 (1994): 385-393.

69. Ji et al. 2003

Ji, J. H., Bae, G. N., Kang, S. H. and Hwang, J.

Effect of particle loading on the collection performance of an electret cabin air filter for submicron aerosols. Journal of Aerosol Science, 34.11 (2003): 1493-1504.

70. Ji et al. 2019

Ji, L. L., Pei, J. J. and Liu, W. L.

Long-term performance of fibrous ventilation/air-cleaner filters for particle removal. Building and Environment, 160. (2019): 106222.

71. Joubert et al. 2010

Joubert, A., Laborde, J. C., Bouilloux, L., Callé-Chazelet, S. and Thomas, D. Influence of Humidity on Clogging of Flat and Pleated HEPA Filters. Aerosol Science and Technology, 44.12 (2010): 1065 -1076.

72. Joubert et al. 2011

Joubert, A., Laborde, J. C., Bouilloux, L., Chazelet, S. and Thomas, D. Modelling the pressure drop across HEPA filters during cake filtration in the presence of humidity. Chemical Engineering Journal, 166.2 (2011): 616-623.

73. Kanaoka et al. 1983

Kanaoka, C., Emi, H. and Tanthapanichakoon, W.

Convective diffusional deposition and collection efficiency of aerosol on a dust‐loaded fiber. AIChE Journal, 29.6 (1983): 895-902.

74. Kasper et al. 2010

Kasper, G., Schollmeier, S. and Meyer, J.

Structure and density of deposits formed on filter fibers by inertial particle deposition and bounce. Journal of Aerosol Science, 41.12 (2010): 1167-1182.

75. Kim et al. 2005

Kim, J. H., Mulholland, G. W., Kukuck, S. R. and Pui, D. Y.

Slip Correction Measurements of Certified PSL Nanoparticles Using a Nanometer Differential Mobility Analyzer (Nano-DMA) for Knudsen Number From 0.5 to 83. J Res Natl Inst Stand Technol, 110.1 (2005): 31-54.

76. Kim et al. 2009

Kim, S. C., Wang, J., Shin, W. G., Scheckman, J. H. and Pui, D. Y. H.

Structural Properties and Filter Loading Characteristics of Soot Agglomerates. Aerosol Science and Technology, 43.10 (2009): 1033-1041.

77. Kirsch and Stechkina 1973

Kirsch, A. and Stechkina, I.

Pressure drop and diffusional deposition of aerosol in polydisperse model filter. Journal of Colloid and Interface Science, 43.1 (1973): 10-16.

78. Kirsch et al. 1974

Kirsch, A., Stechkina, I. and Fuchs, N.

Gas flow in aerosol filters made of polydisperse ultrafine fibres. Journal of Aerosol Science, 5.1 (1974): 39-45.

79. Kousaka et al. 1990

Kousaka, Y., Okuyama, K., Shimada, M. and Takii, Y.

Development of a Method for Testing Very High-Efficiency Membrane Filters for Ultrafine Aerosol-Particles. Journal of Chemical Engineering of Japan, 23.5 (1990): 568-574.

80. Kuwabara 1959

Kuwabara, S.

The Forces experienced by Randomly Distributed Parallel Circular Cylinders or Spheres in a Viscous Flow at Small Reynolds Numbers. Journal of the Physical Society of Japan, 14.4 (1959): 527-532.

81. Langmuir et al. 1942

Langmuir, I., Rodebush, W. H. and Lamer, V. K.

Filtration of aerosols and development of filter materials. OSRD-865, Office of Scientific Research and Development, Washington, DC (1942).

82. Letourneau et al. 1991

Letourneau, P., Mulcey, P. and Vendel, J.

Aerosol penetration inside HEPA filtration media. (1991).

83. Li and Wang 2003

Li, Z. and Wang, H.

Drag force, diffusion coefficient, and electric mobility of small particles. I. Theory applicable to the free-molecule regime. Phys Rev E Stat Nonlin Soft Matter Phys, 68.6 Pt 1 (2003): 061206.

84. Liang and Shen 2010

Liang, Z. and Shen, H.

Study on the characteristics of high temperature filter material for bag type dust removal. Proceeding of National HVAC Refrigeration Annual Conference (2010). (In Chinese)

85. Lin et al. 2013

Lin, Z., Wu, C., Lu, T. and Xia, J.

The unsteady filtration efficiency of fiber filter medium in the dust holding stage. Journal of Tongji University (Natural Science), 41.06 (2013): 920-925. (In Chinese)

86. Lindquist et al. 2014

Lindquist, G. J., Pui, D. Y. H. and Hogan, C. J.
Porous particulate film deposition in the transition regime. Journal of Aerosol Science, 74. (2014): 42-51.

87. Liu et al. 2002
Liu, J., Peng, W. and Xiang, X.
Study on the unsteady filtration efficiency of fiber surface layer. Building Energy & Environment, 03. (2002): 16-19+22. (In Chinese)

88. Liu et al. 2013
Liu, J., Swanson, J. J., Kittelson, D. B., Pui, D. Y. H. and Wang, J.
Microstructural and loading characteristics of diesel aggregate cakes. Powder Technology, 241. (2013): 244-251.

89. Liu and Xu 2009
Liu, S. and Xu, B.
Application of HBT/PPS gradient special filter material in flue gas dust removal of power plant. National Workshop on Dust Removal Technology of Bag Filters (2009). (In Chinese)

90. Mahdavi et al. 2015
Mahdavi, A., Haghighat, F., Bahloul, A., Brochot, C. and Ostiguy, C.
Particle loading time and humidity effects on the efficiency of an N95 filtering facepiece respirator model under constant and inhalation cyclic flows. Ann Occup Hyg, 59.5 (2015): 629-640.

91. Maze et al. 2007
Maze, B., Tafreshi, H. V., Wang, Q. and Pourdeyhimi, B.

A simulation of unsteady-state filtration via nanofiber media at reduced operating pressures. Journal of Aerosol Science, 38.5 (2007): 550-571.

92. Miguel 2003

Miguel, A. F.

Effect of air humidity on the evolution of permeability and performance of a fibrous filter during loading with hygroscopic and non-hygroscopic particles. Journal of Aerosol Science, 34.6 (2003): 783-799.

93. Molter and Fissan 1997

Molter, W. and Fissan, H.

Modelling of inhomogeneous fibrous filter media - Discussion and application of the representative element size to calculate the filtration performance numerically. Gefahrstoffe Reinhaltung Der Luft, 57.5 (1997): 201-205.

94. Mostofi et al. 2010

Mostofi, R., Wang, B., Haghighat, F., Bahloul, A. and Jaime, L.

Performance of Mechanical Filters and Respirators for Capturing Nanoparticles -Limitations and Future Direction. Industrial health, 48.3 (2010): 296-304.

95. Novick et al. 1992

Novick, V. J., Monson, P. R. and Ellison, P. E.

The effect of solid particle mass loading on the pressure drop of HEPA filters. Journal of Aerosol Science, 23.6 (1992): 657-665.

96. Payatakes 1976

Payatakes, A. C.

Model of the dynamic behavior of a fibrous filter. Application to case of pure interception during period of unhindered growth. Powder Technology, 14.2 (1976): 267-278.

97. Payatakes 1977

Payatakes, A. C.

Model of transient aerosol particle deposition in fibrous media with dendritic pattern. AIChE Journal, 23.2 (1977): 192-202.

98. Payatakes and Tien 1976

Payatakes, A. C. and Tien, C.

Particle deposition in fibrous media with dendrite-like pattern: A preliminary model. Journal of Aerosol Science, 7.2 (1976): 85-100.

99. Penicot et al. 1999

Penicot, P., Thomas, D., Contal, P., Leclerc, D. and Vendel, J.

Clogging of HEPA fibrous filters by solid and liquid aerosol particles: An experimental study. Filtration & Separation, 36.2 (1999): 59-64.

100. Podgorski et al. 2006

Podgorski, A., Balazy, A. and Gradon, L.

Application of nanofibers to improve the filtration efficiency of the most penetrating aerosol particles in fibrous filters. Chemical Engineering Science, 61.20 (2006): 6804-6815.

101. Qian et al. 2013

Qian, F., Huang, N., Zhu, X. and Lu, J.

Numerical study of the gas–solid flow characteristic of fibrous media based on SEM using CFD–DEM. Powder Technology, 249.11 (2013): 63-70.

102. Qian et al. 2010a

Qian, F., Wang, H. and Chen, G.

Numerical study on the filtration performance of the surface coated multilayer composite fiber filter material. Acta Scientiae Circumstantiae, 30.12 (2010a): 2392-2398. (In Chinese)

103. Qian et al. 2010b

Qian, F., Wang, H., Qian, F. and Wang, H.

Study of the filtration performance of a plain wave fabric filter using response surface methodology. Journal of Guangzhou University, 176.4 (2010b): 377-378.

104. Rebaï et al. 2010a

Rebaï, M., Prat, M., Meireles, M., Schmitz, P. and Baclet, R.

Clogging modeling in pleated filters for gas filtration. Chemical Engineering Research and Design, 88.4 (2010a): 476-486.

105. Rebaï et al. 2010b

Rebaï, M., Prat, M., Meireles, M., Schmitz, P. and Baclet, R.

A semi-analytical model for gas flow in pleated filters. Chemical Engineering Science, 65.9 (2010b): 2835-2846.

106. Ribeyre et al. 2017

Ribeyre, Q., Charvet, A., Vallières, C. and Thomas, D.

Impact of relative humidity on a nanostructured filter cake – Experimental and modelling approaches. Chemical Engineering Science, 161. (2017): 109-116.

107. Rief et al. 2006

Rief, S., Latz, A. and Wiegmann, A.

Computer simulation of Air Filtration including electric surface charges in three-dimensional fibrous micro structures. Filtration, 6.2 (2006): 169-172.

108. Rong and Zhang 1992

Rong, W. and Zhang, G.

Theoretical analysis and experimental study of fiber layer unsteady filtration. Building Energy & Environment03 (1992): 8-12+29. (In Chinese)

109. Rudnick and First 1978

Rudnick, S. N. and First, M. W.

Specific resistance (K2) of filter dust cakes: Comparison of theory and experiments. the Third Symposium on Fabric Filters for Particulate Collection (1978).

110. Sakano et al. 2000

Sakano, T., Otani, Y., Namiki, N. and Emi, H.

Particle collection of medium performance air filters consisting of binary fibers under dust loaded conditions. Separation and Purification Technology, 19.1-2 (2000): 145-152.

111. Saleh et al. 2013

Saleh, A. M., Hosseini, S. A., Vahedi Tafreshi, H. and Pourdeyhimi, B.

3-D microscale simulation of dust-loading in thin flat-sheet filters: A comparison with 1-D macroscale simulations. Chemical Engineering Science, 99. (2013): 284-291.

112. Sangani and Acrivos 1982

Sangani, A. S. and Acrivos, A.

Slow Flow Past Periodic Arrays of Cylinders with Application to Heat-Transfer. International Journal of Multiphase Flow, 8.3 (1982): 193-206.

113. Schmidt and Löffler 1990

Schmidt, E. and Löffler, F.

Preparation of dust cakes for microscopic examination. Powder Technology, 60.2 (1990): 173-177.

114. Schmidt and Löffler 1991

Schmidt, E. and Löffler, F.

The Analysis of Dust Cake Structures. Particle & Particle Systems Characterization, 8.1-4 (1991): 105-109.

115. Shen 2006

Shen, H.

Research and development and application of new filter material for bag filter of coal - fired boiler. Building Energy & Environment, 25.5 (2006): 30-33. (In Chinese)

116. Silva et al. 1999

Silva, C. R. N., Negrini, V. S., Aguiar, M. L. and Coury, J. R.

Influence of gas velocity on cake formation and detachment. Powder Technology, 101.2 (1999): 165-172.

117. Song et al. 2006

Song, C. B., Park, H. S. and Lee, K. W.

Experimental study of filter clogging with monodisperse PSL particles. Powder Technology, 163.3 (2006): 152-159.

118. Spielman and Goren 1968

Spielman, L. and Goren, S. L.

Model for predicting pressure drop and filtration efficiency in fibrous media. Environmental Science & Technology, 2.4 (1968): 279-287.

119. Steffens and Coury 2007

Steffens, J. and Coury, J. R.

Collection efficiency of fiber filters operating on the removal of nano-sized aerosol particles: I - Homogeneous fibers. Separation and Purification Technology, 58.1 (2007): 99-105.

120. Tan and Wang 1990

Tan, Z. and Wang, J.

Theoretical analysis and experimental study of surface unsteady filtration. Building Energy & Environment01 (1990): 1-4. (In Chinese)

121. Thomas 2017

Thomas, D.

Filtration of Solid Aerosols. Aerosol Filtration. D. Thomas, A. Charvet, N. Bardin-Monnier and J.-C. Appert-Collin, Elsevier (2017): 123-159.

122. Thomas et al. 2016

Thomas, D., Charvet, A., Bardin-Monnier, N. and Appert-Collin, J.-C. Aerosol filtration, Elsevier (2016).

123. Thomas et al. 1999

Thomas, D., Contal, P., Renaudin, V., Penicot, P., Leclerc, D. and Vendel, J. Modelling pressure drop in hepa filters during dynamic filtration. Journal of Aerosol Science, 30.2 (1999): 235-246.

124. Thomas et al. 2014

Thomas, D., Ouf, F. X., Gensdarmes, F., Bourrous, S. and Bouilloux, L. Pressure drop model for nanostructured deposits. Separation and Purification Technology, 138. (2014): 144-152.

125. Thomas et al. 2001

Thomas, D., Penicot, P., Contal, P., Leclerc, D. and Vendel, J. Clogging of fibrous filters by solid aerosol particles Experimental and modelling study. Chemical Engineering Science, 56.11 (2001): 3549-3561.

126. Tian et al. 2019

Tian, E., Gao, Y. and Mo, J. Electrostatically assisted air coarse filtration for energy efficient ambient particles removal: Long-term performance in real environment and influencing factors. Building and Environment, 164. (2019): 106348.

127. Tian et al. 2018

Tian, E., Mo, J. and Li, X.

Electrostatically assisted metal foam coarse filter with small pressure drop for efficient removal of fine particles: Effect of filter medium. Building and Environment, 144. (2018): 419-426.

128. Walsh and Stenhouse 1997

Walsh, D. C. and Stenhouse, J. I. T.

The effect of particle size, charge, and composition on the loading characteristics of an electrically active fibrous filter material. Journal of Aerosol Science, 28.2 (1997): 307-321.

129. Wang et al. 2013

Wang, H., Zhao, H., Wang, K., He, Y. and Zheng, C.

Simulation of filtration process for multi-fiber filter using the Lattice-Boltzmann two-phase flow model. Journal of Aerosol Science, 66. (2013): 164-178.

130. Wang et al. 2016

Wang, Q., Lin, X. and Chen, D.-R.

Effect of dust loading rate on the loading characteristics of high efficiency filter media. Powder Technology, 287. (2016): 20-28.

131. Wise et al. 2008

Wise, M. E., Martin, S. T., Russell, L. M. and Buseck, P. R.

Water uptake by NaCl particles prior to deliquescence and the phase rule. Aerosol Science and Technology, 42.4 (2008): 281-294.

132. Xia and Chen 2020

Xia, T. L. and Chen, C.

Toward understanding the evolution of incense particles on nanofiber filter media: Its influence on PM2.5 removal efficiency and pressure drop. Building and Environment, 172. (2020): 106725.

133. Xiang et al. 2002a

Xiang, X., Liu, J. and Peng, W.

Study on unsteady filtration of fiber layer surface. Environmental Engineering06 (2002a): 31-34+33. (In Chinese)

134. Xiang et al. 2002b

Xiang, X., Zhu, D. and Peng, W.

Study on pressure Loss of unsteady filtration and dust removal. Gongye Anquan yu Huanbao09 (2002b): 5-7. (In Chinese)

135. Xu et al. 1993

Xu, X., Deng, C., Luo, Q. and Kang, Y.

Fractal study of filter cake structure. Metal Mine09 (1993): 42-44+53. (In Chinese)

136. Xu 2014

Xu, Z.

Principle of air cleaning technology, SCIENCE PRESS (2014). (In Chinese)

137. Xu and Zhou 2014

Xu, Z. and Zhou, B.

Fundamentals of Air Cleaning Technology and Its Application in Cleanrooms, Springer Berlin Heidelberg (2014).

138. Yan 2006

Yan, C.

Experimental study on dust removal filter material for boiler flue gas purification in coal-fired power plant, Donghua University (2006). (In Chinese)

139. Ye and Chen 2013

Ye, X. and Chen, J.

Haze and particulate hygroscopic growth. Chinese Journal of Nature, 35.05 (2013): 337-341. (In Chinese)

140. Yun et al. 2007

Yun, K. M., Hogan, C. J., Mastubayashi, Y., Kawabe, M., Iskandar, F. and Okuyama, K.

Nanoparticle filtration by electrospun polymer fibers. Chemical Engineering Science, 62.17 (2007): 4751-4759.

141. Zaatari et al. 2016

Zaatari, M., Novoselac, A. and Siegel, J.

Impact of ventilation and filtration strategies on energy consumption and exposures in retail stores. Building and Environment, 100. (2016): 186-196.

142. Zhang et al. 2016

Zhang, H., Zhen, Q., Wang, H., Qian, X. and Liu, Y.

Structure and properties of high temperature resistant fiber filter materials with gradient structure. Journal of Textile Research, v.37;No.362.05 (2016): 22-27. (In Chinese)

143. Zhang et al. 2018

Zhang, W., Deng, S., Wang, Y. and Lin, Z.

Dust Loading Performance of the PTFE HEPA Media and its Comparison with the Glass Fibre HEPA Media. Aerosol and Air Quality Research, 18.7 (2018): 1921-1931.

144. Zhong and Pan 2016

Zhong, W. and Pan, N.

Aerosol Filtration by Fibrous Filters: A Statistical Mechanics Approach. Textile Research Journal, 77.5 (2016): 284-289.

145. Zhou 2015

Zhou, L.

Experimental study on the Purification of PM2.5 by air filter in centralized air conditioning system, Donghua University (2015). (In Chinese)

146. Zhu 2009

Zhu, H.

Computer simulation of dust particles deposited on the surface of fiber filter medium, Donghua University. Master (2009): 102. (In Chinese)

147. Zhu et al. 2013

Zhu, H., Fu, H. and Kang, Y.

Numerical simulation of particles deposition and rebound on fiber surface. Zhongnan Daxue Xuebao (Ziran Kexue Ban)/Journal of Central South University (Science and Technology), 44.7 (2013): 3086-3094.

148. Zuraimi et al. 2017

Zuraimi, M. S., Vuotari, M., Nilsson, G., Magee, R., Kemery, B. and Alliston, C.

Impact of dust loading on long term portable air cleaner performance. Building and Environment, 112. (2017): 261-269.